## CONTACT

Turkish JournalPark ACADEMIC

## Environmental Research & Technology

http://dergipark.gov.tr/ert

# **Editorial Board**

## Environmental Research & Technology

http://dergipark.gov.tr/ert

## TABLE OF CONTENTS

Environmental Research & Technology

## EDITORIAL

## Editorial for the 2nd Issue of ER&T

Guleda Onkal Engin[1,*]

[1]Yildiz Technical University, Civil Engineering Faculty, Environmental Engineering Department, 34220, Esenler, Istanbul, TURKIYE

I am honored when our editor-in-chief asked me to write an editorial for the second issue of the *Environmental Research & Technology Journal*. After a tiring and long journey of preparatory work with a lot of effort put forward by our Editor-In-Chief, and warm support from the other co-editors, the first issue of the *Environmental Research & Technology* was launched at the beginning of the year 2018. We, as the co-editors, feel very fortunate to publish yet another issue of *Environmental Research & Technology*. We are also delighted and eager to work with our outstanding scientists and authors, reviewers, co-editors, and our only staff for the next years to come.

The main aim of the *Environmental Research & Technology* is to publish the state-of-the-art of current research revealing environmental problems and solutions. This is only the second issue and I wish *Environmental Research & Technology* will serve you by publishing your most interesting researches and achievements in the years to come. Although there are many other journals available dealing with environmental problems and concerns, many researchers face the difficulty in finding the right journal for their manuscripts most of the time. This is mainly due to the fact that manuscripts may not seem to "fit" within the scope of a particular journal. I believe *Environmental Research & Technology* will serve as the right place for publishing as it covers a broad scope of the environmental sciences and engineering from its basics to advanced research.

It's been quite a while since the World Water Forum which was organized in Istanbul in 2009. In this Forum, one of the prominent issues was the access to sanitary water. Although, I feel really very lucky that this is not an issue in this part of the world, I feel really very sorry for those who could not find any means for irrigation for food security or energy production, let alone those who cannot reach clean potable water. It is already announced by the renowned researchers that the water stress in many parts of the world will increase gradually due to the negative effects of climate change and pollution. The existing cooperation among the countries in this sense must be improved to mitigate the foreseen effects. To my personal belief, political discussions, disagreements and conflicts will always be there, however, the main problem is the lack of understanding and confidence at the technical level. This is the main barrier to enhance cooperation and to provide sound solutions. This will only be achieved by producing quality evidence-based research. I hope *Environmental Research & Technology* will provide the chance to those who would work for a better (not just from the point of environment) world.

In this issue, I believe you will find quite interesting papers from a variety of areas from wastewater treatment to leachate injection system and from biodiesel production to air quality management.

As I final word, I would like to thank again all our colleagues, authors and co-editors whose support and suggestions have made this new issue possible.

Turkish **JournalPark** ACADEMIC

## Environmental Research & Technology

RESEARCH ARTICLE

# Effect of gas composition on the selective reduction of NO$_x$ with ammonia over Vanadia based catalysts

Souad Djerad[1,*], Marcus Crocoll[2], Lakhdar Tifouti[1], Werner Weisweiler[2]

[1] Laboratory of Environmental Engineering, Department of Process Engineering, University of Annaba, P.O. Box 12, Annaba, ALGERIA
[2] Institut für Chemische Technik und Polymer Chemie, Universität Karlsruhe (TH), GERMANY

## ABSTRACT

The catalytic reduction of NO$_x$ under different oxygen concentrations leading to different NO/NO$_2$ compositions has been studied in the presence of V3W9Ti and V8W9Ti catalysts in a tubular flow reactor. The results have shown that increasing O$_2$ concentration leads to increase the NO$_x$ reduction in low temperature range [150-275 °C]. Slight effect of O$_2$ concentration on NO$_x$ conversion was observed at higher temperatures. SCR reaction also occurred in the absence of gaseous oxygen but with low NO conversion indicating the strong redox properties of both catalysts. Aged catalysts exhibited relative good activities in NO$_x$ reduction. This is probably due to the sol gel method used for the preparation of the catalysts known to improve the catalysts properties.

*Keywords:* SCR; Oxygen concentration; NO-NO$_2$ mixture; ammonia oxidation; TPD; aging

## 1. INTRODUCTION

Nitrogen oxides remain a major source in air pollution [1]. Nowadays, it is known that not only NO$_x$ but also N$_2$O contributes to the greenhouse effect and to the depletion of the ozone layer. Both gases are emitted from many industrial processes and from all means of transport.

From a global warming perspective, diesel engines are presently preferred alternatives to conventional Otto engines in heavy-duty vehicles due to lower fuel consumption and hence lower emissions of CO$_2$.

An established technique for stationary units, which recently has gained increased attention for automotive applications, is selective catalytic reduction of NO$_x$ using ammonia-releasing compounds (e.g, urea) as the reducing agent (NH$_3$-SCR) [2]. Ammonia is added to the exhaust gas, where it reacts selectively with the NO$_x$ over a catalyst to form harmless nitrogen and water. Catalytic systems constituted by V$_2$O$_5$ dispersed over a TiO$_2$-anatase support are widely used in the selective catalytic reduction (SCR) of NO$_x$ with NH$_3$ [3]. Vanadia supported on the anatase type of titania is a commercial catalyst for the SCR process due to the high NO removal activity and its relatively strong resistance to the poisons including SO$_2$, which is commonly contained in the flue gas. WO$_3$ frequently used with vanadia presents a much lower activity in both denitrification and SO$_2$ oxidation reactions and is used to preserve the structural and morphological characteristics of TiO$_2$-anatase upon addition of vanadia [4].

It is known that the catalytic mechanism is divided into a reduction reaction where a vanadium atom is reduced due to an electron transfer from the adsorbate and a reoxidation reaction where +5 oxidation state of vanadium atom is restored by a reverse electron transfer involving gaseous oxygen [5]. Since O$_2$ is important for the reoxidation of vanadium atom and restore the initial sites, it is an interesting task to study the effect of its concentration but also its absence on the course of the NO$_x$ reduction. In this study, two catalysts with low (3%) and high (8%) vanadia contents were prepared and tested for the catalytic reduction of NO$_x$ in the absence and in the presence of gaseous O$_2$. Aging the catalysts may restrict their use, and therefore the activities of aged catalysts have been also studied.

## 2. EXPERIMENTAL

### 2.1. Catalyst preparation

Two catalysts: $3\%V_2O_5$-$9\%WO_3/TiO_2$ (w/w) and $8\%V_2O_5$-$9\%WO_3/TiO_2$ (w/w) were prepared by sol-gel method. The cordierite used as support has a cell density of 64 cells $cm^{-2}$ and a volume of 9.4 $cm^3$ and was coated with 200 mg of each catalyst labelled V3 and V8. Further details on the catalyst preparation are given in a previous publication [6].

BET measurements were performed with a Quantachrome Autosorb 1C using Nitrogen. X-ray diffraction patterns were obtained with a Siemens D-500 powder X-ray diffractometer using CuKα radiation (λ= 1,5406 Å) in step mode between 20° and 80°, using a step size of 0,02° $s^{-1}$. Mesopores distribution measurements have been obtained by mercury penetration method using a porosimeter Autopore III.

### 2.2. Activity measurements

The catalytic activity measurements were carried out in a quartz tubular fixed bed reactor (i.d 30 mm). The composition of the feed was 500 ppm NO, 500 ppm $NH_3$ with varying the oxygen concentration (2, 4, 6, 8, 10 and 15 % vol $O_2$). The $N_2$ being a carrier gas (total flow rate = 2000 mL $min^{-1}$). K-type thermocouples provided the exhaust temperature before the catalyst. The temperature of all gas lines was kept at 150°C.

The activity data were collected at different temperatures in the range 150-500°C, each temperature was maintained until steady-state conditions were reached. The NO and $NO_2$ concentrations in the inlet and outlet gases were measured continuously by mean of a Chemiluminescence detector CLD 700 EL ht. $NH_3$ and $N_2O$ were analysed with non-dispersive IR spectrometry with a Siemens Ultramat 5E and Binos 4b.1 devices, respectively. The results of the catalytic tests performed over $V_3$ and $V_8$ catalysts are shown in terms of $NO_x$ conversion $XNO_x$ = 1-([$NO_x$]out/[$NO_x$]in) and $N_2$ selectivity $SN_2$ = [$N_2$]/([$N_2$] + [$N_2O$]), respectively. The moles of $N_2$ were determined from the following atomic nitrogen balance:

$N_{2out}$ = $1/2$([$NO_x$]$_{in}$-[$NO_x$]$_{out}$) + $1/2$([$NH_3$]$_{in}$-$NH_3$]$_{out}$) - $N_2O_{out}$. All measurements were run in duplicates

## 3. RESULTS

### 3.1. Characteristics of the prepared catalysts

Table 1 shows that BET surface areas of both catalysts $V_3$ and $V_8$ decreased with increasing the calcination temperature, while the mean pore radius increased. The effect of calcination temperature was more pronounced with $V_8$ due to the high vanadia content.

X-ray analyses show that up to 600°C, $V_3$ catalyst was monophasic and only anatase polymorph was formed (Fig. 1a). At 700°C the rutile form was detected and the transformation was complete at 800°C. No $V_2O_5$ crystallites were formed at high calcination

temperatures, probably because vanadia was highly dispersed as isolated $VO_x$ species [7].

With the catalyst V8, rutile form of titania was detected at 600°C (58%) (Fig.1b) and weak peaks at $2\theta$ = 20.3-26.3 and 31.2° appeared revealing the formation of crystalline $V_2O_5$ on the catalyst surface. Over this temperature, crystallites of vanadia disappeared again suggesting the formation of a solid solution between vanadia and titania support [8].

### 3.2. Catalytic activity measurements

Activity measurements were carried out with the catalysts $V_3$ and $V_8$ calcined at 500°C for 2 hours. Their surface areas were respectively 77 and 22 $m^2$ $g^{-1}$ (Table 1). Preliminary reactions were carried out in the absence of oxygen over both catalysts (Fig. 2a-b). Low NO conversions were observed in temperature range [150-325°C]. Over 325°C, $NO_x$ conversions increased gradually with increasing temperature. The conversion of NO with $V_3$ was slightly higher than that with $V_8$ over the whole temperature range. Furthermore, differences were observed in the amounts of $N_2$ and $N_2O$ formed during the SCR reactions. In fact, higher amount of $N_2$ was produced in the presence of $V_3$ in temperature range [400-500°C] (not shown). In contrast, higher $N_2O$ amount was formed in the presence of $V_8$ in the whole temperature range (Fig. 3a-b). It was also observed that ammonia conversion was lower than that of NO in the whole temperature range in both cases (not shown).

The effect of oxygen concentration on the $NO_x$ conversion was also investigated in the temperature range [150-500°C] (Fig. 2 a - b).

$NO_x$ in diesel exhaust is usually composed of >90% NO. Therefore, the main reaction of SCR with ammonia will be:

$$4NH_3 + 4NO + O_2 \rightarrow 4N_2 + 6H_2O \quad (1)$$
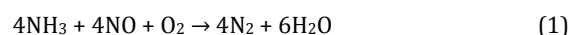
The reaction between NO and ammonia may also proceed in a different way, giving rise to the unwanted $N_2O$:

$$4NH_3 + 4NO + 3O_2 \rightarrow 4N_2O + 6H_2O \quad (2)$$
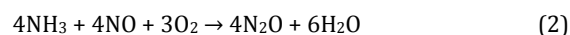
The presence of oxygen revealed in the interval of temperature [150-500°C] two quite distinct zones. In the first zone [150-250°C], the influence of the oxygen content was remarkable in the presence of both catalysts. Indeed, $NO_x$ conversion increased with the increase in the oxygen content and temperature. Catalyst V8 had the highest activity compared to $V_3$ in this temperature range.

In the second zone [250-500°C], the effect of $O_2$ was weak. We observed however, that with 2, 4 and 6 % $O_2$ in the presence of $V_3$, the $NO_x$ conversions were maintained at 100% in the temperature range [250-400°C] before decreasing. With 8, 10 and 15% $O_2$, $NO_x$ conversions were less than those observed at lower $O_2$ concentrations. At higher temperatures [400-500°C], the conversion of $NO_x$ in the presence of $V_3$ decreased slowly and reached 68% at 500°C regardless of the oxygen content.

**Table 1.** Morphological properties

| Catalyst | T (°C) | $S_g$ (m²/g) | Phase | $D_c$ (Å) | $V_p$ (cm³/g) | $rp_{exp}$ (Å) |
|---|---|---|---|---|---|---|
| | 400 | 115 | A | 265 | 0.336 | 16.6 |
| V3W9Ti | 500 | 77 | A | 319 | 0.289 | 20 |
| | 600 | 22 | A | 579 | 0.248 | 23.2 |
| | 800 | - | R | 783 | - | - |
| | 400 | 154 | A | 265 | 0.31 | 30 |
| V8W9Ti | 500 | 22 | A | 682 | 0.29 | 72 |
| | 600 | 14 | 43%A+57%R | 1068 | - | - |
| | 800 | - | - | - | - | - |





**Fig 2.** NOx conversion over V₃W₉Ti (a) and V₈W₉Ti (b) during the SCR reaction (Experimental conditions: catalyst weight: 200mg, flow rate: 2000 mL min⁻¹, feed: N₂ + 500 ppm NH₃ + 500 ppm NO, (2-4-6-8-10-15% volO₂))

**Fig 1.** X-ray powder diffraction patterns of (a) V3W9Ti and (b) V8W9Ti calcined from 400 to 800°C

In the presence of $V_8$, the maximum of $NO_x$ conversion was obtained in temperature range [250-350°C] with 2-4-6% $O_2$. With 15% $O_2$, the $NO_x$ conversion had the lowest value in temperature range [250-500°C]. The $NO_x$ conversion decreased abruptly over 375°C with all $O_2$ concentrations and reached negative values over 475°C due probably to ammonia oxidation which produced $NO_x$. With both catalysts, 6% $O_2$ seems to be the best $O_2$ concentration since a better stability in the results was observed in the whole temperature range.

The $N_2O$ production in the presence of $V_3$ during the SCR reaction started at 300°C (Fig. 3a). Its amount increased quickly with increasing temperature and decreased however with the increase in oxygen content. A total selectivity to $N_2$ in the presence of $V_3$ was observed in a large temperature range [150-300°C] and it decreased slowly starting from 325°C to reach values ranging between 60 and 70% at 500°C (not shown).

In the presence of $V_8$, the $N_2O$ was produced during the SCR reaction starting from 250°C (Fig. 3b) and reached a maximum at 450°C over which it decreased. This behaviour was not observed in the presence of $V_3$. The selectivity to $N_2$ was total up to 250°C over which it decreased reaching values ranging between 20 and 30 % at 500°C (not shown).

According to our experiments, $NO_2$ concentration increased with increasing $O_2$ content upstream the catalysts as shown in Table 2, which caused the increase in the SCR rate reaction in low temperature range. We can conclude that the presence of $NO_2$ in the inlet flow increased the catalytic activity of V-W-Ti catalysts.

At 15% $O_2$ the gas composition did not reach the equimolar composition between NO and $NO_2$ to be referred as "Fast SCR reaction". In automotive application 90~95% of the $NO_x$ in Diesel exhaust is NO and the fast SCR is promoted by an oxidizing catalyst upstream to the SCR catalyst that forms $NO_2$ to yield a near optimum of $NO/NO_2=1$ [9].

In our experiments, no oxidation catalyst was used and $NO_2$ was formed through the thermodynamic equilibrium which depends on the $O_2$ concentration and temperature:

$$NO + \tfrac{1}{2} O_2 \leftrightarrow NO2 \qquad (3)$$

### 3.3. Ammonia oxidation

For a better understanding of the side reactions, catalytic tests were also carried out in which the feed contained only $NH_3$ and $O_2$ under the same operation conditions as those conducted for the SCR reaction experiments.

The ammonia may be oxidized by oxygen instead of NO through one of the following ways:

$$2NH_3 + 3/2\ O_2 \rightarrow N_2 + 3H_2O \qquad (4)$$
$$2NH_3 + 2O_2 \rightarrow N_2O + 3H_2O \qquad (5)$$
$$2NH_3 + 5/2\ O_2 \rightarrow 2NO + 3H_2O \qquad (6)$$
$$4NH_3 + 7O_2 \rightarrow 4NO_2 + 6H_2O \qquad (7)$$
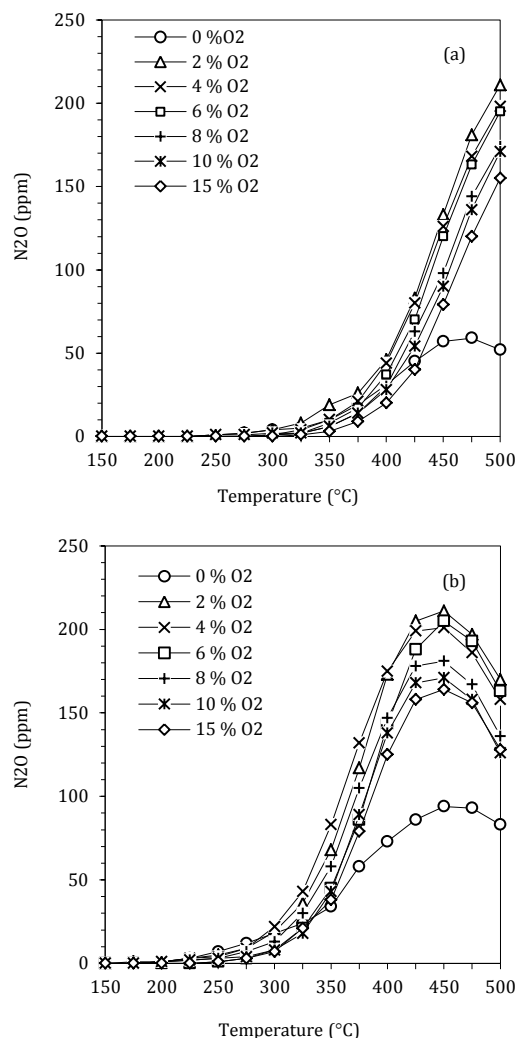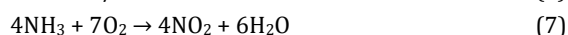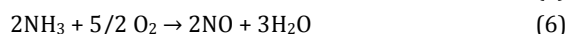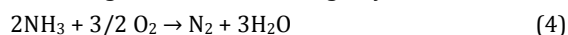




**Fig 3.** $N_2O$ formation during the SCR reaction over $V_3W_9Ti$ (a) and $V_8W_9Ti$ (b) (Experimental conditions: catalyst weight: 200mg, flow rate: 2000mL/min, feed: $N_2$ + 500 ppm $NH_3$ + 500 ppm NO, (2-4-6-8-10-15% vol $O_2$))

**Table 2.** Composition of $NO_x$ versus $O_2$ concentration

| Oxygen concentration | Composition of $NO_x$ (ppm) | Composition of $NO_x$ (%) |
|---|---|---|
| 0% vol | $500NO+0NO_2$ | $100\%NO+0\%NO_2$ |
| 2% vol | $460NO+40NO_2$ | $92\%NO+08\%NO_2$ |
| 4% vol | $420NO+80NO_2$ | $84\%NO+16\%NO_2$ |
| 6% vol | $400NO+100NO_2$ | $80\%NO+20\%NO_2$ |
| 8% vol | $375NO+125NO_2$ | $75\%NO+25\%NO_2$ |
| 10% vol | $360NO+140NO_2$ | $72\%NO+28\%NO_2$ |
| 15% vol | $310NO+190NO_2$ | $62\%NO+38\%NO_2$ |

In the presence of oxygen, the decrease in the ammonia concentration during its oxidation was observed over both catalysts. In the presence of $V_3$, ammonia oxidation started at 275°C producing only $N_2$ (Fig. 4a). The $N_2O$ was formed starting from 300°C (Fig. 4b) and increased gradually until 130 ppm at 500°C regardless of $O_2$ content. The production of NO was very weak and started at 450°C reaching a

maximum of 18 ppm at 500°C with 2% vol $O_2$ (Fig. 4c). NO formation of $NO_2$ was observed under our experimental conditions.







**Fig 4.** $N_2$ (a), $N_2O$ (b) and NO (c) formation during $NH_3$ oxidation over $V_3W_9Ti$ (Experimental conditions: catalyst weight: 200mg, flow rate: 2000mL/min, feed: $N_2$ + 500 ppm $NH_3$ + (2-4-6-8-10-15 % vol $O_2$))

Higher activity in $NH_3$ oxidation was achieved in the presence of $V_8$ with the formation of $N_2$, $N_2O$, NO and $NO_2$ (Fig. 5a-d). In fact, ammonia oxidation produced $N_2$ starting from 225°C (Fig. 5a) which quickly reached a first maximum at 350°C and decreased thereafter up to 425°C before increasing again. The formation of $N_2O$ started at 275°C and reached a maximum at 425°C coinciding with the minimum of $N_2$ produced (Fig. 5b). The formation of NO started at

375°C (Fig. 5c) and the amounts produced were more important than those of $N_2$ and $N_2O$ at higher temperatures. The formation of $NO_2$ was the last reaction to occur starting at 425°C (Fig. 5d). The oxidation of ammonia in the presence of $V_8$ gave all the products indicated by the thermodynamic namely $N_2$, $N_2O$, NO and $NO_2$ while $V_3$ produced only $N_2$, $N_2O$ and NO. This multitude of products formed with $V_8$ indicated a more active surface in the ammonia oxidation. It should be noticed that $O_2$ content affected slightly the amount of the products formed during ammonia oxidation in the presence of both catalysts on the contrary of its effect on the SCR reaction.

The amounts of $N_2O$ produced during the SCR reaction in the presence of both catalysts were slightly higher than those produced by the oxidation of ammonia. Comparing the $N_2O$ amounts formed during SCR reaction and ammonia oxidation with $V_3$ for example, shows that increasing $O_2$ content leads to increase the importance of ammonia oxidation in the $N_2O$ formation. In fact, with 2% $O_2$ at 450°C, 42% of the total $N_2O$ amount formed during the SCR reaction was due to the ammonia oxidation. This value increased with increasing oxygen concentration until reaching 100% with 8, 10 and 15% $O_2$ at the same temperature.

Thus, it can be concluded that the main $N_2O$ amount produced during the SCR reaction in the presence of both catalysts was due to ammonia oxidation (R5), the remainder $N_2O$ was produced by the secondary SCR reaction (R2).

### 3.4. TPD measurements

It is usually agreed that SCR activity is positively related to the surface acidity of the vanadia-based catalysts [9-11]. The acidic properties of the catalysts were evaluated by temperature programmed desorption of ammonia. TPD experiments were performed in situ with V3 and V8 with the same reactor used for the catalytic tests. Before the experiments, the samples were pre-treated with $N_2$ at 500°C for 1h to remove adsorbed $H_2O$ and other gases. After that the samples were cooled down to 50°C, the $N_2$ flow was switched to a flow of 500 ppm $NH_3/N_2$. When NDIR analysis showed that the concentration of $NH_3$ has stabilized, the reactor was then purged with $N_2$ for 1 h. The temperature was raised at 10°C/min to 500°C. The TPD profiles of ammonia on $V_3$ and $V_8$ are shown in figures 6a and 6b. Ammonia desorption was observed over a wide temperature range for $V_3$. Two main peaks were found at 105 °C (203 ppm) and 210°C (142 ppm). Ammonia profile with $V_8$ showed a predominant feature in the low temperature region with two maxima at 118°C (137 ppm) and 215°C (68 ppm). $NH_3$ desorption signal drops down after a shoulder-like feature around 286°C (23 ppm) but continued to show small quantities of $NH_3$ desorption at higher temperatures.

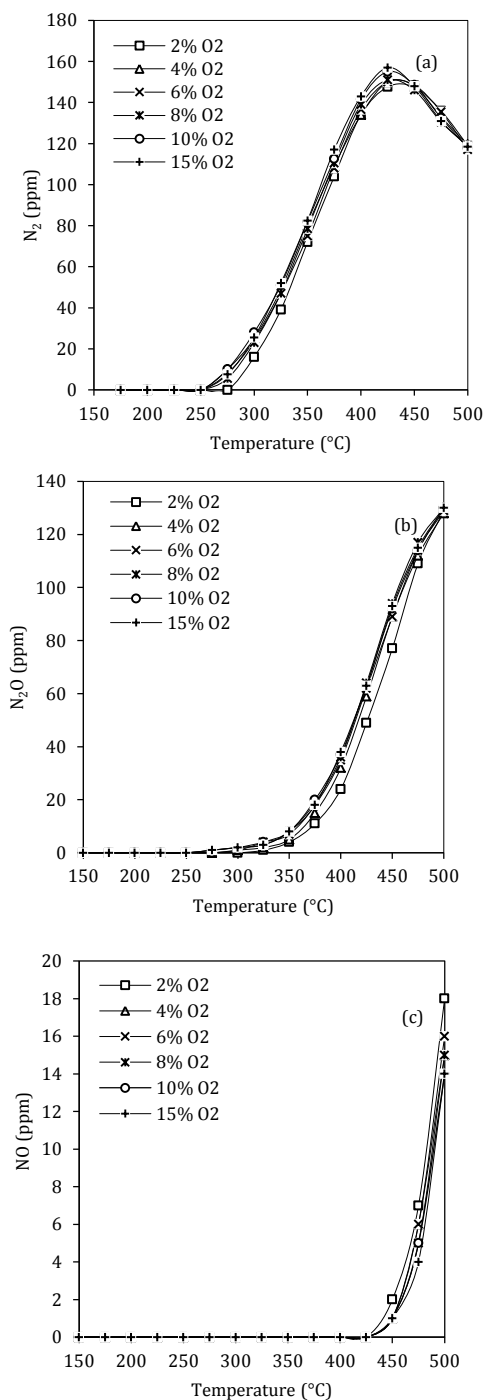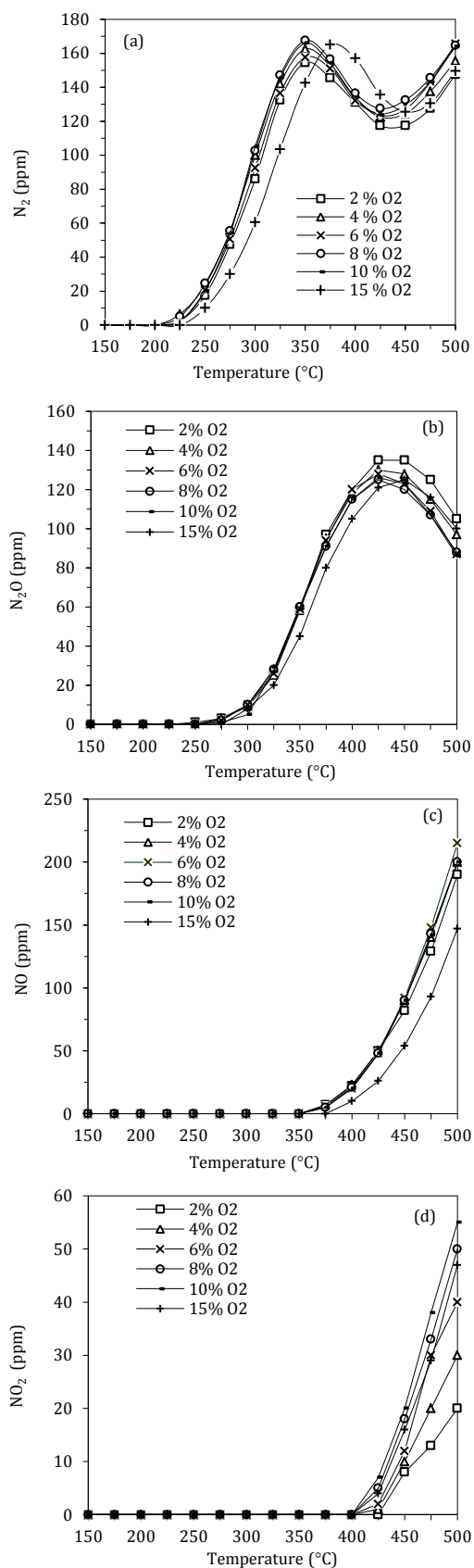**Fig 5.** $N_2$ (a), $N_2O$ (b), NO (c) and $NO_2$ (d) formation during $NH_3$ oxidation over V8W9Ti (Experimental conditions: catalyst weight: 200mg, flow rate: 2000 mL min$^{-1}$, feed: $N_2$ + 500 ppm $NH_3$ + (2-4-6-8-10-15 % vol $O_2$))

The amount of $NH_3$ desorbed from V8 was lower than that desorbed from V3. For both catalysts, the features

obtained from ammonia desorption indicated the presence of different types of adsorbed species.

The total amount of ammonia desorbed was calculated by integration of the areas under the curves in the temperature range between 50°C and 500°C. Higher amount of ammonia was desorbed from $V_3$ surface compared to that desorbed from $V_8$, but the amount of the desorbed ammonia per unit of surface area indicated that the density of acidic surface sites was significantly higher for V8 (8.43 μmole/m$^2$) compared to V3 (4.85 μmole/m$^2$).
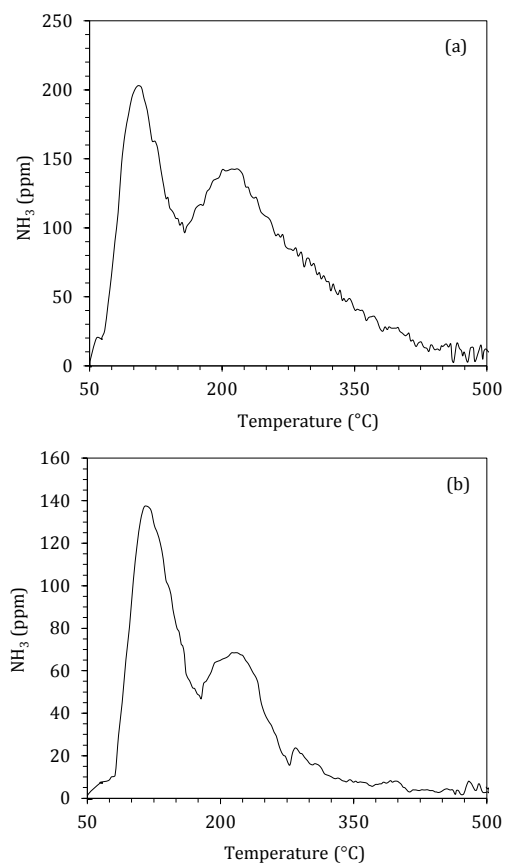


**Fig 6.** Temperature Program Desorption of ammonia for V3W9Ti (a) and V8W9Ti (b)

### 3.5. Aged samples

The catalysts V3 and V8 were calcined for 25 hours at 500°C to evaluate their durability. Activities (with 6% $O_2$ vol) in SCR reaction as well as the surface characteristics of these catalysts were evaluated after this treatment.

The specific surface area of aged V3 was 72 m$^2$/g with a multimodal pore distribution (rp=18-35-57-70Å) while that of fresh one was 77 m$^2$/g with a monomodal pore distribution (rp=20 Å) (not shown). The X-ray results did not show any rutile form of titania on the aged V3 (Fig. 7a), but an increase in the crystallinity was observed.

The aged V3 catalyst exhibited the same activity as that of the fresh one in temperature range [250-500°C] (Fig. 8a). In low temperature range, $NO_x$ conversion over the aged catalyst was slightly lower

than that of the fresh one. Higher amount of $N_2O$ was produced in the presence of aged V3 (not shown) but the difference remained slight. Thus, we can assume that a prolonged exposure of V3 to 500°C did not affect greatly the physicochemical characteristics of the catalyst. Aged V8 catalyst showed a decrease in the activity at low and high temperatures ranges compared to the fresh one (Fig. 8b). The same $NO_x$ conversion as that of fresh V8 was obtained in a tighter temperature range [250-350°C]. Higher amount of $N_2O$ was also formed compared with the fresh V8 (not shown). The specific surface area of aged V8 was 15 m²/g with a multimodal pore distribution (rp = 49-63-257Å).

As for V3, the X-ray analysis of aged V8 did not reveal traces of rutile but an increase in the crystallinity of the sample was also observed (Fig. 7b). Thus, a long exposure to 500°C affected more V8 than V3. The presence of high vanadia loading on V8 has probably accelerated the sintering process even there was no rutile form detected on the catalyst surface.
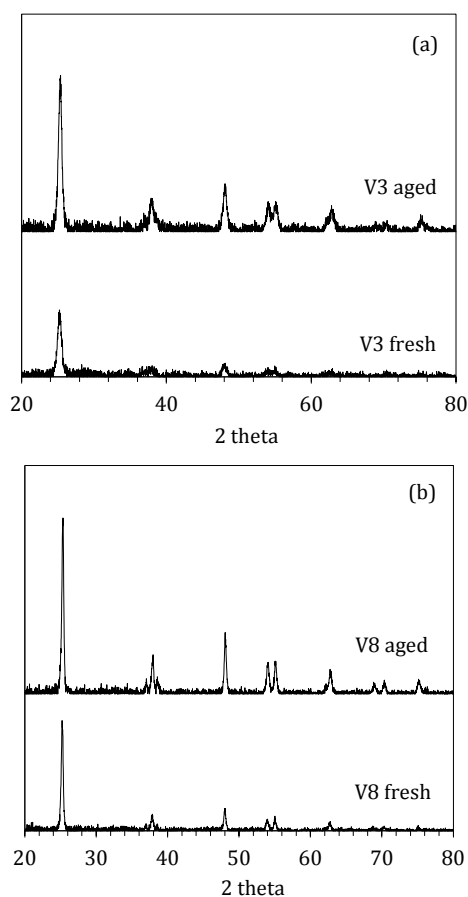


**Fig 7.** X-Ray analysis before and after aging the catalysts V3W9Ti (a) and V8W9Ti (b) at 500°C - 25 hours
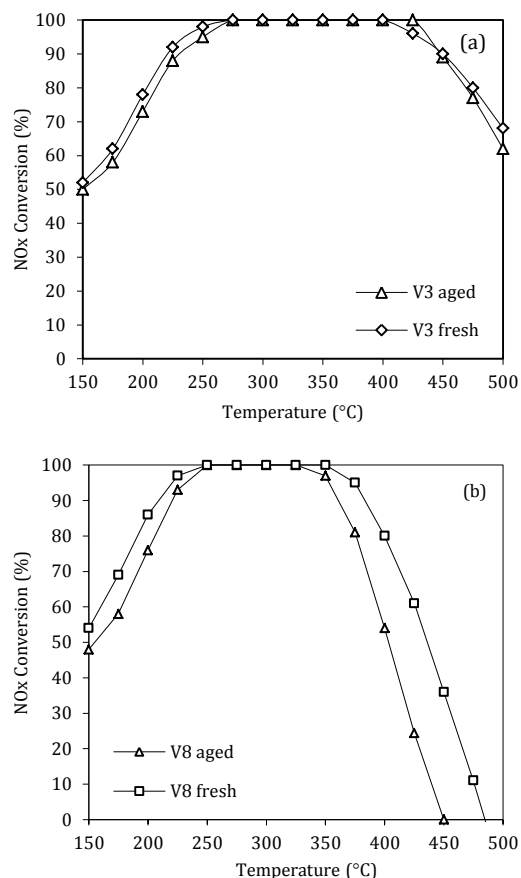


**Fig 8.** NOx conversion before and after aging the catalysts V3W9Ti (a) and V8W9Ti (b) at 500°C - 25 hours

## 4.  DISCUSSION

The conditions used for the preparation of V3 and V8 catalysts allowed the occurrence of the SCR reaction in the absence of oxygen but with lower rates and efficiencies compared to the reactions in the presence of $O_2$. The SCR reaction of NO was rarely elucidated with the mobility of oxygen and even less in case of the absence of gaseous oxygen. There is a report published by Garcia el al. [12] where they attribute the increase in SCR activity in the absence of gaseous oxygen to the mobility of the lattice oxygen, which promoted the oxidation of the reduced vanadium. Thus, the fact that the SCR reactions did not stop in the absence of oxygen in our case suggested that the surface of catalysts contained enough oxygen surface available for incorporation into the reactions and that the bridging oxygen species that link the vanadia or tungsta species to the surface or the units of vanadyl species to each other provided a continuing source of unlabeled oxygen to the surface leading to the reaction:

$$2NH_3 + 2NO + O_l \rightarrow 2N_2 + 3H_2O \qquad (8)$$
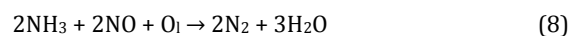
The fact that the NO conversions remained low (<20%) in temperature range [150-325°C] indicated that there was another kind of oxygen (lattice oxygen) that was involved in the SCR mechanism. Over 325°C, the SCR reaction may proceed without the need of

oxygen as reported by Lietti and Forzatti [13] to form $N_2$ and $N_2O$ as follows:

$$4NH_3 + 6NO \rightarrow 5\,N_2 + 6H_2O \qquad (9)$$

$$2NH_3 + 8NO \rightarrow 5N_2O + 3H_2O \qquad (10)$$
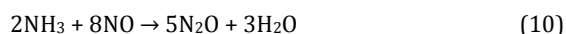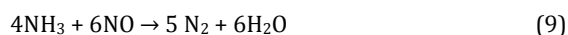
In fact, the authors reported that the SCR reaction in the absence of oxygen was observed above the temperature that roughly corresponded to the threshold of the reactions (9) and (10) at T≥300°C. Our results have shown differences between both catalysts in $N_2$ and $N_2O$ amounts formed during NO conversion in the absence of oxygen over 325°C. Furthermore, our TPD results showed strong acid strength of both catalysts favouring the adsorption of ammonia and its activation. This indicated that the surfaces participate to the reaction leading to different products as observed in our results.

Rosanska et al. [14] reported that $N_2O$ may reoxidize the reduced vanadyl groups and that it is a less effective oxidizing agent compared to gaseous oxygen. Thus, we can speculate that as the reaction (10) proceeded the produced $N_2O$ may reoxidize the reduced vanadium sites allowing the reaction (8) to occur in the same time of reactions (9) and (10). This can explain the increase in NO conversions observed over 325°C. In the presence of oxygen, the catalytic activity of V3 and V8 clearly increased with increasing $O_2$ concentration in temperature range [150-275°C]. Over 275°C the NOx conversion almost stabilized up to 425°C and decreased thereafter up to 500°C. The $O_2$ concentration of 6% registered higher $NO_x$ conversion with V3 and V8. The results indicated that the reaction mechanism included the oxidation of NO to $NO_2$ in gas phase. We have observed that the higher the $NO_2$ content in the feed gas, the faster was the SCR reaction. However, we do not know the mechanistic model of the primary reactions involved in the SCR reaction in our case. Despite its importance, there is no clear consensus in the literature on the details of the mechanism of $NO_x$ reduction with ammonia over vanadia based catalysts, nor other catalytic systems active in the SCR reaction. Many mechanistic studies have been proposed to explain the SCR model. All authors agree that oxygen is involved in the reoxidation of the catalyst, whereas different opinions are available concerning its interaction with the catalytic surface since the chemistry of the SCR reaction involving NO, $NH_3$ and $O_2$ at the interface of oxide materials is very complex [5].

Inomata et al. [15] and later agreed by most authors [16], concluded that on vanadia based catalysts, the ammonia reacts from a strongly adsorbed state while NO reacts from the gaseous or weakly adsorbed state. In our previous paper [6], we have studied the adsorption of NO over V3 catalyst. The exposed catalyst did not show DRIFT bands even after exposure to NO for 3 hours. The introduction of oxygen (6% vol) into the same flow gas caused the appearance of bands due to the adsorbed $NO_2$ [17-19]. Ammonia was also strongly adsorbed over V3 catalyst. Furthermore, TPD of NO conducted over V3 and V8 catalysts did not show any NO adsorption. These data allowed us to suggest that in our case, NO reacted in gaseous phase with adsorbed ammonia and

that $NO_2$ when present was effective in the SCR mechanism.

Koebel et al. [20] proposed a mechanism for the SCR reaction where $NO_2$ was involved in the reoxidation of the reduced sites of vanadia. They suggested that the $V^{4+}$ species formed during the reduction of NO with ammonia are reoxidized faster by $NO_2$ than by $O_2$:

$$2V^{4+}\text{-}OH + NO_2 \rightarrow 2V^{5+}=O + NO + H_2O \qquad (11)$$
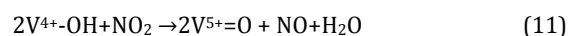
Resulting in an increased rate of the SCR reaction. NO formed from the reaction (11) reacted with $NH_3$ and $NO_2$ according to the following reaction:

$$4NH_3 + 2NO + 2NO_2 \rightarrow 4N_2 + 6H_2O \qquad (12)$$
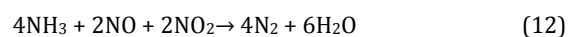
On the other hand, Tagaki et al. [21] suggested that NO-$NH_3$ reaction in the presence of oxygen over vanadia based catalyst proceeded via the two adsorbates, $NO_2$(ad) and $NH_4^+$(ad), which reacted through a Langmuir-Hinshelwood mechanism. Many different ways and reaction schemes are possible, in theory, to perform the reduction of $NO_x$ by ammonia in the presence of oxygen. In our case, we can suppose that the SCR reaction involved the preliminary oxidation of NO to $NO_2$ in gas phase (according to our results), and since there is adsorption of $NO_2$ on the active surfaces as shown in our previous paper [6], we think that in low temperature range, several reactions may occur such as :

- Adsorption of ammonia and its reaction with gaseous NO,
- Adsorption of $NO_2$ and its reaction with adsorbed ammonia,
- Reoxidation of reduced sites with $NO_2$ (the reoxidizing role of oxygen was substituted by $NO_2$ in this case considered as more effective than $O_2$).

With increasing the temperature, the thermodynamic equilibrium: NO + ½ $O_2$ ↔ $NO_2$ tends to left side. We can thus suppose that $NO_2/NO_x$ ratio decreased which implied that the SCR reaction evolved toward a limiting mechanism in which NO became a main reagent. The reoxidation of the active phase was then performed by gas phase oxygen instead of $NO_2$. Oxygen is known to be weaker oxidant than $NO_2$. Furthermore, there will be less adsorbed $NO_2$ reacting with the adsorbed ammonia. We do not know however, if this is the major reason for the decrease of the $NO_x$ conversion at higher temperature. A general relationship between the $NO_2$ content and the reaction rate was observed. Our point of view is that both mechanisms (Eley-Rideal and Langmuir-Hinshelwood) occurred under our reaction conditions, and that both mechanisms could be affected when the feed composition changed.

However, several details on the proposed reaction scheme are still to be better clarified. These aspects include the catalyst characterization, the nature of the active sites and of the active ammonia species.

It was shown by Myamoto et al. [22] that the V=O species of supported vanadia catalysts played an important role in the selective catalytic reduction of NO with ammonia. In the proposed mechanism, V=O is reduced to V-OH, which is then reoxidized by gaseous

oxygen. The oxidation of V-OH may be more important with $NO_2$ in our case. Srnak et al. [23] proposed that both reaction mechanisms could be valid, depending on the reaction conditions. On the other hand, Tuenter et al. [24] have shown that above approximately 0.5% vol oxygen, the reaction rate was almost independent of the oxygen concentration. However, in the present study, we have observed that the higher the $O_2$ concentration, the faster the SCR reaction in temperature range [150-275°C]. It is interesting to note that despite of the relatively low surface area of V8 ($22m^2/g$) comparatively to that of V3 ($77m^2/g$), its activity in $NO_x$ conversion was higher in temperature range [150-275°C]. Thus, a simple relation does not apparently exist between the surface area and the SCR activity. This is certainly due to the complexity of the surface with the simultaneous presence of several species of vanadia in V-W-Ti mixed oxides [25]. One can speculate that the presence of high vanadia content may reduce the $TiO_2$ surface area so that the vanadium coverage is eventually increased. This will favour the formation of polyvanadate species which are associated with superior redox properties [12, 26]. This was observed in case of V8. In fact, over 450°C the $NO_x$ conversion was negative indicating that ammonia oxidation into nitrogen oxides occurred on a very active surface. Low vanadia loading leads to well dispersion of vanadia on Ti support improving the selectivity towards $N_2$. It was reported that specific activity on polymeric vanadate species was 10-30 times larger than on monomeric vanadyl, and 5 times larger than on crystalline $V_2O_5$ [26-28]. Moreover, these structural properties depended on several factors namely: the amount of vanadia phase on the support, the surface area and nature of the support, the method adopted for the preparation of the catalyst, the nature of chemicals and thermal treatments of the catalyst.

The role of vanadia with different forms in the reaction, if actually existing, is still far from being completely clarified. Our results have also shown that increasing oxygen concentration did not affect the temperature at which the maximum of $NO_x$ conversion was attained in the presence of V3 and V8. In fact, lower than 275°C with V3 and 250°C with V8, $NO_x$ conversion was less than 100% even with high $O_2$ concentration (15%). This indicated that the effect of temperature on the $NO_x$ conversion was more important than $O_2$ content, since we could use 2% vol $O_2$ with V3 for example at 275°C to reach the same $NO_x$ conversion as with 15% $O_2$ at the same temperature. This effectively determines the maximum catalyst operating temperature and $O_2$ concentration.

Aging both catalysts did not have a great effect on their physico-chemical characteristics. This may be due to the sol-gel method used for the preparation of both catalysts which is known to improve the V-Ti interactions resulting in a general good behaviour of the catalysts in the NOx reduction.

## 5. CONCLUSION

The SCR reaction was influenced by vanadia content and gas composition. In our case, SCR reaction occurred in the absence of oxygen due to the superior redox properties of the catalysts that allow the reoxidation of the reduced sites of vanadium.

In the presence of oxygen, V8 was more active than V3 at temperatures lower than 250°C, whereas V3 had lower ammonia oxidation during SCR reaction and better $N_2$ selectivity.

The results have shown that NO was partially oxidized in feed gas by $O_2$ into $NO_2$. Increasing $O_2$ concentration led to increase the $NO_2$ content which enhanced the low temperature $NO_x$ reduction on V3 and V8 catalysts. However, once the maximum of $NO_x$ conversion was attained the effect of $O_2$ concentration was less effective. On the other hand, the sol gel method used for the preparation of both samples led to good stabilities for the aged catalysts.

## ACKNOWLEDGEMENT

## REFERENCES

[1]. J. Jiang and D. Li, "Theoretical analysis and experimental confirmation of exhaust temperature control for diesel vehicle $NO_x$ emissions reduction," *Applied Energy*, Vol. 174, pp. 232-244, 2016.

[2]. I. Nova and E. Tronconi (Eds.), "*Urea-SCR Technology for deNO$_x$ after treatment of diesel exhausts*," Springer, 2014.

[3]. A. Marberger, M. Elsener, D. Ferri and O. Kröcher, "$VO_x$ surface coverage optimization of $V_2O_5/WO_3$-$TiO_2$ SCR catalysts by variation of the V loading and by aging," *Catalysts,* Vol. 5, pp. 1704-1720, 2015.

[4]. C. Wang, S. Yang, H. Chang, Y. Peng, J. Li, "Dispersion of tungsten oxide on SCR performance of $V_2O_5WO_3/TiO_2$: Acidity, surface species and catalytic activity," *Chemical Engineering Journal,* Vol. 225, pp. 520-527, 2013.

[5]. L. Arnarson, H. Falsig, S. B. Rasmussen, J.V. Lauritsen and P.G. Moses, "The reaction mechanism for the SCR process on monomer $V^{5+}$ sites and the effect of modified Brønsted acidity," *Physical Chemistry Chemical Physics,* Vol. 18, pp. 17071-17080, 2016.

[6]. S. Djerad, M. Crocoll, S. Kureti, L. Tifouti and W. Weisweiler, "Effect of oxygen concentration on the NOx reduction with ammonia over $V_2O_5$–$WO_3/TiO_2$ catalyst," *Catalysis Today,* Vol. 113, pp. 208-214, 2006.

[7]. A. Marberger, D. Ferri, M. Elsener, A. Sagar, C. Artner, K. Schermanz and O. Kröcher, "Relationship between structures and activities of supported metal vanadates for the selective

catalytic reduction of NO by NH₃," *Applied Catalysis B: Environmental,* Vol. 218, pp. 731-742, 2017.

[8]. M.A. Banares, L. J. Alemany and M. Carmen Jimenez, "The role of vanadium oxide on the titania transformation under thermal treatments and surface vanadium states," *Journal of Solid State Chemistry,* Vol. 124, pp. 69-76, 1996.

[9]. L. Arnarson, H. Falsig, S.B. Rasmussen, J.V. Lauritsen, P.G. Moses, "A complete reaction mechanism for standard and fast selective catalytic reduction of nitrogen oxides on low coverage VO$_x$/TiO$_2$(001) catalysts," *Journal of Catalysis,* Vol. 346, pp. 188–197, 2017.

[10]. H. Schneider, S. Tsuchudin, M. Schneider, A. Wokaun, A. Baiker, "In situ diffuse reflectance FTIR study of the selective catalytic reduction of NO by NH₃ over vanadia-titania aerogels," *Journal of Catalysis,* Vol. 147, pp. 5-14, 1994.

[11]. M.A. Centeno, I. Carrizosa, J. A. Odriozola, "In situ DRIFTS study of the SCR reaction of NO with NH₃ in the presence of O₂ over lanthanide doped V₂O₅/Al₂O₃ catalysts," *Applied Catalysis B*, Vol. 19, pp. 67-73, 1998.

[12]. E. Garcia-Bordejé, J. L. Pinilla, M. J. Làzaro, R. Moliner, J. L. G. Fierro, "Role of sulphates on the mechanism of NH₃-SCR of NO at low temperatures over presulphated vanadium supported on carbon-coated monoliths," *Journal of Catalysis*, Vol. 233, pp. 166-175, 2005.

[13]. L. Lietti, P. Forzatti, "Temperature programmed desorption/reaction of ammonia over V₂O₅/TiO₂ De-NOxing catalysts," *Journal of Catalysis,* Vol. 147, pp. 241-249, 1994.

[14]. X. Rosanska, E. V. Kondratenko, J. Sauer, "Oxidative dehydrogenation of propane: Differences between N₂O and O₂ in the reoxidation of reduced vanadia sites and consequences for selectivity," *Journal of Catalysis,* Vol. 256, pp. 84-94, 2008.

[15]. M. Inomata, A. Miyamoto, Y. Murakami, "Mechanism of the reaction of NO and NH₃ on vanadium oxide catalyst in the presence of oxygen under the dilute gas condition," *Journal of Catalysis*, Vol. 62, pp. 140-148, 1980.

[16]. G. Busca, L. Lietti, G. Ramis and F. Berti, "Chemical and mechanistic aspects of the selective catalytic reduction of NO$_x$ by ammonia over oxide catalysts: A review," *Applied Catalysis,* Vol. 18, pp. 1-36, 1998.

[17]. G. Ramis, G. Busca, V. Lorenzelli, P. Forzatti, "Fourier transform-infrared study of the adsorption and coadsorption of nitric oxide, nitrogen dioxide and ammonia on vanadia-titania and mechanism of selective catalytic reduction," *Applied Catalysis,* Vol. 64, pp. 259-278, 1990.

[18]. T. J. Dines, C. H. Rochester, A. M. Ward, "Infrared study of the reaction between nitrogen oxides and ammonia on titania-supported vanadia catalysts," *Journal of the Chemical Society, Faraday Transactions,* Vol. 87, pp. 1473-1477, 1991.

[19]. M. Hesse, H. Meier, B. Zeeh, "*Spektroskopische methoden in den organischen chemie,*" Georg Thieme Verlag, Stuttgart, New York, 1995.

[20]. M. Koebel, G. Madia, F. Raimondi, A. Wokaun, "Enhanced Reoxidation of Vanadia by NO₂ in the Fast SCR Reaction," *Journal of Catalysis*, Vol. 209, pp. 159-165, 2002.

[21]. M. Tagaki, T. Kowai, M. Soma, T. Onishi, K. Tamaru, "The mechanism of the reaction between NO$_x$ and NH₃ on V₂O₅ in the presence of oxygen," *Journal of Catalysis*, Vol. 50, pp. 441-446, 1977.

[22]. [22] A. Miyamoto, K. Kobayashi, M. Inomata, Y. Murakami, "Nitrogen-15 tracer investigation of the mechanism of the reaction of nitric oxide with ammonia on vanadium oxide catalysts," *The Journal of Physical Chemistry*, Vol. 86, pp. 2945-2950, 1982.

[23]. T. Z. Srnak, J. A. Dumesic, B. S. Clausen, E. Tornquist, N. Y. Topsoe, "Temperature-programmed desorption/reaction and in situ spectroscopic studies of vanadia/titania for catalytic reduction of nitric oxide," *Journal of Catalysis,* Vol. 135, pp. 246-262, 1992.

[24]. G. Tuenter, W. F. Van Leewen, L. J. M. Snepvangers, "Kinetics and mechanism of the NO$_x$ reduction with NH₃ on V₂O₅- WO₃-TiO₂ Catalyst," *Industrial & Engineering Chemistry Product Reseacrh and Development,* Vol. 25, pp. 633-636, 1986.

[25]. L. Arnarson, S. B. Rasmussen, H. Falsig, J. V Lauritsen and P. G. Moses, "Coexistence of square pyramidal structures of oxo vanadium (+5) and (+4) species over low-coverage VOX/TiO₂ (101) and (001) anatase catalysts," *Journal of Physical Chemistry C.,* Vol. 119, pp. 23445–23452, 2015.

[26]. G. T. Went, L. J. Rosin, R. R, A. T. Bell, "The effects of structure on the catalytic activity and selectivity of V₂O₅/TiO₂ for the reduction of NO by NH3," *Journal of Catalysis,* 134, 492-505, 1992.

[27]. A. Baiker, P. Dollenmeier, M. Glinski, A. Reller, "Selective catalytic reduction of nitric oxide with ammonia: I. monolayer and multilayers of vanadia supported on titania," *Applied Catalysis,* Vol. 35, pp. 351-364, 1987.

[28]. W. J. Stark, K. Wegner, S. E. Pratsinis, A. Baiker, "Flame aerosol synthesis of vanadia–titania nanoparticles: structural and catalytic properties in the selective catalytic reduction of NO by NH₃," *Journal of Catalysis,* Vol. 197, pp. 182-191, 2001.

Turkish
JournalPark
ACADEMIC

Environmental Research & Technology

http://dergipark.gov.tr/ert

RESEARCH ARTICLE

# Straightforward assessment of horizontal leachate injection system using frequency domain electromagnetic induction method

Rémi Clément[1,*], Marine Audebert [2], Simon Loisel[3], Sylvain Moreau [2]

[1]Irstea, UR REVERSAAL, centre de Lyon-Villeurbanne, 5 rue de la Doua CS 20244, 69625, Villeurbanne, FRANCE
[2]Irstea, Hydrosystems and Bioprocesses Research Unit, 1 rue Pierre-Gilles de Gennes, CS10030, 92161 Antony, FRANCE
[3]SAS Les Champs Jouault, Lieu-dit Les Champs Jouault, 50670 Cuves, France, 92161 Antony, FRANCE

## ABSTRACT

In municipal solid waste landfills operating as bioreactor process, leachate recirculation is the key process for increasing moisture content in order to optimize the waste biodegradation. Given that liquid flows exhibit a complex behaviour in very heterogeneous porous media, in situ monitoring methods are required to assess horizontal leachate injection system. Among the physical measurements available, the authors propose a prompt geophysical investigation using Frequency Domain Electromagnetic Method (FDEM). During leachate injection event, this technique highlights changes in electrical conductivity of the waste deposit cell induced by variations of water content. Measurement procedure and preliminary monitoring results are presented applied to a waste deposit cell operated as a bioreactor. First results suggest that this technique is suitable for a quick assessment of horizontal leachate injection systems at industrial scale.

*Keywords:* Geophysics, leachate recirculation, frequency domain electromagnetic method, bioreactor

## 1. INTRODUCTION

The concept of bioreactor landfill is studied and tested since 1970 in the US and for more than two decades in Europe. This technology aims at enhancing the waste biodegradation in municipal solid waste landfills (MSWL) by optimising water content. Many studies have pointed out the potential benefits of the bioreactor approach: for example, (i) a quicker stabilization of organic matter can be achieved [1] and (ii) the rate of biogas production goes up inducing a more efficient energy recovery. In situ operation of a bioreactor landfill requires a  monitoring and control of the operating parameters [2]. The anaerobic methanogenesis is enhanced by a high water content that can only be reached by adding leachate to waste [3]. Indeed, after waste deposit cell closure, the waste mass is generally too dry to insure an optimal biodegradation and leachate recirculation appears as a solution. Different methods of water measurements in landfills are available and some of them were presented by Imhoff [4]. However, the optimization of leachate injection systems is a particular case which remains a challenge for bioreactor landfill operators.

In the literature, many studies deal with the assessment of leachate injection system using geophysical method [5-9]. Among them, Electrical Resistivity Tomography (ERT) has been widely used for leachate injection monitoring because the electrical resistivity is very sensitive to the water content variation. This method provides 2D or 3D electrical resistivity distribution and can be employed in time-lapse mode to study the infiltration dynamics. However, ERT is rarely used by the landfill operators because implementation of electrodes measurement needs to be located in contact with waste mass under the geomembrane cover. Post-processing numerical tools are also complex to obtain the electrical resistivity distribution [10, 11]. Moreover, recent papers have shown electrical resistivity distribution plenty of artefacts where no changes are expected, leading to false interpretations of the ERT results [5], [12-14]. Industrial community requires an easier method without contact and complex post-processing analysis to investigate the first 4-5 meters of waste mass. Frequency Domain Electromagnetic Method (FDEM) is a popular geophysical method widely used for soil surveying, which has been outlined by McNeill [15]. This method is based on the electrical

conductivity (in S.m$^{-1}$) measurement (inverse of electrical resistivity in ohm.m). FDEM seems well adapted to focus on leachate diffusion, very conductive (5-10 mS/cm), compared to the waste mass less conductive , comprised between 0.1 and 2 mS cm$^{-1}$ [16-20]. No article describes the validity of the FDEM method to assess the leachate injection systems and this paper demonstrates its relevance in delimiting the lateral extent of the infiltration zone at the industrial scale.

## 2. MATERIALS AND METHODS

### 2.1. Experimental site description

The experimental landfill site is located in Cuves, France, (e.g. Fig 1-a and b) and is managed by the company SAS Les Champs Jouault. It is a non-hazardous municipal waste landfill fully operated as a bioreactor. The waste deposit cell spreads across more than 5000 m², 100 m long, 50 m wide, 15 m at its maximum height and approximatively 65,000 t of household waste were landfilled (e.g. Fig 1-c). The layering structure of the MSWL cell consists in a 1-m soil cover overlaying a layer of waste for a total thickness up 10–15 m. The bottom of the MSWL cells consists in a 0.5 m layer of granular drainage materials (e.g. Fig 1-c) and the whole cell is lined by a double seal barrier: a passive one composed by a clay layer (e.g. Fig 1-d) and an active one using HDPE geomembranes. The waste deposit cell is composed by a drainage system at the bottom, biogas extraction system into the waste mass and biogas and leachate mixed landfill horizontal trenches installed at the top of the cell (e.g. Fig 1-d). Biogas extraction is performed continuously using pumping systems which keep the waste deposit cell in depression. Then biogas is conducted to a biogas valorisation system. At the bottom of the waste deposit cell, a pumping system is switched on periodically (or automatically when the leachate level exceeds a level of 30 cm) and discharges the leachate to the storage tank. The study is managed in the waste deposit cell 4 operated between September 2011 and July 2012 (e.g. Fig 1-b).

### 2.2. Leachate injection monitoring using FDEM

FDEM profiling has been widely used for environmental surveying [21-23] and many devices are available for electrical conductivity measurements. In our study, the EM31 (Geonics Ltd) was chosen to study leachate infiltration. Basically, EM31 device generates a primary electromagnetic field in the first coil named Transmitter coil (at frequency of 9800 Hz, e.g. Fig 2), which induces electrical currents in the soil with the same frequency. These currents generate a secondary electromagnetic field, which is monitored by the receiver coil. Under known conditions as "low induction numbers EM condition", the secondary field is proportional to the ground current and is used to compute the electrical conductivity for the volume of soil profiled [22, 24]. In theory, the investigation depth is linked to the distance between the transmitter and the receiver (Tx–Rx) and the coil orientations used (vertical or

horizontal dipole). The EM31 device has a fix horizontal coil spacing of 3.66 m which provides an investigation between 3 to 5 m deep.
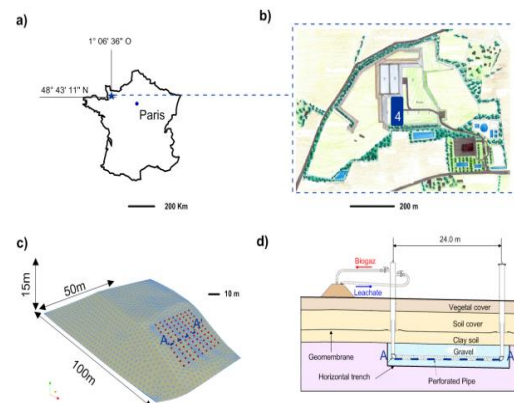


**Fig 1.** (a) Location (b) industrial site description (c) geometry of experimental waste deposit cell, location of FDEM measurement (red point) and perforated pipe (AA') (d) mixed horizontal trenches for biogas collection and leachate injection

Electromagnetic measurement was performed at the surface of the waste deposit cell (e.g. Fig 1-c), during leachate injection event: 87 m³ were injected in 7 hours using the leachate injection system shown in Fig 1-d. Different locations were necessary to map the resistivity measurements recorded by EM equipment (following the numeration of each station - Fig 2-b). One of the problems is to move the equipment to the same plots for each sequence during leachate injection monitoring. To achieve our measurements, we followed this procedure: (i) we calibrated the device according to the manufacturer's recommendations described here (http://www.geonics.com/), (ii) we chose to acquire a sequence of 99 fixed stations around the perforated pipe every 30 min (e.g. Fig 2-b), (iii) we always kept the same orientation coils (transmitter in the East and receiver in the West) and (iv) the FDEM device position was always parallel to the ground. The 99 points were required 12 min.
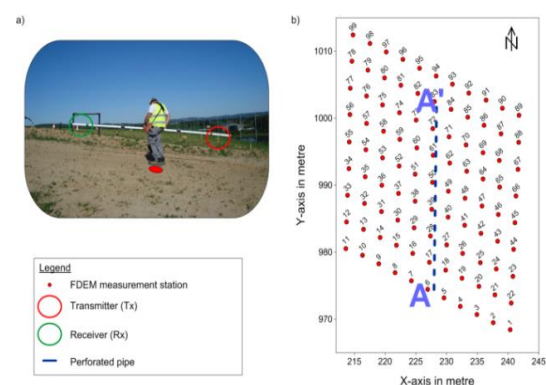


**Fig 2.** a) FDEM equipment during prospection b) location of FDEM fixes stations and acquisition sequence

## 3.  RESULTS & DISCUSSION

Fig 3 presents the resistivity value ρa0 (inverse of the conductivity, in ohm.m), measured by the EM31 device before starting the infiltration. The injection system is symbolized by a blue line (from A to A') and is located at the position X of 227 m. The resistivity values are comprised between 6 and 11 ohm.m with an increase of up to 14 ohm.m at the end of injection pipe.
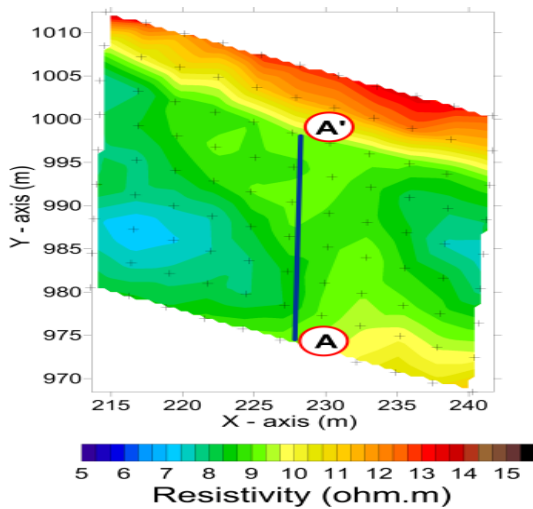


**Fig 3.** Map representing the resistivity values (in ohm.m) recorded before infiltration

Fig 4 shows electrical resistivity variations $\Delta\rho_a$ for ten time steps (a to j) recorded before, during and after the leachate injection and expressed as follows:

$$\Delta\rho_a = \left[\frac{\rho_{at}}{\rho_{a0}} - 1\right] \times 100 \qquad (1)$$

where $\rho_{at}$ and $\rho_{a0}$ (in mS m$^{-1}$) are the apparent electrical resistivity of the data sets at time t and of the initial data sets at t0, respectively. Each electrical resistivity variation map has been plotted using Kriging interpolation method. To assess the measurement noise linked to the geophysical device used and to the environment around the waste mass studied, three acquisitions were carried out before infiltration where no resistivity changes are expected (e.g. Fig 4 – a and b).

For all the points on the field, $\Delta\rho_a$ values were calculated before recirculation and varied between 0 and 7%. It corresponds to a classical variation range of $\Delta\rho_a$ observed on the field for this kind of geophysical survey and allowed us to consider only the variations higher than 7% as reliable.

During the injection event, we can observe a decrease in resistivity around the leachate pipe and for each time step (e.g. Fig 4 – c to h). This area corresponds to the leachate infiltration and is delimited by a black line (corresponding to the non-reliable variation range of -7%). Between the third and the eighth time step (respectively 30 min and 7 h after the beginning of the injection), the size of this area increases and the variation in resistivity is comprised between -7 and -25%. At each time step, the resistivity variation is

increasingly lower. Eight hours after the beginning, the leachate injection was stopped. For the two last maps (e.g. Fig 4 - i and j), we can observe that the size of the infiltration area decreases compared to the previous steps. Moreover, the resistivity variation increases with a variation range comprised between -7 and -16% for the ninth step (e.g. Fig 4 – i) and between -7 and -13 % for the tenth step (e.g. Fig 4 – j). These electromagnetic measurements of electrical resistivity variations are in accordance to the physical process studied: the size of the infiltration area increases during the leachate injection and decreases just after the end of injection.

According to these results linked to the hydraulic conditions tested, we can assess approximatively the maximum lateral extent of the infiltration area which goes from 220 m to 237 m, corresponding to 7 m on the left of the injection system and to 10 m on its right. Due to the slope of the waste deposit cell (e.g. Fig 1-c); it makes sense that the infiltration is larger on the right of the injection system than on the left. We can also observe that the vertical extent of the infiltration area does not exceed the length of the injection system.

Thus, this result on the horizontal infiltration area can help landfill operators to assess their injection system. For example, different flow rates can be tested to calculate distance between each injection system to avoid location without injection impact or location wetted by two leachate pipes.
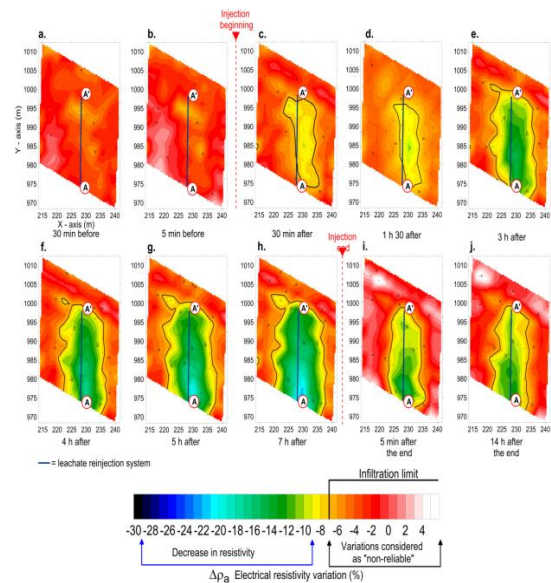


**Fig 4.** 10 maps of electrical resistivity variations during 10 h of leachate injection

## 4.  CONCLUSIONS

Through this short paper, the authors showed the ability to use the FDEM for assessing leachate injection systems. The FDEM is a fast acquisition and non-intrusive method without contact and complex data post-processing. With the suggested protocol used, the authors have shown that it is possible to monitor the evolution of the electrical resistivity of

*Clément et al.*

waste mass linked with the variation of the water content and conductivity of the injected leachate. They estimated lateral propagation of the infiltration in the upper horizon layer of the waste deposit cell (0-5m with depth investigation of selected equipment) and can concluded on the injection system efficiency. The company SAS Les Champs Jouault will use this device for assessment of their injection systems to check their functioning. Equipment used in this study does not allow a deeper investigation?, and consequently are not adapted to study large industrial sites. For larger sites, new equipment has been recently developed and allows deeper exploration. These results open new perspectives for industrial application of the FDEM; however, to refine the lateral position of the leachate infiltration, work on the analysis of the FDEM sensitivity with different equipment and exploration depth will be required.

## ACKNOWLEDGEMENT

## REFERENCES

[1]. J. Pacey, D.R. Reinhart, D.L. Hansen, G.T. Townsend, and W. H. Johnson, "Landfill bioreactor – an innovation in solid waste management," *in 22nd Annual LFG Symposium.*, 1999.

[2]. D.R. Reinhart and T.G. Townsend, Landfill Bioreactor Design & Operation. New York, USA: Lewis Publishers, 1998.

[3]. D.R. Reinhart and A.B. AlYousfi, "The impact of leachate recirculation on municipal solid waste landfill operating characteristics," *Waste Management & Resource.* Vol. 14 (4), pp. 337–346, 1996.

[4]. P.T. Imhoff, D.R. Reinhart, M. Englund, R. Guérin, N. Gawande, B. Han, S. Jonnalagadda, T.G. Townsend, and R. Yazdani, "Review of state of the art methods for measuring water in landfills," *Waste Management,* Vol. 27 (6), pp. 729–745, 2007.

[5]. R. Clément, M. Descloitres, T. Günther, L. Oxarango, C. Morra, J.P. Laurent, and J.P. Gourc, "Improvement of electrical resistivity tomography for leachate injection monitoring," *Waste Management,* Vol. 30 (3), pp. 452–464, 2010.

[6]. R. Clément, L. Oxarango, and M. Descloitres, "Contribution of 3-D time-lapse ERT to the study of leachate recirculation in a landfill," *Waste Management*, Vol. 31 (3), pp. 457–467, 2011.

[7]. R. Guérin, M. L. Munoz, C. Aran, C. Laperrelle, M. Hidra, E. Drouart, and S. Grellier, "Leachate recirculation: moisture content assessment by

means of a geophysical technique," *Waste Management,* Vol. 24 (8), pp. 785–794, 2004.

[8]. H. Rosqvist, T. Dahlin, and C. Lenhé, "Investigation of water flow in a bioractor landfill using geoelectrical imaging techniques," *in tenth International Waste Management and landfill Symposium,* 2005.

[9]. M. Audebert, R. Clément, J. Grossin-Debattista, T. Günther, N. Touze-Foltz, and S. Moreau, "Influence of the geomembrane on time-lapse ERT measurements for leachate injection monitoring.," *Waste Management*, Vol. 34 (4), pp. 780–790, 2014.

[10]. T. Günther, C. Rücker, and K. Spitzer, "Three-dimensional modelling and inversion of dc resistivity data incorporating topography – II. Inversion," *Geophysical Journal International,* Vol. 166 (2), pp. 506–517, 2006.

[11]. M. H. Loke, J. E. Chambers, D. F. Rucker, O. Kuras, and P. B. Wilkinson, "Recent developments in the direct-current geoelectrical imaging method," *Journal of Applied Geophysics,* Vol. 95, pp. 135–156, 2013.

[12]. R. Clement, M. Descloitres, T. Gunther, O. Ribolzi, and A. Legchenko, "Influence of shallow infiltration on time-lapse ERT: Experience of advanced interpretation," *Comptes Rendus Geoscience,* Vol. 341 (10–11), pp. 886–898, 2009.

[13]. K. Singha and S. M. Gorelick, "Saline tracer visualized with three-dimensional electrical resistivity tomography: Field-scale spatial moment analysis," *Water Resources Research*, Vol. 41 (5), 2005.

[14]. M. Descloitres, J. P. Laurent, C. Morra, R. Clément, L. Oxarango, and J.P. Gourc, "Monitoring resistivity in non-hazardous waste landfill using Time Domain Electromagnetism (Drôme, France)," *in International Conference EAGE "Near Surface 2008,"* 2008.

[15]. D.J. McNeill, Electromagnetic terrain conductivity measurements at low induction numbers. GEONICS, Technical Note TN-6. [Online]. Available: www.geonics.com, 1980.

[16]. I. San and T. T. Onay, "Impact of various leachate recirculation regimes on municipal solid waste degradation," *Journal of Hazardous Materials.* Vol. 87 (1–3), pp. 259–271, 2001.

[17]. B. Olofsson, H. Jernberg, and A. Rosenqvist, "Tracing leachates at waste sites using geophysical and geochemical modelling," *Environmental Geology,* Vol. 49 (5), pp. 720–732, 2006.

[18]. Q.Y. Zhou, C.P. Ling, J.G. Liu, Y.W. Xue, R.Li, and Y. Y. Zhang, "The electrical resistivity tomography for column bioreactor ," *3rd International Conference o3rd International Conference on Engineering for Waste and Biomass Valorisationn Engineering for Waste and Biomass Valorisation*, May 17-19, 2010, 2010.

[19]. S. Grellier, R. Guérin, H. Robain, A. Bobachev, F. Vermeersch, and A. Tabbagh, "Monitoring of Leachate Recirculation in a Bioreactor Landfill by 2-D Electrical Resistivity Imaging," *Journal of*

*Environmental Engineering and Geophysics,* Vol. 13 (4), pp. 351–359, 2008.

[20]. S. Moreau, F. Ripaud, F. Saidi, and J.-M. Bouyé, "Laboratory test to study waste moisture from resistivity," *Proc. ICE - Waste Resour. Manag.* Vol. 164 (1), pp. 17–30, 2011.

[21]. D. C. Nobes, M. J. Armstrong, and M. E. Close, "Delineation of a landfill leachate plume and flow channels in coastal sands near Christchurch, New Zealand, using a shallow electromagnetic survey method," *Hydrogeology Journal,* Vol. 8 (3), pp. 328–336, 2000.

[22]. J. A. Doolittle and E. C. Brevik, "The use of electromagnetic induction techniques in soils studies," *Geoderma,* Vol. 223–225, pp. 33–45, 2014.

[23]. D. V Fitterman and M. T. Stewart, "Transient electromagnetic sounding for groundwater," *Geophysics,* Vol. 51 (4), pp. 995–1005, 1986.

[24]. W. M. Telford, L. P. Geldart, and R. E. Sheriff, Applied Geophysics, 2nd Edition. Cambridge University Press, 1990.

Turkish **JournalPark**
ACADEMIC

# Environmental Research & Technology

http://dergipark.gov.tr/ert

**RESEARCH ARTICLE**

# Simplified method for derivatization of extractable glyphosate and aminomethylphosphonic acid and their determination by high performance liquid chromatography

Jamilu Garba[1], Abd Wahid Samsuri [2,*], Radziah Othman[2], Muhammad Saiful Ahmad Hamdani[3]

[1]Zamfara State College of Education, Department of Agricultural Education, 1002 Maru, Zamfara, NIGERIA
[2]Department of Land Management, Faculty of Agriculture, Universiti Putra Malaysia, 43400 UPM Serdang, Selangor, MALAYSIA
[3]Department of Crop Science, Faculty of Agriculture, Universiti Putra Malaysia, 43400 UPM Serdang, Selangor, MALAYSIA

## ABSTRACT

This work presents a simple procedure for pre-column derivatization of glyphosate and aminomethylphosphonic acid (AMPA) and their determination by high-performance liquid chromatography (HPLC). Derivatization was achieved by mixing a solution of 0.02 M FMOC-Cl, 0.05 M borate buffer and glyphosate or AMPA, then shaken for 1 hour, later washed with diethyl ether and ready for analysis. The quantification was performed by HPLC with fluorescent (FLD) or diode array detector (DAD). The result of the HPLC-FLD/DAD showed high linearity ($R^2 \geq 0.995$) of both compounds over eight point's concentration range and their high recovery from water compared to soil matrixes. The relative standard deviation (RSD) range from 0.1 to 30 % from the aforementioned matrixes. The limit of detection of HPLC-FLD for glyphosate from water, sandy and clay soil was 0.008 mg L$^{-1}$, 0.021 and 0.132 mg kg$^{-1}$ respectively while that of AMPA was 0.004 mg L$^{-1}$, 0.74 and 0.224 mg kg$^{-1}$. Meanwhile, the limit of detection of HPLC-DAD for glyphosate from water, sandy and clay soils was 0.024 mg L$^{-1}$, 0.731 and 0.122 mg kg$^{-1}$ respectively while that of AMPA for water sample was 0.076 mg L$^{-1}$. This study was unable to determine lower detection limit for AMPA from soil matrixes by HPLC-DAD thus suggested for more repeated extraction for increasing quantification of the compound.

*Keywords:* Glyphosate, aminomethylphosphonic acid, derivatization, analytical method, water, soil

## 1. INTRODUCTION

Glyphosate {N-(phosphonomethyl) glycine} is increasingly applied for weed control in agricultural and non-agricultural lands. The global estimate of application of glyphosate (GLY) active ingredient in 2014 was 8.2 million metric tons with the application rate of 2.13 and 1.94 kg ha$^{-1}$ to agricultural and non-agricultural lands respectively [1]. This amount was 0.2% higher than estimated amount applied in 2013. Glyphosate is foliage applied herbicide thus not active while in soil and is completely mineralized by microbes with aminomethylphosphonic acid (AMPA) as its major metabolite [2–4]. Glyphosate had high efficacy in weed control [5] also, its residual impact on soil and water is of great environmental concern. Glyphosate was therefore, reported to have negative effect on soil microbes [4, 6], aquatic habitat [7, 8] and numerous health consequences to humans [9, 10]. In

order to protect food contamination and health hazard, maximum GLY residue limit in food and water has been set up by various countries. For instance maximum acceptable limit of GLY in water was set as 0.7 and 0.28 mg L$^{-1}$ by US environmental protection agency and health Canada respectively [11]. Monitoring GLY residue is therefore, achieve through the development of analytical technique for its determination. There are different analytical techniques used in determination of GLY and AMPA however, gas and liquid chromatography are the most widely used. Unlike other organic herbicides, GLY and its metabolite have unique properties of insolubility in organic solvent but highly soluble in water [4]. Moreover, due to none possession of chromophores and fluorophores in the molecular structure of GLY and its metabolite [12], there is difficulty in their direct detection with gas or liquid chromatography. In gas or liquid chromatography, GLY analysis is usually

done after derivatization as it was reported to reduce polarity and its enhance volatility hence, easily detected when derivatized [13]. The feasible derivatization of GLY and AMPA in aqueous solution with requiring less or no sample pre-treatments coupled with compatibility of the derivatized sample with reverse-phase chromatographic separation makes liquid chromatography (LC) the preferred technique[14]. The GLY and AMPA are basically derivatized either by pre-column or post-column procedure. The pre-column is more preferred because it has fewer restrictions, easy in controlling reaction condition and can be perform manually because it does not require complicated equipment [15, 16].

Several reagents are used in pre-column derivatization of GLY and AMPA, however, 9-flourenyl methyl chloroformate (FMOC-Cl) is the most widely used reagent. It has the ability in reacting with both secondary and primary amino group of GLY and AMPA respectively[15]. The use of FMOC-Cl in pre-column derivatization of GLY and AMPA was pioneered by Moye and Boning [12]. The authors performed the reaction under aqueous alkaline condition thus, it achieved through addition of 0.01 M FMOC-Cl solution, 0.025 M sodium borate solution and acetone to the GLY and AMPA standard solutions. The mixture was incubated for 20 minutes at temperature of 23oC on a laboratory bench without shaking or stirring. Later the derivatives were washed with ethyl ether to remove the excess reagents then analysed using ion exchange chromatography. Several other methods were reported afterward, which optimized Moye and Boning work for better resolution and detection of these compounds. One of the earlier work stirred the mixture for 30 minutes and acidified it with 0.1N HCl. Then FMOC-GLY derivatives was extracted with ethyl acetate and dried using rotor-evaporator before analysis[17]. Druart and co-workers [18] derivatized GLY and AMPA with solution of FMOC-Cl in acetonitrile under alkaline condition through addition of 0.05 M borate buffer. The mixture later agitated with magnetic stirrer for 1 hour then washed with ethyl ether before analysis. Recently, Skeff and co-workers [19] derivatized GLY and AMPA with 1 mM solution of FMOC-Cl in acetonitrile and 0.07 M borate buffer through vigorous shaking for 4 hours at room temperature.

These differences in the derivatization process necessitates a continuous optimization on GLY and AMPA pre-column derivatization. On the other hand, some of the methods of GLY and AMPA analysis by LC employed pre-treatments for sample clean-up prior to derivatization. These includes solid phase extraction [20], ions exchange [21] and column coupling [22] which all require additional sophisticated and costly apparatus. The FMOC-GLY and AMPA can be separated and detected using LC with mass spectrometry, fluorescent or ultraviolet detector. Mass spectrometry gives better resolution and separation however, it has very complex operating procedure thus require high skill. Fluorescent detector is widely used due to its simplicity in operation. Even though, Franz and co-workers [4] reported that, FMOC derivatives of GLY and AMPA had both fluorescent and ultraviolet properties but still less attention is given to the use of ultraviolet

detector. It is of much interest therefore, to develop a method which is simple, sensitive and economically affordable for detection and quantification of GLY and AMPA in the environmental matrixes. In this study, our aim was to optimize FMOC-Cl pre-column derivatization of GLY and AMPA based on the previously reported studies, and to determine GLY and AMPA by LC with fluorescent and diode array detector (DAD).

## 2. MATERIAL AND METHODS

### 2.1. Chemicals

All the chemicals were of analytical grade unless otherwise stated and Millipore® Direct UV-Q water was used throughout in preparing solutions. Glyphosate (99.7%), AMPA (99%) and FMOC-Cl (97%) were purchased from Sigma Aldrich® (Seelze, Germany). Acetonitrile and diethyl ether were purchased from QREC®, Malaysia. Analytical reagent grade $CaCl_2$ and $KH_2PO_4$ were purchased from Emsure® Germany while $Na_2B_4O_7.10H_2O$ were purchased from Sigma Aldrich® (India). Stock solutions of GLY and AMPA (500 mg $L^{-1}$) and working standard were prepared Millipore water. A 0.05 M $Na_2B_4O_7.10H_2O$ (pH 9), 0.01 M and 0.05 M $KH_2PO_4$ solutions were prepared in Millipore water while 0.02 M FMOC-Cl was prepared in acetonitrile.

### 2.2. Instruments

The LC system Agilent 1100 series (Agilent Santa Clara, USA.) consisted of two detectors fluorescence (model G1321A) and DAD (model G1315B) detectors; it is equipped with a vacuum degasser (model G 1322A), quaternary pump of high pressure gradient (model G1311A), autosampler unit (model G1313A) and column compartment (model G1316A); all connected to Chemstat computer software. The analytical column was reverse-phase $C_{18}$ Agilent® Zorbax Eclipse plus (4.6 x 150mm, 5µm).

### 2.3. Determination of Glyphosate and AMPA by HPLC-FLD

In other to identify the peaks of GLY and AMPA, a blank Millipore water and samples containing 1 mg $L^{-1}$ of either GLY or AMPA standard solutions were derivatized and analysed. Afterwards, calibration curves were obtained by derivatization and analysis of samples containing GLY or AMPA solutions at 8 point different concentrations ranging between of 0 mg $L^{-1}$ and 2 mg $L^{-1}$. Later calibration curves of GLY or AMPA was plotted from the peak areas versus their respective concentration.

The extraction of GLY and AMPA from soil matrix was achieved through spiking 0.5 ml each of 1 mg $L^{-1}$ of GLY and AMPA in 2 grams of either clay or sandy soils which later followed addition of 20 ml 0.01 M $KH_2PO_4$ then the mixture was shaken on rotary shaker for 2 hours. After which it was centrifuged at 10000 rpm for 10 minutes and the supernatants were filtered

using 0.45 μm syringe filter and kept for derivatization.

### 2.4. Determination of Glyphosate and AMPA by HPLC-DAD

A blank Millipore water and samples containing 5 mg L$^{-1}$ of either GLY or AMPA standard solutions were derivatized and analysed for the identification of GLY and AMPA peaks. Later GLY or AMPA solution at 8 point different concentrations ranging between of 0 mg L$^{-1}$ and 40 mg L$^{-1}$ derivatized and analysed. This followed by plotting peak areas versus their respective concentration for the development of calibration curve.

A 0.5 ml each of 5 mg L$^{-1}$ solutions of GLY and AMPA was spiked in 2 grams of either clay or sandy soils weighed into 50 ml centrifuge tubes then added with 20 ml 0.01 M KH$_2$PO$_4$ and shake for 2 hours on rotary shaker. This followed by centrifugation at 10,000 rpm for 10 minutes after which, the supernatants were filtered using 0.45 μm syringe filter and kept for derivatization.

### 2.5. Derivatization Procedure of Glyphosate and AMPA

A blank samples or samples containing GLY and /or AMPA from standard solution and soil extract were derivatized by addition of 1 mL of each into 25 mL centrifuge tubes then followed by addition of 1 mL 0.02 M FMOC-Cl and 2 mL 0.05 M borate buffer. The mixture was shaken at 180 rpm for 1 hour on end-to-end shaker after which 2 mL diethyl ether was added to each tubes and vortex for 2 minutes to remove unreacted FMOC. This resulted in formation of two layers; organic and aqueous layer thus the organic layer was discarded through a careful pipetting and the aqueous solution containing FMOC-GLY and/or FMOC- AMPA was transferred to HPLC vials for analysis.

### 2.6. Chromatographic Conditions

Mobile phase solvent was acetonitrile and 0.05 M KH$_2$PO$_4$ mixture (30:70 v/v) using isocratic mode. The running time was 20 minutes with flow rate of 0.7mL min$^{-1}$ and column temperature of 40$^o$C while the injection volume was 20μl. For the HPLC-DAD analysis, two wave length were used, 206 and 210 nm while for the HPLC- FLD analysis, excitation and emission wave lengths were set at 270 nm and 315 nm respectively.

### 2.7. Validation of the Method

The methods was validated based on the following parameters; specificity, linearity, accuracy, precision, limit of detection and quantification. Specificity of the present method was achieved through comparative analysis of the blanks and samples containing GLY and/or AMPA. For the linearity, a calibration curves were obtained for eight concentration range of GLY or AMPA standard solutions. The precision was

evaluated through replicate analysis of the eight concentration range spiked in water and soils then later relative standard deviation (RSD) was calculated as;

$$RSD = \frac{standard\ deiviation}{mean} \times 100 \qquad (1)$$

The accuracy of this method was evaluated through calculated percent recovery of GLY and AMPA from water, as well as the GLY and AMPA extracted from clay and sandy soils spiked with eight different concentration range of GLY and AMPA. The limit of detection (LOD) was calculated as standard deviation of the concentration of three replicates multiplied by 3.3 while limit of quantification (LOQ) was calculated as standard deviation of the concentration of three replicates multiplied by 10 [23].

## 3. RESULTS AND DISCUSSION

### 3.1. Derivatization and Determination of Glyphosate and AMPA

Derivatization of GLY or AMPA occurs in alkaline condition and is based on the reaction between FMOC-Cl and amino functional group of GLY or AMPA thus, is achieved through a substitution of H atom from GLY or AMPA with aromatic ring of FMOC-Cl yielding FMOC-GLY or FMOC-AMPA and HCl [24] as shown in Fig 1. These resultant derivatives are compounds with both polar and non-polar properties. They derived their polar properties from GLY or AMPA while the non-polar characteristics was from FMOC-Cl. These FMOC-derivatives of GLY and AMPA resembles each other except that in AMPA there is presence of H atom instead of CH$_2$COOH functional group in GLY. Borate buffer (pH 9) increases the pH of the mixture to alkaline condition which help in promoting the reactivity of amines functional groups of GLY or AMPA as well stabilizing the solubility of FMOC-Cl in acetonitrile [25]. Ghanem and co-workers [21] reported that, the ratio between analyte, borate buffer and FMOC-Cl affects derivatized product formation Hence, Bernal and co-workers [14] obtained best result using the volume ratio of 1:2:1 of analyte, borate buffer and FMOC-Cl (v/v/v) which makes the adoption of this ratio in the present work. Adequate homogenization of the mixture gives good derivatives due to better interaction of FMOC and GLY or AMPA, which is why Druart and co-workers [18] used magnetic stirrer for homogenizing analyte, borate buffer and FMOC-Cl solution. However, the magnetic stirrer is only for one sample at a time hence the stirring can be difficult and time consuming when dealing with many samples. The present study therefore, used end-to-end shaker which handled many samples at a time. Adequate time is required for complete reaction hence replacement of Cl from FMOC-Cl by amino functional groups of GLY or AMPA. However, no standard time limit was set [24] but, Druart and co-workers [18] noticed no significant increase in reaction between FMOC-Cl and GLY or AMPA above 1 hour. This makes it possible for the present study to choose 1 hour reaction time for achieving complete reaction. The excess un-derivatized FMOC-Cl do interfere with the analyte

during analysis. The function of ethyl ether therefore, was to removed/reduced this excess solvent [26] which helps in increasing absorption of fluorescence

or UV light by the analyte for good peaks and better separation of the compounds.
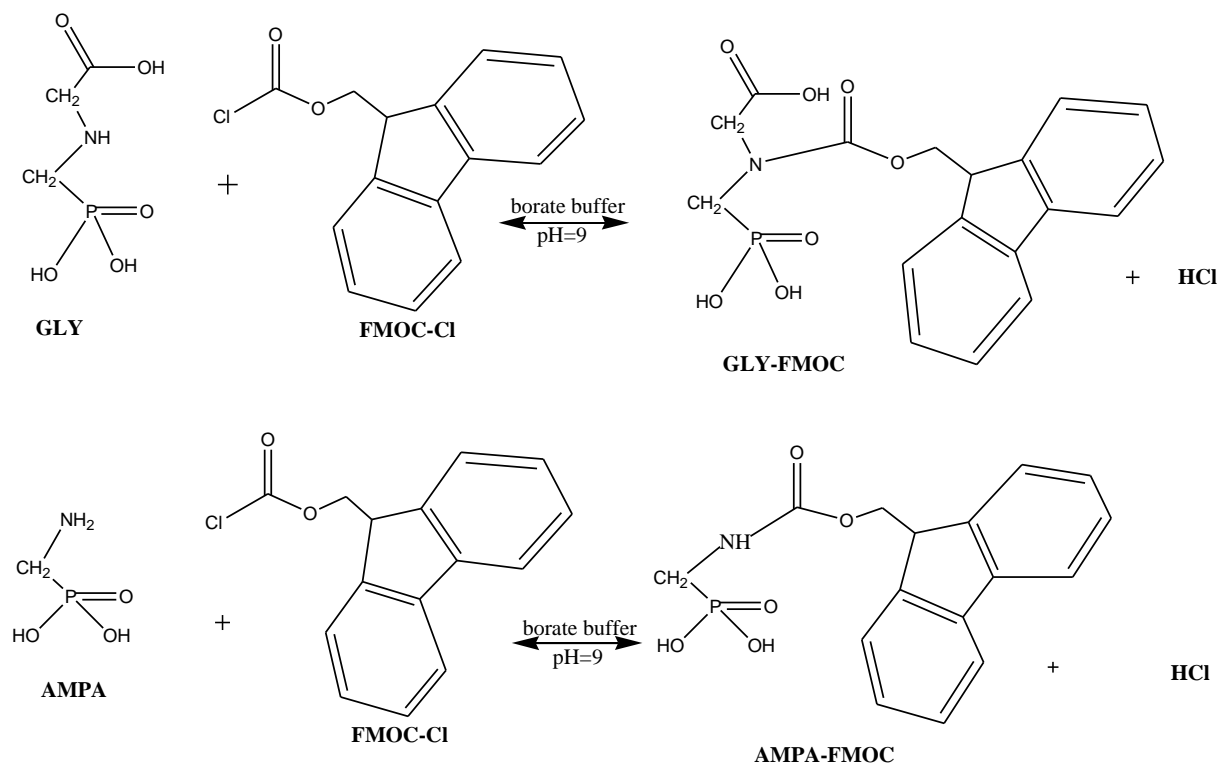


**Fig 1.** Derivatization reaction of glyphosate and AMPA with FMOC-Cl

The separation of FMOC-GLY and/or FMOC-AMPA was achieved by using the C18 column as a stationary phase while a mobile phase was acetonitrile and a solution buffer of 0.05 M $KH_2PO_4$ in an isocratic elution. Acetonitrile is a polar solvent with polarity index of 5.8, it controls the separation of these compounds while 0.05 M $KH_2PO_4$ buffer solution aids in neutralizing FMOC-GLY or FMOC-AMPA for increased retention on the stationary phase. The 40oC temperature is high enough to reduce viscosity between the analyte and mobile phase thereby enhancing the solubility and chromatographic efficiency [27]. The chromatograms produced by the column used in the present work shows that, apart from FMOC-GLY or FMOC-AMPA derivatives, there was also FMOC-OH and unknown by-products. Nedelkoska and Low [28] reported co-elution of FMOC-OH with GLY which was presented by a large peak in front of GLY thus interfere in its separation. However, in this work we recorded success in early elution of FMOC-GLY or FMOC-AMPA before FMOC-OH as can be observed from the FLD-chromatograms but there was appearance of FMOC-OH large peak

before that of FMOC-GLY or FMOC-AMPA from the DAD-chromatograms.

### 3.2. HPLC-FLD Method Performance and Validation

As shown in the Fig 2-a, there was no peak of either GLY or AMPA in the chromatogram of blank neither does it produced a large peak of FMOC-OH as expected, this might be due to low or no reaction between FMOC-Cl and water. The chromatograms of the standard solutions (Fig 2-b and c) shows the retention time of 2.54 and 5.23 minutes for GLY and AMPA respectively. There is also a presence of large peak of FMOC-OH eluted very late (10 minutes) than that of GLY or AMPA hence no overlapped or interference between the FMOC-OH and compounds of interest. The absence of any peak from control chromatograms and the presence of peaks in the chromatograms of GLY and/or AMPA standard solutions indicate selectivity and specificity of this method.
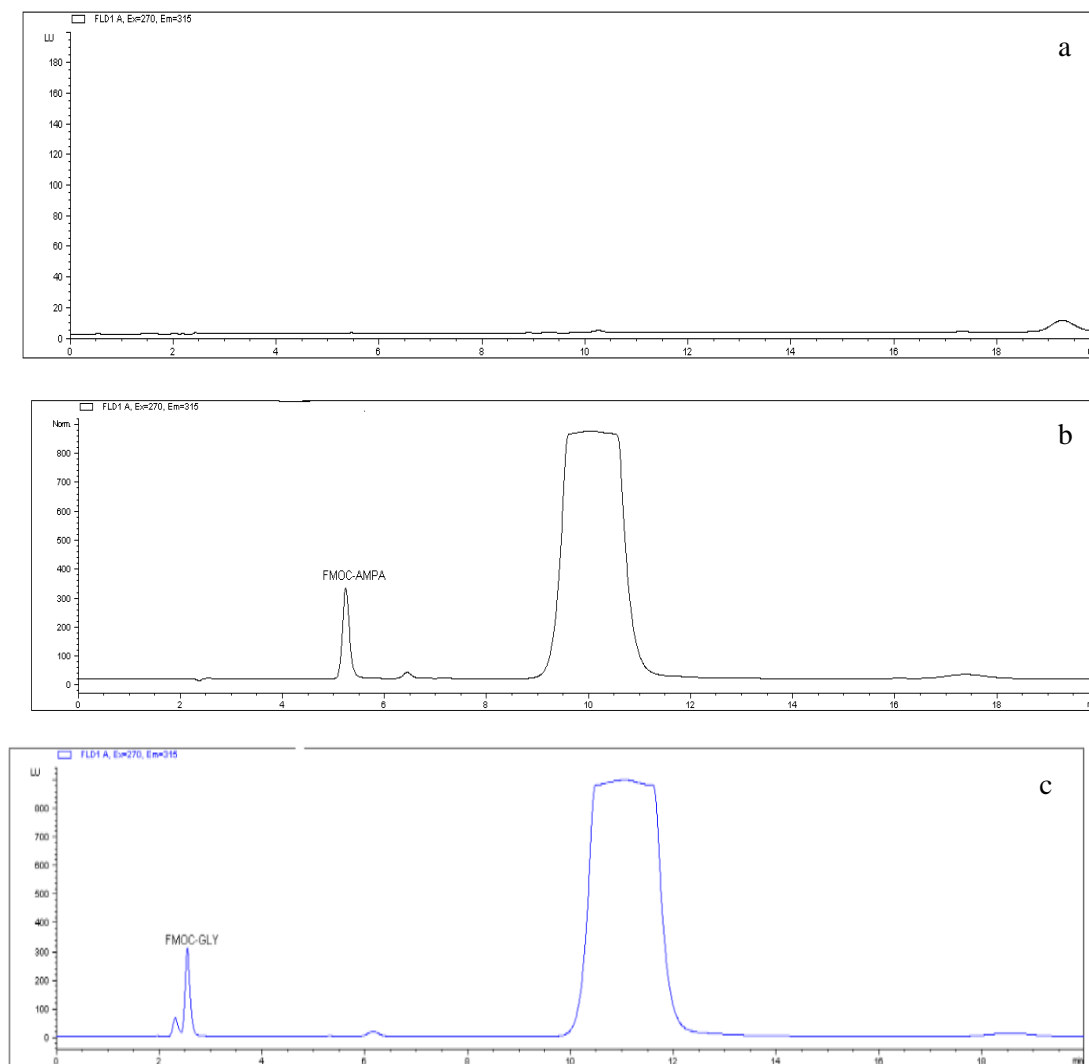
**Fig 2.** Chromatograms of control (a), 1 mg L-1 AMPA (b) and glyphosate (c) standard solutions by LC-FLD

Eight different concentrations ranging between 0 mg L$^{-1}$ and 2 mg L$^{-1}$ of GLY or AMPA standard solution were analysed for linear calibration curve. The response values shows high linear regression (Table 1) which indicated the linearity and reliability of this method.

Fig 3 is the chromatograms of GLY and AMPA in water and extracted residues from the spiked soils. The retention time of GLY and AMPA from water was 2.45 and 5.23 minutes respectively while from soil it was 2.42 and 5.37 minutes for GLY and AMPA respectively.

The percent recovery (Table 2) of eight different concentrations ranging between 0 mg L$^{-1}$ and 2 mg L$^{-1}$ of GLY and AMPA in water indicated a very good recovery for GLY (80-110%) and AMPA (73-103%) hence the accuracy of this method. The calculated LOD and LOQ for GLY in water was 0.008 mg L$^{-1}$ and 0.028 mg L$^{-1}$ while AMPA had 0.004 mg L$^{-1}$ and 0.015mg L$^{-1}$ respectively. Moreover the RSD for these eight concentration was 0.2-1% and 0.1-0.7% for GLY and AMPA respectively. This indicated that the method is repeatable, efficient and have a very good precision. The recovery of GLY (34-74%) and AMPA (37-51%)

from clay soil was low compared to that sandy soil which shows 49-105% for GLY and 32-70% for AMPA.

The recovery of both compounds in both water and soil samples increased with increasing concentrations. The LOD and LOQ of GLY in clay soil was 0.132 mg kg$^{-1}$ and 0.399 mg kg$^{-1}$ while AMPA had 0.224 mg kg$^{-1}$ and 0.678 mg kg$^{-1}$. The sandy soil shows low LOD and LOQ of both compounds compared to clay thus, LOD and LOQ from this soil was 0.021 mg kg$^{-1}$ and 0.064 mg kg$^{-1}$ for GLY while AMPA had 0.074 mg kg$^{-1}$ and 0.331 mg kg$^{-1}$ respectively. Furthermore, the RSD of the analysed extracted solutions was 12-24% for GLY and 10-26% for AMPA in clay soils while sandy soil had 6-30% and 10-28% for GLY and AMPA respectively.

**Table 1.** Linearity AMPA and Glyphosate standard solutions by LC-FLD

| Compounds | Regression equation (n=8) | $R^2$ |
|-----------|---------------------------|-------|
| AMPA | y= 2886.9x+43.001 | 0.998 |
| Glyphosate | y= 1265.8x+84.005 | 0.994 |
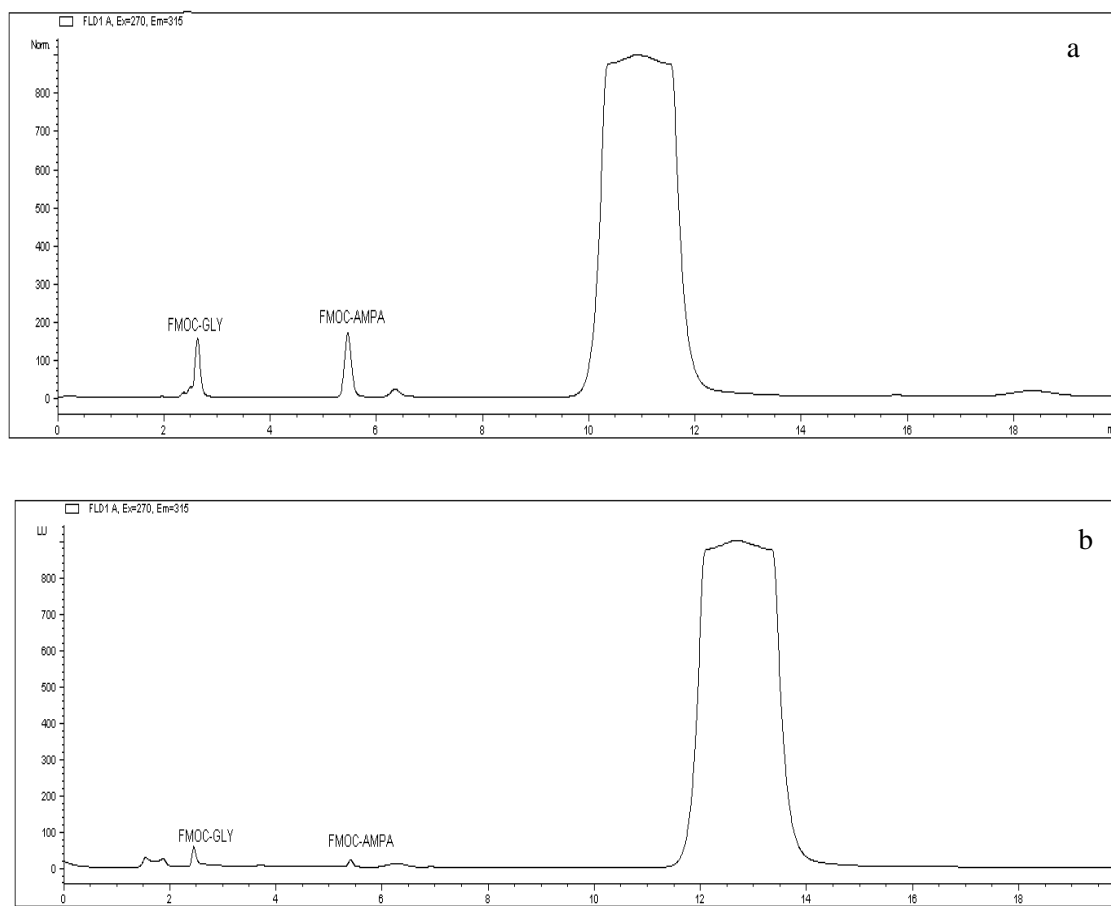
**Fig 3.** Chromatograms of 1 mg L-1 glyphosate and AMPA in water (a) and extracted residues (b) from spiked clay soil by LC-FLD

**Table 2.** Validation parameters for method of glyphosate and AMPA analysis by LC-FLD

| Compound | Matrix | Parameters | | | |
|---|---|---|---|---|---|
| | | Recovery (%) | RSD (%) | LOD | LOQ |
| GLY | Water | 80-110 | 0.2-1 | 0.008 mg L$^{-1}$ | 0.028 mg L$^{-1}$ |
| | Clay soil | 34-74 | 12-24 | 0.132 mg kg$^{-1}$ | 0.399 mg kg$^{-1}$ |
| | Sandy soil | 49-105 | 6-30 | 0.021 mg kg$^{-1}$ | 0.064 mg kg$^{-1}$ |
| AMPA | Water | 73-103 | 0.1-0.7 | 0.004 mg L$^{-1}$ | 0.015 mg L$^{-1}$ |
| | Clay soil | 35-51 | 10-26 | 0.224 mg kg$^{-1}$ | 0.678 mg kg$^{-1}$ |
| | Sandy soil | 32-70 | 10-28 | 0.074 mg kg$^{-1}$ | 0.331 mg kg$^{-1}$ |

The present method involved simple steps and direct determination of GLY and AMPA without further clean up prior to derivatization hence very cost effective. The high linear regression and specificity of both compounds indicated that, the method can be reproducible and has very good reliability. The result

of the method validation showed high recovery of both compounds with low RSD from water samples compared to the soils. Glyphosate was reported to strongly adsorbed to Fe and Al oxides minerals, polyvalent cations and soil organic matter [29]. Table 3 indicated that both soils had substantial content of sesquioxides and soil organic matter with clay soils having high content than sandy soil. Therefore, this low recovery of both compounds from soils was attributed to adsorption by oxide minerals and soil organic colloids. Similarly, the greater content of sesquioxides and organic matter in clay were

suggested to cause low recoveries of these compounds as well as their high LOD and LOQ compared to the sandy soil. Glyphosate and AMPA rapidly formed non-extractable residues in soils due to their strong adsorption [30] therefore, most studies experienced low recovery from many soils [31]. The KH$_2$PO$_4$ solution extracts both soluble and weekly adsorbed form of these compounds hence their recovery depends on soil clays, organic matter, pH, inorganic phosphorus and exchangeable actions [29–32]. The KH$_2$PO$_4$ is the best extracting solution of GLY and AMPA from soil and extraction by agitation was shown to provide best efficient recovery [18, 30]. This evidently shows that, the low recovery of these compounds from soils compared to the water samples was attributed to their adsorption by these soils. However, this extraction procedure can still be applied with soils where adsorption of these compounds was less. The average GLY recovery obtained from sandy (77%) and clay (54%) from the

present study was still high than what was reported for clay loam, sandy loam and silty clay loam soil extracted with 0.1 M $KH_2PO_4$ solution [30]. The LOD of GLY from both sandy and clay soil were less than that reported by Glass [17] from sandy- loam soils (5 mg $kg^{-1}$) and clay-loam soils (50 mg $kg^{-1}$). Miles and Moye [33] also extracted GLY from two soils and reported the LOD of 0.5 mg $kg^{-1}$ for sandy soils and 1 mg $kg^{-1}$ for clay soils. However, a recent study conducted by Druart and co-workers [18] on clay-loam soils reported LOD for GLY and AMPA as 0.1 mg $kg^{-1}$ and 0.016 mg $kg^{-1}$ respectively, the values which are similar to the present study. The LOD of both compounds from water samples were very low than the maximum GLY residue level in drinking water set by US environmental protection agency and health Canada [16]

**Table 3.** Selected properties of the soils used for method validation

| Property | Sandy soil | Clay soil |
|---|---|---|
| Free FeO (%) | 0.473 | 2.297 |
| Amorphous FeO (%) | 0.218 | 0.655 |
| Free AlO (%) | 0.476 | 1.815 |
| Amorphous AlO (%) | 0.262 | 0.550 |
| SOM (%) | 5.233 | 10.567 |
| CEC (coml(+) $kg^{-1}$) | 12.667 | 11.905 |

### 3.3. HPLC-DAD Method Performance and Validation

As shown in Fig 4, there was only large peak of FMOC-OH from the control chromatograms which evidently showed a high sensitivity of FMOC-OH to UV light compared to fluorescent. The retention time of GLY and AMPA for LC-DAD as shown by analysis of 5 mg $L^{-1}$ standard solution (Fig 5) were 2.38 and 5.30 minutes respectively, the times which are similar to LC-FLD. The presence of FMOC-OH peaks only from blank and elution of GLY and AMPA peaks from standard solutions indicated the specificity of this method even with DAD. Table 4 shows regression equations and coefficient of determination of nine concentration of GLY and AMPA standard solution (0 – 40 mg $L^{-1}$) with greater linear regression from both compounds ($R^2 > 99\%$) thus, indicating the linearity of LC-DAD. Fig 6 is the chromatograms of GLY and AMPA in water and extracted residues from the spiked soils. The retention time of GLY and AMPA from clay soils was 2.57 and 5.38 minutes respectively.

**Table 4.** Linearity AMPA and Glyphosate standard solutions by LC-DAD

| Compounds | Regression equation (n=9) | $R^2$ |
|---|---|---|
| AMPA | y= 73.201x+6.1748 | 0.996 |
| Glyphosate | y= 59.956x+51.172 | 0.996 |
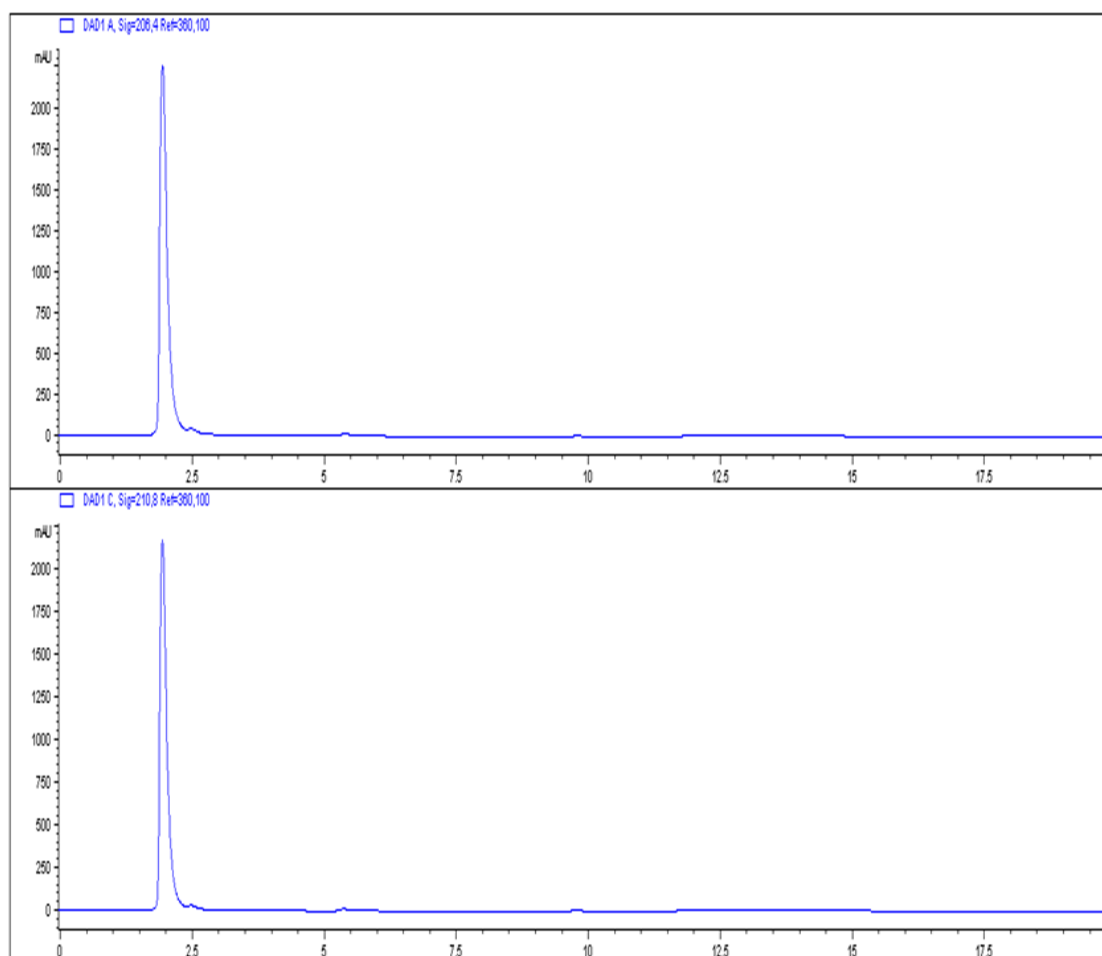


**Fig 4.** Chromatograms of the blank sample by LC-DAD
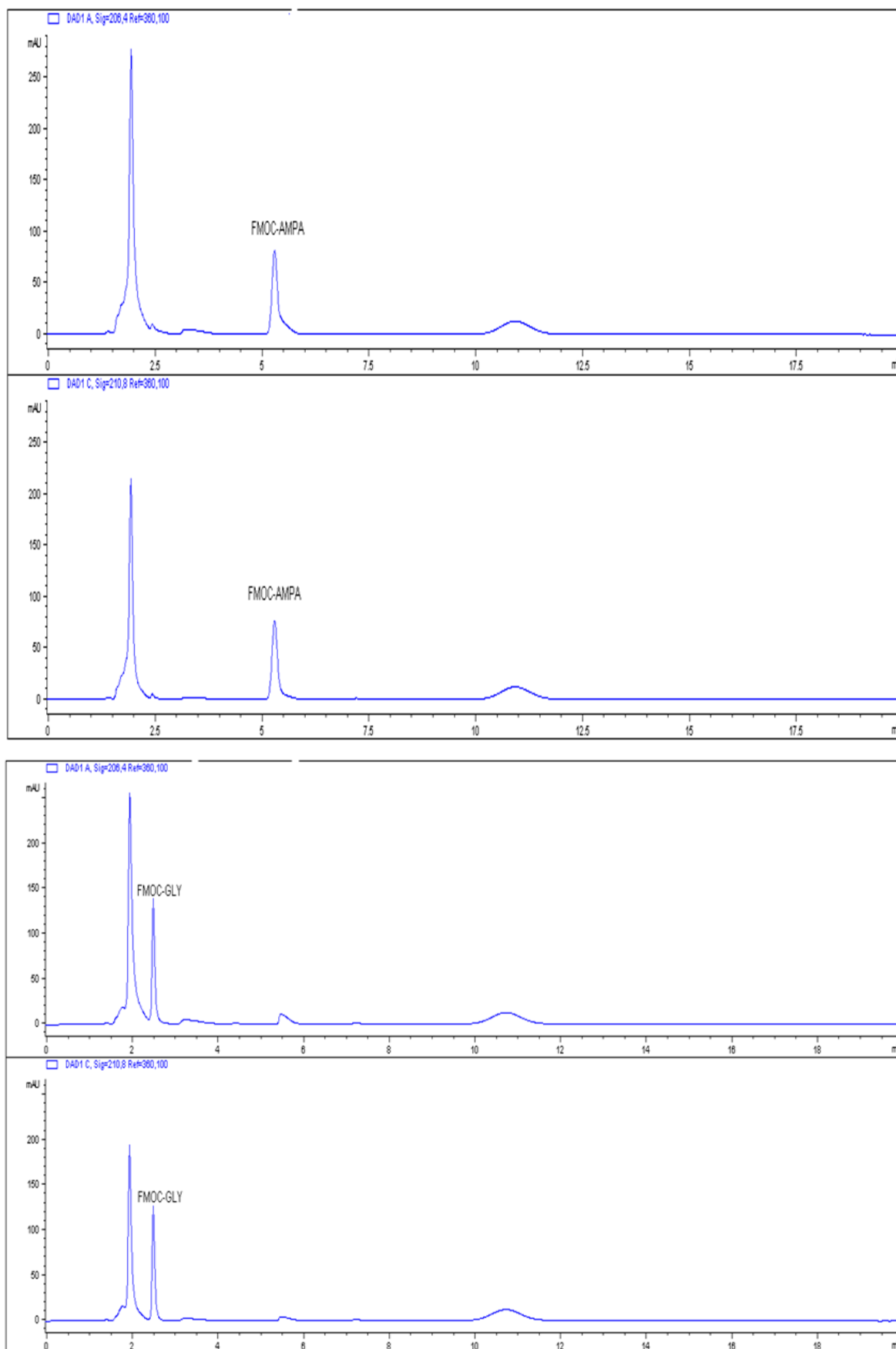
**Fig 5.** Chromatograms of 5 mg L$^{-1}$ of AMPA or glyphosate standard solution by LC-DAD
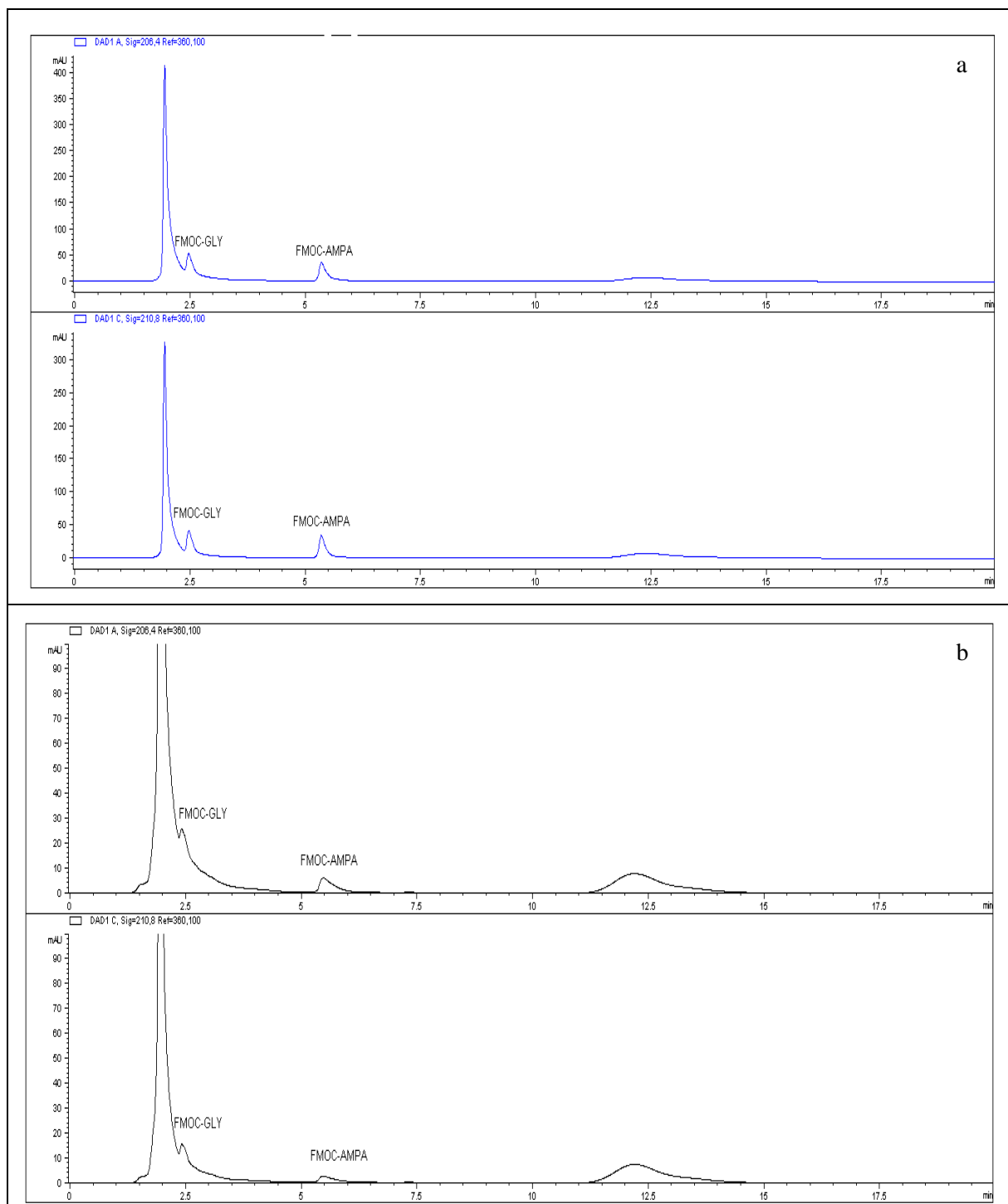
**Fig 6.** Chromatograms of 5mg $L^{-1}$ glyphosate and AMPA in water (a) and extracted from clay soil (b) by LC-DAD

The percent recovery of GLY and AMPA in water from nine different concentrations (0-40 mg $L^{-1}$) as shown in Table 5 indicated a very good recovery ranging from 93% to 110% for GLY and 86% to 106% for AMPA hence reproducibility of the method even with DAD. The calculated LOD and LOQ for GLY from water sample was 0.024 mg $L^{-1}$ and 0.083 mg $L^{-1}$ while AMPA had 0.076 mg $L^{-1}$ and 0.247 mg $L^{-1}$ respectively. The RSD was 0.7-4% and 0.2-2% for GLY and AMPA

respectively. This indicates that, the method is repeatable, efficient and has a very good precision. The percent recovery of GLY from the clay soil was 18-58% while the sandy soil had 27-64%. The LOD and LOQ of GLY from clay soil was 0.122 mg $kg^{-1}$ and 0.360 mg $kg^{-1}$ while the sandy soil had 0.731 mg $kg^{-1}$ and 1.242 mg $kg^{-1}$ respectively. The RSD was 1-5% for the clay soil and 6%-24% for sandy soil.

**Table 5.** Validation parameters for method of glyphosate and AMPA analysis by LC-DAD

| Compound | Matrix | Parameters | | | |
|---|---|---|---|---|---|
| | | Recovery (%) | RSD (%) | LOD | LOQ |
| GLY | Water | 93-110 | 0.7-4 | 0.024 mg $L^{-1}$ | 0.083 mg $L^{-1}$ |
| | Clay soil | 18-58 | 1 -5 | 0.122 mg $kg^{-1}$ | 0.360 mg $kg^{-1}$ |
| | Sandy soil | 27-64 | 6-24 | 0.731 mg $kg^{-1}$ | 1.242 mg $kg^{-1}$ |
| AMPA | Water | 86-106 | 0.2-2 | 0.076 mg $L^{-1}$ | 0.247 mg $L^{-1}$ |

The FMOC- derivatives of GLY and AMPA are rarely analysed with LC with ultraviolet detector (UV) hence, we laid our hand only on Peruzzo and co-workers [34] despite the fact that Franz and co-workers [4] reported both derivatives to have ultraviolet properties. The common reagents used in pre-column derivatization and LC analysis of GLY and AMPA with UV detector includes 1-flouro-2,4-dinitrobenzene (FDNB) [3], p-toluenesulphonyl chloride (TsCl) [35], p-nitrobenzoyl chloride (PNBC) [36] , 4-chloro-3,5-dinitrobenzotriflouride (CNBF) [37] and 2,5-dimethoxy benzenesulfonyl chloride (DMOSC) [38]. The present work therefore agrees with Peruzzo and co-workers [34], which evidently shows that both FMOC- GLY and AMPA- derivatives can be analysed with LC-UV. Even though FLD has high sensitivity than DAD as shown by their respective LOD and LOQ. As an equipment, both detectors are bound to have technical problems and considering the high cost of FLD lamp compared to DAD, the latter can serve as alternative in case FLD got faulty especially when using a machine with dual detectors like the one in the present work. The present study therefore, re-explore the potential of DAD in detecting GLY and AMPA thus,

serve as additional advantage of simple procedure which uses available analytical equipment. The LC-DAD shows high linear regression of standard solutions and high percent recovery of GLY and AMPA in water which indicated its reliability and repeatability. However, the percent recovery of GLY from both soils studied was poor but considering the LOD of GLY in both soils, the method can still be use in routine analysis of GLY extracted from matrixes other than soil . On the other hand,  AMPA was poorly extracted which led to very low/no quantification hence resulted in rather similar values for all concentration range which makes it impossible to calculate LOD and LOQ from both soils. This was attributed to its strong adsorption to soil minerals and organic colloids. Therefore, it is possible to improve the AMPA quantification by more repeated extraction. This might likely help in extracting adsorbed compound [31] which will result in increased in quantification and recovery. The LOD and LOQ of GLY from the clay soil are similar to that reported by Peruzzo and co-workers [34] for soils and sediment (0.10 mg $kg^{-1}$ and 0.25 mg $kg^{-1}$) but the sandy soil had greater values than what the authors have reported.

**Table 6.** Comparison of some LC-UV methods for glyphosate and AMPA analysis

| Matrix | Enrichment/pre-treatment | Reagent for derivatization | LOD | | Reference |
|---|---|---|---|---|---|
| | | | GLY | AMPA | |
| Soil | Ion exchange extraction, evaporation | FDNB | 0.05 µg $g^{-1}$ | 0.1 µg $g^{-1}$ | [3] |
| Fruits juice | Supported-liquid membrane | TsCl | 0.01 mg $L^{-1}$ | 0.01 mg $L^{-1}$ | [35] |
| Apple | Solid phase extraction | CNBF | 0.01 µg $g^{-1}$ | NA | [39] |
| water | evaporation | MOBSF | 0.001 mg $L^{-1}$ | 0.001 mg $L^{-1}$ | [16] |
| water | none | DMOSC | 0.067 mg $L^{-1}$ | NA | [35] |
| Water | none | FMOC-Cl | 0.024 mg $L^{-1}$ | 0.076 mg $L^{-1}$ | This work |
| Soil | none | FMOC-Cl | 0.122 µg $g^{-1}$ | NA | This work |

NA no analysis

## 4.   CONCLUSIONS

The present work demonstrate a simple pre-column derivatization of GLY and AMPA with FMOC-Cl and HPLC analysis of the derivatives with FLD or DAD. The derivatization reaction was completed in 1 hour at room temperature and diethyl ether was used in washing the excess FMOC for clear separation of the analyte. The FMOC- derivatives of GLY and AMPA eluted long before FMOC-OH in LC-FLD. The method recorded good recovery in both water and sandy soil especially for GLY hence, considered reliable for quantitative determination of GLY and AMPA. Similarly, these derivatives were quantified using LC-DAD also, a clear separation was obtained between FMOC-GLY, FMOC-AMPA and FMOC-OH. Even though, there was low GLY recovery from the soil matrixes but considering its low LOD, the LC-DAD can still be used in routine analysis of GLY especially in soil will less

adsorption phenomena. We were unable to calculate LOD and LOQ for AMPA from soil matrixes which was attributed to its strong adsorption by soil minerals and organic colloids as well low sensitivity of DAD for AMPA. We therefore, suggested for more repeated extraction, which might increase quantification and recovery of the compound.

### ACKNOWLEDGEMENT

## REFERENCES

[1].  C. M. Benbrook, "Trends in glyphosate herbicide use in the United States and globally," *Environmental Sciences Europe*, Vol 28(3), pp. 1-15, 2016.

[2].  P. Sprankle, W. F. Meggitt, and D. Penner, "Adsorption, Mobility, and Microbial Degradation of Glyphosate in the Soil," *Weed Science*, Vol. 23 (3), pp. 229–234, 1975.

[3].  L.N. Lundgren, "New Method for the determination of glyphosate and (Aminomethy1) phosphonic acid residues in soils," *Journal of Agricultural and Food Chemistry, Vo*l. 34 (3), pp. 535–538, 1986.

[4].  J. E. Franz, M. K. Mao, and J. A. Sikorski, "*Glyphosate: a unique global herbicide",* American Chemical Society, 1997.

[5].  W. Wibawa, "Development of method for residue analysis of three herbicides in the soil by high performance liquid chromatography (HPLC)," *Journal of Environmental Chemistry and Ecotoxicology*, vol. 5 (8), pp. 220–226, 2013.

[6].  J.P. Giesy, S. Dobson and K.R. Solomon, "Ecotoxicological risk assesment for roundup herbicide," *Reviews of Environmental Contamination and Toxicology*, Vol. 167, pp. 35–120, 2000.

[7].  C. J. Henry, K. F. Higgins, and K. J. Buhl, "Acute toxicity and hazard assessment of Rodeo, X-77 Spreader, and Chem-Trol to aquatic invertebrates," *Archives of Environmental Contamination and Toxicology, V*ol. 27 (3), pp. 392–399, 1994.

[8].  M. T. K. Tsui and L. M. Chu, "Aquatic toxicity of glyphosate-based formulations: Comparison between different organisms and the effects of environmental factors," *Chemosphere*, Vol. 52 (7), pp. 1189–1197, 2003.

[9].  Y. S. Hu, Y. Q. Zhao, and B. Sorohan, "Removal of glyphosate from aqueous environment by adsorption using water industrial residual," *Desalination*, Vol. 271 (1–3), pp. 150–156, 2011.

[10]. I. Herath, P. Kumarathilaka, M. I. Al-Wabel, A. Abduljabbar, M. Ahmad, A. R. A. Usman, and M. Vithanage, "Mechanistic modeling of glyphosate interaction with rice husk derived engineered biochar," *Microporous Mesoporous Materials*, Vol. 225, pp. 280–288, 2016.

[11]. H.-Y. Chuang, T.-P. Hong, and C.-W. Whang, "A simple and rapid screening method for glyphosate in water using flow-injection with electrochemiluminescence detection," *Analytical Methods*, Vol. 5 (21), pp. 6186–6191, 2013.

[12]. H. A. Moye and A. J. Boning Jr, "A versatile fluorogenic labelling reagent for primary and secondary amines: 9-fluorenylmethyl chloroformate," *Analytical Letters*, Vol. 12 (1), pp. 25–35, 1979.

[13]. C. V. Waiman, M. J. Avena, M. Garrido, B. Fernández Band, and G. P. Zanini, "A simple and rapid spectrophotometric method to quantify the herbicide glyphosate in aqueous media: Application to adsorption isotherms on soils and goethite," *Geoderma*, Vol. 170, pp. 154–158, 2012.

[14]. J. Bernal, M. T. Martin, M. E. Soto, M. J. Nozal, I. Marotti, G. Dinelli, and J. L. Bernal, "Development and application of a liquid chromatography-mass spectrometry method to evaluate the glyphosate and aminomethylphosphonic acid dissipation in maize plants after foliar treatment.," *Journal of Agricultural and Food Chemistry*, Vol. 60 (16), pp. 4017–4025, 2012.

[15]. Y. Zhang, Y. Zhang, Q. Qu, G. Wang, and C. Wang, "Determination of glyphosate and aminomethylphosphonic acid in soybean samples by high performance liquid chromatography using a novel fluorescent labeling reagent," *Analytical Methods*, Vol. 5 (22), pp. 6465 - 6472, 2013.

[16]. Y. Sun, C. Wang, Q. Wen, G. Wang, H. Wang, Q. Qu, and X. Hu, "Determination of glyphosate and aminomethylphosphonic acid in water by LC using a new labeling reagent, 4-methoxybenzenesulfonyl fluoride," *Chromatographia*, Vol. 72 (7–8), pp. 679–686, 2010.

[17]. R. L. Glass, "Liquid chromatographic determination of glyphosate in fortified soil and water samples," *Journal of Agricultural and Food Chemistry*, Vol. 31 (2), pp. 280–282, 1983.

[18]. C. Druart, O. Delhomme, A. de Vaufleury, E. Ntcho, and M. Millet, "Optimization of extraction procedure and chromatographic separation of glyphosate, glufosinate and aminomethylphosphonic acid in soil," *Analytical and Bioanalyticaal Chemistry*, Vol. 399 (4), pp. 1725–173232, 2011.

[19]. W. Skeff, C. Neumann, and D. E. Schulz-Bull, "Glyphosate and AMPA in the estuaries of the Baltic Sea method optimization and field study," *Marine Pollution Bulletin*, Vol. 100 (1), pp. 577–585, 2015.

[20]. M. E. Báez, E. Fuentes, M. J. Espina, and J. Espinoza, "Determination of glyphosate and aminomethylphosphonic acid in aqueous soil matrices: a critical analysis of the 9-fluorenylmethyl chloroformate derivatization reaction and application to adsorption studies," *Journal of Seperation Science*, Vol. 37 (21), pp. 3125–3132, 2014.

[21]. A. Ghanem, P. Bados, L. Kerhoas, J. Dubroca, and J. Einhorn, "Glyphosate and AMPA analysis in sewage sludge by LC-ESI-MS/MS after FMOC derivatization on strong anion-exchange resin as solid support," *Analytical Chemistry*, Vol. 79 (10), pp. 3794–3801, 2007.

[22]. C. Hidalgo, C. Rios, M. Hidalgo, V. Salvadó, J. V Sancho, and F. Hernández, "Improved coupled-column liquid chromatographic method for the determination of glyphosate and aminomethylphosphonic acid residues in environmental waters," *Journal of Chromatography A*, Vol. 1035 (1), pp. 153–157, 2004.

[23]. L. C. Schrübbers, M. Masís-Mora, E. Carazo Rojas, B. E. Valverde, J. H. Christensen, and N. Cedergreen, "Analysis of glyphosate and aminomethylphosphonic acid in leaves from Coffea arabica using high performance liquid chromatography with quadrupole mass spectrometry detection," *Talanta*, Vol. 146, pp. 609–620, 2016.

[24]. T. C. P. G. Catrinck, A. Dias, M. C. S. Aguiar, F. O. Silverio, P. H. Fidencio, and G. P. Pinho, "A simple and efficient method for derivatization of glyphosate and AMPA using 9-fluorenylmethyl chloroformate and spectrophotometric analysis," *Journal of the Brezilian Chemical Society*, Vol. 25 (7), pp. 1194–1199, 2014.

[25]. J. Patsias, A. Papadopoulou, and E. Papadopoulou-Mourkidou, "Automated trace level determination of glyphosate and aminomethyl phosphonic acid in water by on-line anion-exchange solid-phase extraction followed by cation-exchange liquid chromatography and post-column derivatization," *Journal of Chromatography A*, Vol. 932 (1–2), pp. 83–90, 2001.

[26]. J. L. Jamison, L. Davenport, and B. W. Williams, "Solvatochromism in the aromatic ketone benzo [b] fluorenone," *Chemical Physics Letters*, Vol. 422 (1), pp. 30–35, 2006.

[27]. K. Robards, P. R. Haddad, and P. E. Jackson, "Principles and practice of modern chromatographic methods", *Academic Press*, 1994.

[28]. T. V. Nedelkoska and G. K. C. Low, "High-performance liquid chromatographic determination of glyphosate in water and plant material after pre-column derivatisation with 9-fluorenylmethyl chloroformate," *Analytica Chimica Acta*, Vol. 511 (1), pp. 145–153, 2004.

[29]. A. A. Piccolo, G. Celano and M. Arienzo, "Adsorption and desorption of glyphosate in some european soils," *Journal of Environmental Science and Health B*, Vol. 29 (6), pp. 1105–1115, 1994.

[30]. A.J.Al-Rajab and O.M. Hakami, "Behavior of the non-selective herbicide glyphosate in agricultural soil," *American Journal of Environmental Sciences*, Vol. 10 (2), pp. 94–101, 2014.

[31]. C. D. Stalikas and C. N. Konidari, "Analytical methods to determine phosphonic and amino acid group-containing pesticides," *Journal of Chromatography A*, Vol. 907 (1-2), pp. 1–19, 2001.

[32]. J. V. Sancho, F. Hernández, F. J. López, E. a. Hogendoorn, E. Dijkman, and P. Van Zoonen, "Rapid determination of glufosinate, glyphosate and aminomethylphosphonic acid in environmental water samples using precolumn fluorogenic labeling and coupled-column liquid chromatography," *Journal of Chromatography A*, Vol. 737 (1), pp. 75–83, 1996.

[33]. C. J. Miles and H. A. Moye, "Extraction of glyphosate herbicide from soil and clay minerals and determination of residues in soils," *Journal of Agricultural and Food Chemistry*, Vol. 36 (3), pp. 486–491, 1988.

[34]. P. J. Peruzzo, A. A. Porta, and A. E. Ronco, "Levels of glyphosate in surface waters, sediments and soils associated with direct sowing soybean cultivation in north pampasic region of Argentina," *Environmental Pollution*, Vol. 156 (1), pp. 61–66, 2008.

[35]. M. V. Khrolenko and P. P. Wieczorek, "Determination of glyphosate and its metabolite aminomethylphosphonic acid in fruit juices using supported-liquid membrane preconcentration method with high-performance liquid chromatography and UV detection after derivatization with p-toluenesulphonyl chloride," *Journal of Chromatography A*, Vol. 1093, pp. 111–117, 2005.

[36]. Y. Hori, M. Fujisawa, K. Shimada, M. Sato, M. Kikuchi, M. Honda, and Y. Hirose, "Quantitative determination of glufosinate in biological samples by liquid chromatography with ultraviolet detection after p-nitrobenzoyl derivatization," *Journal of Chromatography B*, Vol. 767 (2), pp. 255–262, 2002.

[37]. K. Qian, T. Tang, T. Shi, F. Wang, J. Li, and Y. Cao, "Residue determination of glyphosate in environmental water samples with high-performance liquid chromatography and UV detection after derivatization with 4-chloro-3,5-dinitrobenzotrifluoride," *Analytica Chimica Acta*, Vol. 635 (2), pp. 222–226, 2009.

[38]. F. Fang, R. Wei, and X. Liu, "Novel pre-column derivatisation reagent for glyphosate by high-performance liquid chromatography and ultraviolet detection," *International Journal of Environmental Analytical Chemistry*, Vol. 94 (7), pp. 1–7, 2014.

[39]. K. Qian, T. Tang, T. Shi, P. Li, J. Li, and Y. Cao, "Solid-phase extraction and residue determination of glyphosate in apple by ion-pairing reverse-phase liquid chromatography with pre-column derivatization," *Journal of Seperation Science*, Vol. 32 (14), pp. 2394–2400, 2009.

Environmental Research & Technology

RESEARCH ARTICLE

# Adsorption properties of activated almond shells for methylene blue (MB)

Ramazan Coskun[1,*], Serpil Savci[2], Ali Delibas[1]

[1] Department of Chemistry, Faculty of Science and Arts, University of Bozok, Yozgat, TURKIYE
[2] Department of Biosystems Engineering, Faculty of Engineering and Architecture, University of Bozok, Yozgat, TURKIYE

## ABSTRACT

In this study, the adsorption properties of activated almond shells for methylene blue (MB) were investigated. For this aim raw almond shells (RAS) were activated with concentrated sulfuric acid. Activated almond shell (SAS) and raw almond shells (RAS) were characterized with FTIR, SEM and BET analysis. After activation, larger and deeper pores similar to chamber were formed and increase in BET surface area and adsorption rate and also new functional groups were observed. Effects of pH, initial concentration of dye and adsorbent dose on adsorption of MB were studied. Adsorption studies were fitted Langmuir isotherm and pseudo second order kinetic models. Experimental results showed that activated almond shells were not affected pH of solution and adsorption capacity were highly increased and it was calculated as 131.58 mg/g from Langmuir isotherm. It was observed that the activated almond shells could be used with high efficiency in a wide pH and concentration ranges and SASs could be desorbed and reusable without losing their activity. As a results, SAS could be used an effective adsorbent for the removal of basic dyes like MB at a wide pH and dye concentration range.

*Keywords:* Adsorption, methylene blue, activated almond shell, efficiently removal

## 1. INTRODUCTION

With developing technology inorganic and organic pollutants discarded to environment are increased day by day. Synthetic dyes have a significant effect within organic pollutants. They use in many industries such as textile, leather tanning, paper production, food technology, photo electrochemical cells, and hair colorings etc. [1-5]. Approximately 10-15% of the used dyes in industry come directly to the nature as waste [6]. As many dye and their degradation products are toxic and carcinogenic, removal of synthetic dyes from effluents have been important study in recent years for health safety [7–9]. MB dye chosen in this study is frequently used in various coloring industries such as paper, cotton, and wool. But, human health is affected adversely by MB especially ingestion of it by human resulted in respiratory illness, diarrhea, nausea, and eye burns [10]. Also, considering that it is a toxic dye, it affects the living life in the water adversely due to high solubility in the water. It is known that many different techniques such as precipitation, membrane technology, ion exchange, electro-coagulation and adsorption are used to remove both inorganic and organic pollutants from aqueous media. But, the adsorption process is the preferred method for removing organic and inorganic contaminants in water and wastewater due to ease, ease of operation and design simplicity [11-13]. To remove various types of pollutants from aquatic environment a large variety of synthetic and natural adsorbents have been used as adsorbent [14-19]. But, their use in wastewater treatment is sometimes restricted due to theirs higher cost, regeneration difficulties, inadequate adsorbent capacity, low adsorption rate and effective use weakness at wide pH and wide concentration range. Removal of dyes from textile wastewater with high efficiency is still an important problem faced by the textile industry today. To this aim, scientists are constantly exploring new, efficient and environmentally friendly materials with low cost. One of the methods used to improve the weak properties of adsorbents is modification. In the modification, acids such as carboxylic, sulphuric, phosphoric acids are generally used. It has been reported that the carboxylic, sulfonic and phosphoric
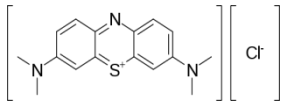
acid groups on the adsorbent are important in the removal of organic and inorganic contaminants [20 - 22]. Our aim in this study is to develop a new adsorbent, which could be quickly regenerable and it would be used at wide pH and wide concentration range effectively removal of cationic dyes such as MB.

## 2. MATERIAL AND METHODS

Raw almond shells (RAS) were supplied from a local farm in Yozgat, Turkey. MB was purchased from Carlo Erba Reagent. It is a cationic dyestuff (chemical formula C16H18CIN3S, dye purity >90%). The characteristics of this dye are presented in Table 1. The solution was prepared by dissolving MB of 1000 mg in 1 L distilled water. All the other used chemicals were Merck and used without any purification.

**Table 1.** Chemical structure and characteristics of methylene blue

| Methylene blue | |
| --- | --- |
| Molecular weight (g/mol) | 319.85 |
| Color | Blue |
| $\lambda_{max}$ (nm) | 665 |
| Dye purity | <90% |
| Chemical formula | $C_{16}H_{18}CIN_3S$ |
| Structure | |

### 2.1. Preparation of adsorbent

Firstly, the almonds were taken out from shells; secondly, they were washed and dried; lastly raw almond shells (RAS) were modified with concentrated sulfuric acid. Certain amounts of RAS (10g/20 mL) were taken and they were shaken with concentrated sulphuric acid for 1 hour at 200 rpm at 60 0C. Then, they were filtered and washed with pure water until pH=7. Then, modified almond shells were dried at 50 °C in oven and stored in desiccator. After that, activated almond shells (SAS) were used as an adsorbent for MB in adsorption studies.

### 2.2. Characterization of adsorbent

Functional groups, surface morphology and surface properties of the RAS, SAS and DSAS were performed with FTIR (Perkin-Elmer Spectrum 400), SEM (FEIQuanta 450 FEG), and BET (Micromeritics Gemini VII Sürfece Area and Porosity) analyses respectively. The pH measurements were made with WTW 32101 model digital pH-meters.

### 2.3. Adsorption studies

Adsorption studies were performed in 100 mL Erlenmeyer Flasks including 0.1 g of almond shells with 30 mL of methylene blue solution. All the adsorption experiments were performed at room temperature (25oC) via batch method. The solution was shaken by a mechanical shaker (VWR) at the constant agitation time (200 rpm) during 24 hours. Then the supernatant was centrifuged (Elektro Mag M 815 M) at 4000 rpm for 10 minutes after the adsorption experiments. The absorbance of methylene blue was measured at maximum wavelength (λmax: 665 nm) by UV–VIS Spectrophotometer (Shimadzu UV 1208). The effect of contact time was evaluated in the time range of 0-360 minutes by using 25, 50 and 100 mg L$^{-1}$ of initial MB concentrations and the initial dye concentration experiments were studied from 50 to 700 mgL$^{-1}$. For the contact time experiments were performed in 25, 50 and 100 mg L$^{-1}$ and the initial dye concentration experiments were studied from 50 to 700 mg L$^{-1}$. All experiments were repeated three times. The removal percentage (R %) and adsorption amount (Q) was calculated with given equation as follow equation 1 and 2 respectively.

$$Removal\ of\ dye\ (R) = \frac{(C_o - C_t)100}{C_o} \tag{1}$$

$$Amount\ of\ adsorption\ (Q) = \frac{(C_o - C_t)V}{m} \tag{2}$$

$C_o$ is the initial dye concentration (mg L$^{-1}$) whereas $C_t$ is the dye concentration after adsorption, $V$ dye volume (mL), $m$ adsorbent mass (g). pH values of the medium were adjusted by addition of 0.10 M HCl or NaOH.

## 3. RESULTS AND DISCUSSION

### 3.1. Characteristics studies

#### 3.1.1. FTIR analysis

Surface functionalities of adsorbent in adsorption process are very important. Functional groups found on its surface of almond shell were determined by FTIR analysis. Fig. 1 indicates the FTIR spectra of RAS, SAS, and DSAS saturated MB dye. As seen in RAS spectrum, the peaks at 3600-3100, 1733, 1591, 1236 and 1020 cm$^{-1}$ belong to different functional groups which are O-H stretch of alcohols and phenols, C=O stretch of ketones and carboxyl groups, C=C stretch of aromatic ring and C-O ether stretching respectively that RAS has many functional groups. New bands were seen in spectra of SAS at 1300-1150 cm$^{-1}$ (S=O), 1000-750 cm$^{-1}$ (S-O) which were not appeared in RAS spectra, suggesting the conversion of ester to carboxylic acid [23]. As seen in DSAS spectra, three new bands which indicated the associated with the C–N stretch (aromatic amines) and C–H bending (CH2 and CH3), and the C–H (aromatics) after the adsorption of MB dye were observed in the DSAS spectrum at 1325 cm$^{-1}$, 1383cm$^{-1}$ and 882 cm$^{-1}$ respectively. These three distinct new bands indicate that the MB joined to SAS. Moreover, expansion in O-H bands shows that hydroxyl groups on adsorbent surface have extremely effect onto removal of MB.
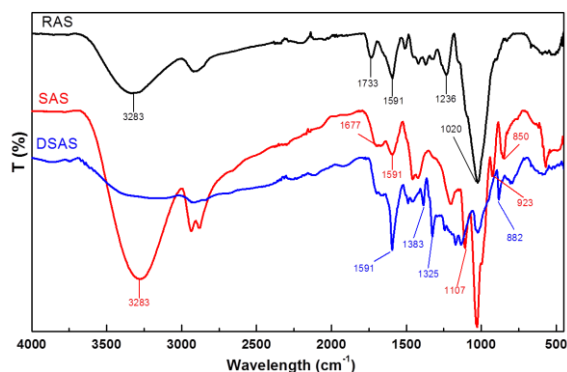
**Fig 1.** ATR-FTIR spectra of RAS, SAS and DSAS

### 3.1.2. SEM analysis

SEM images of RAS, SAS and DSAS were shown in Fig. 2. As shown in Fig. 2, while there are many micro pores in SEM image of RAS, there are many larger and deeper pores similar to chamber in SEM images of SAS. These chambers could be seen clearly in Fig. 2-c with higher magnification (x5000). These chambers can make positive effects on both the adsorption capacity of SAS and the rate of methylene blue removal of SAS. After adsorption of MB, the chambers were filled with dye evidently as seen in Fig. 2-d. The other words, it can be said that the dye molecules bind to the chamber of adsorbent. Compare to the literature it can be seen that same activator (sulphuric acid) has different effect on adsorbent surface which was used biosorbent [24].
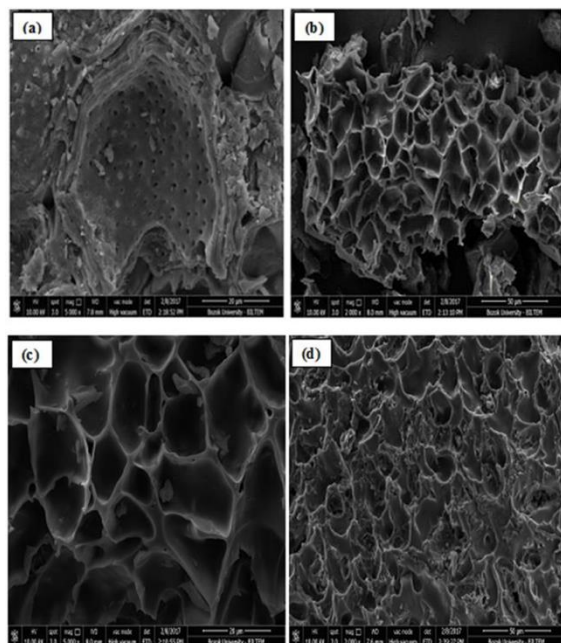


**Fig 2.** SEM images of a) RASx5000 b) SASx2000 c) SASx5000 d) DSASx2000

### 3.1.3. BET analysis

The adsorbent surface structure such as surface area and pore structure that are crucial for adsorption can be changed with used activation reagent [24-26]. BET analysis results of RAS and SAS were given in Table 2. As seen in Table 2, the surface properties of RAS

which is important for adsorption substantial varied with the acid employed. Particularly, pore volume and the pore size were increased significantly.

**Table 2.** BET results of almond shells

| Adsorbent Type | Single point surface area (m² g⁻¹) | Pore Volume (m³ g⁻¹) | Pore Size (A⁰) |
|---|---|---|---|
| RAS | 0.1504 | 0.000564 | 224.8282 |
| SAS | 0.2073 | 0.000643 | 283.1749 |

### 3.2. Batch adsorption studies

### 3.2.1. Effect of adsorbent dose

Adsorbent dose is an important parameter for adsorption capacity. Fig. 3 shows the relationship adsorbent dose, removal (%) and adsorption capacity. As seen in Fig. 3, the amount of adsorption decreased with the increasing amount of adsorbent, while the removal percentage increased until a certain amount of adsorbent then the removal percentage remained constant further increasing the adsorbent amount. While this unchanging in adsorption amount can be interpreted by the saturation of the adsorbent, decreasing of adsorption amount can be explained by unit adsorbent. Because adsorption amount is calculated per unit of adsorbent, the amount of adsorption (Q) decreased. Similar results have been observed in some studies in the literature [27-29]. The optimum amount of adsorbent was determined to be about 3.4 g L⁻¹ and this value was used in subsequent studies.
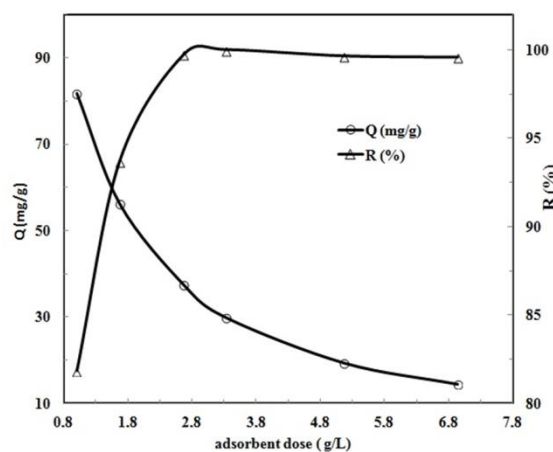


**Fig 3.** Effect of adsorbent dose [T = 25°C; t= 5 h; Ci = 100 ppm; pH = 10]

### 3.2.2. Effect of pH

The effect of pH on removal of MB onto RAS and SAS was shown in Fig. 4. As shown in Fig. 4, removal of MB by RAS increased with pH change but removal of MB by SAS was almost not changed with pH change together with high removal efficiency. Similar observations have been reported in literature for the adsorption of methylene blue on different adsorbent [30, 31]. At low pH, low adsorption of RAS can be explained due to the competitive adsorption between cationic dye and excess H⁺ in the solution. Increased

pH enhances negativity of adsorbent and this situation leads to the strong attraction between the negatively charged surfaces and positively charged MB dye as a result adsorption increases. The fact that the amount of adsorption of SAS does not change with increasing pH can be explained by the decreasing pHZBC of SAS [24]. As seen in Table 3, SAS can be used a wide pH range without much change in adsorption capacity and removal efficiency compared with the given some studies in literature. In this case there is no need for pH adjustment. The use of a large pH range without pH adjustment is a great advantage over pH-sensitive adsorbents in wastewater treatment. The results indicate that the SAS can be used for dye removal in different media. Also, when compared to the other adsorbents given in Table 3, SAS has superiority with high efficiency in a wide pH range.
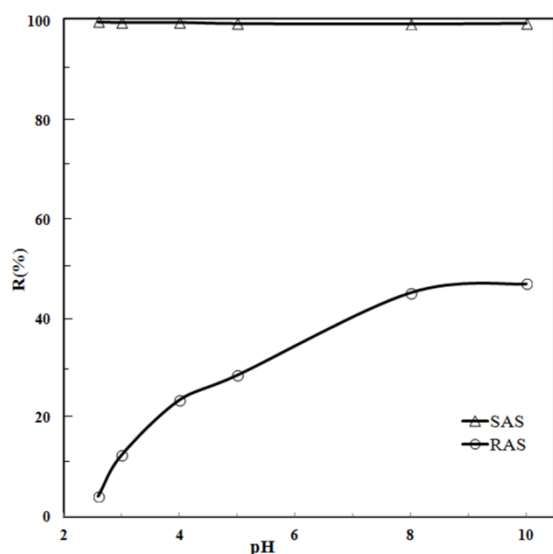


**Fig 4.** Effect of p [T = 25°C; t= 5 h; Ci = 100 ppm]

**Table 3.** Comparison of solution pH on the adsorption of MB by different adsorbents

| Adsorbents | pH range | Percentage of | References |
|---|---|---|---|
| Activated-clay | 2–9 | 60–95 | [33] |
| Pine leaves | 2–11 | 20–80 | [34] |
| Pine cone | 3.47–7.28 | 63.83–94.82 | [35] |
| Tobacco Stem Ash | 2.08–7.93 | 60–81 | [36] |
| Fly ash | 2–8 | 36–45 | [37] |
| Activated-carbon | 2–11 | Increase | [38] |
| Modified sawdust | 2–11 | Increase | [39] |
| SALC | 3 - 11 | 60-85 | [40] |
| EB bio-char | 4.8–11.3 | 53.4- 80.5 | [41] |
| SAS | 2-10 | 99.88-99.59 | This study |

### 3.2.3.    *Effect of dye concentration*

The effect of the initial dye concentration on the adsorption amount and removal (%) of methylene blue on SAS is shown in Fig. 5. As shown in Fig. 5, initial dye concentration increasing from 50 to 500 mg L$^{-1}$, the adsorption capacity of SAS increased from 14.95 to 131 mg g$^{-1}$ due to increased driving force

[32]. While the increase in dye concentration over 500 mg L$^{-1}$, the adsorption capacity did not change. This phenomenon indicates that the SAS has reached saturation. Also as shown Fig. 5, high removal (%) did not change until 400 mg L$^{-1}$. This high removal at wide concentration range is important in industrial application. After that, dye concentration increased from 400 mg L$^{-1}$ to 700 mg L$^{-1}$, removal (%) of dye decreased from 99.67 to 67.44 respectively. SAS can be an effective adsorbent for MB removal in the broad concentration range compared to the adsorbents in literatures (Table 4). As a result, it has been observed that SAS has remarkable absorptive efficiency.
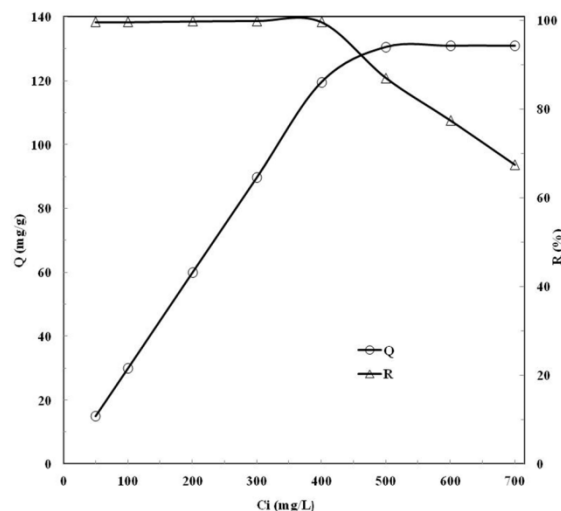


**Fig 5.** Effect of initial dye concentration [pH = 10; T = 25 °C; t = 5 h]

**Table 4.** Comparison of initial dye concentration on the adsorption of MB by different adsorbents

| Adsorbents | Initial Dye Concentration range (ppm) | Percentage of removal range (%) | References |
|---|---|---|---|
| Kaolin | 10-40 | 90–62 | [42] |
| Modified sawdust | 25-500 | 91.2–66.3 | [39] |
| Raw mango seed | 50-250 | 99.1–92.5 | [43] |
| Modified mango seed | 50-250 | 99.9–96.9 | [43] |
| SALC | 50-200 | 95-91 | [40] |
| EB bio-char | 10-100 | 80.5- 36.8 | [41] |
| SAS | 50-400 | 99.9-99.6 | This study |

### 3.2.4.    *Effect of time*

In the adsorption studies, rapid removal for a good adsorbent is as important as high adsorption capacity. The effect of contact time on adsorption of MB onto SAS was studied at room temperature from 0 to 360 min and the obtained results were shown in Fig. 6. The adsorption of MB on the SAS was observed very quickly in the first hour for all of studied dye concentration due to initially the abundance of active sites and the increase in contact time did not

significantly increase the adsorption because of saturation of active sites on the SAS.
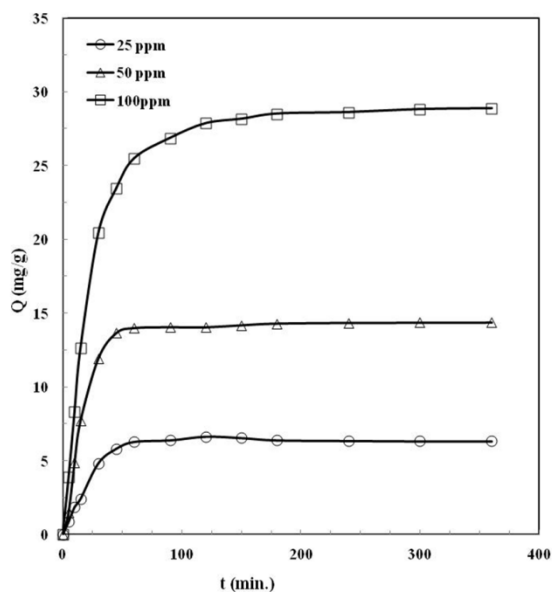


**Fig 6.** Effect of time [pH = 10; T = 25 °C]

### 3.3. Adsorption isotherms

Adsorption isotherms are necessary for understanding the surface properties of the adsorbents, for the determination of the capacities and to be able to explain the possible mechanism of adsorption. Also, they describe how the pollutants interact with the adsorbent material. The most commonly used adsorption models Langmuir and Freundlich isotherm models were used to describe the experimental data of MB adsorption onto SAS.

Langmuir model, given equation below, describes the monolayer adsorption of dye molecules on a homogeneous surface.

$$\frac{C_e}{q_e} = \frac{1}{K_L} + \left(\frac{a_L}{K_L}\right) C_e \qquad (3)$$

where; $C_e$ is the equilibrium concentration of adsorbate in solution after adsorption (mg L$^{-1}$), $q_e$ is the equilibrium solid phase concentration (mg g$^{-1}$), as well as $K_L$ (L g$^{-1}$) and $a_L$ (L mg$^{-1}$) are the Langmuir constants.

However, the Freundlich isotherm supposes a heterogeneous surface with a non-uniform distribution and can be expressed by Eq. 4:

$$\log q_e = \log K_F + \frac{1}{n} log \, C_e \qquad (4)$$

where $K_F$ (L g$^{-1}$) is the adsorption capacity at unit concentration and $1/n$ is adsorption intensity. The plot of $C_e/q_e$ vs. $C_e$ for Langmuir isotherm model (Fig. 7) and $log \, q_e$ vs $log \, C_e$ for Freundlich model (not given) were drawn from the experimental data given in Fig. 5. In this study, obtained isotherm parameters were shown in Table 5. As seen in the Table 5, the adsorption of methylene blue on the SAS was found to be the best fitted to the Langmuir Isotherm because of the higher correlation coefficient and closeness of $q_{exp}$ and $q_e$ [41]. Thus, adsorption centers on SAS are

identical energetic and it can be said that methylene blue adsorption on SAS is monolayer. Found adsorption capacity of SAS was compared in Table 6 that of another adsorbents capacities given in literature. It makes clearly that the SAS has a high adsorption capacity for MB compared with other materials.

The separation factor ($R_L$) [40] for adsorption of MB on SAS was calculated from the Langmuir adsorption isotherm parameters and given in Fig. 8. As can see in Fig. 8, the value of $R_L$ varies from 0.0120 to 0.0009 for the initial MB dye concentration of 100-700 mg L$^{-1}$. This indicates that the adsorbent prepared from the almond shell is favorable for adsorption of MB [41].
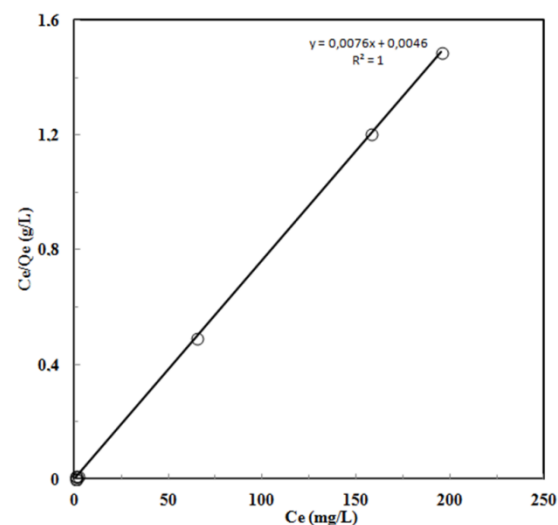


**Fig 7.** Langmuir isotherm plot of almond shell

**Table 5.** Isotherm parameters onto SAS of MB obtained from equilibrium models

| Isotherm Models | Parameter (unit) | Value |
|---|---|---|
| Langmuir | $K_L$ (L g$^{-1}$) | 227.272 |
| | $a_L$ (L mg$^{-1}$) | 1.727 |
| | $Q_{max}$ (mg g$^{-1}$) | 131.578 |
| | $R^2$ | 1 |
| Freundlich Isotherm | $n_F$ | 5.546 |
| | $K_F$ | 57.108 |
| | $R^2$ | 0.4934 |

**Table 6.** Comparison of found adsorption capacity of MB with various adsorbents

| Adsorbent | Q (max) | References |
|---|---|---|
| Powdered activated carbon | 91 | [44] |
| Nut shell activated carbon | 5.3 | [45] |
| Palm tree activated carbon | 128 | [46] |
| Act. almond shell (750 °C) | 1.33 | [47] |
| Activated carbon from Walnut shell | 3.53 | [47] |
| Coir pith activated carbon | 5.87 | [48] |
| Activated carbon from Hazelnut shell | 8.82 | [47] |
| SAS | 131.58 | This study |

### 3.4. Adsorption kinetics

Three kinetic models, pseudo-first order, pseudo-second order and intraparticle diffusion model which were used frequently in the adsorption studies, were used in order to investigate the adsorption mechanism of MB on SAS. Pseudo-first order [40], pseudo-second order [41–43] and intraparticle diffusion model [44–46] were given in 5, 6 and 7 equation respectively.

$$ln(Q_e - Q_t) = lnQ_e - k_1 t \tag{5}$$

$$\frac{t}{Q_t} = \frac{1}{k_2 Q_e^2} + \frac{1}{Q_e} t \tag{6}$$

$$Q_t = k_{id} t^{1/2} \tag{7}$$

Where, $Q_t$ and $Q_e$ (mg g$^{-1}$) are the amount of adsorption on the activated SAS at time $t$ and equilibrium, $k_1$ (min$^{-1}$), $k_2$ (g mg$^{-1}$min$^{-1}$) and $k_{id}$ (mg g$^{-1}$ min$^{-1/2}$) are the rate constant for the pseudo-first-order, the pseudo-second-order and the intraparticle diffusion models respectively. For first order kinetic model the linear plot of $ln$ $(Q_e - Q_t)$ vs $t$ and for intraparticle diffusion model $Q_t$ vs $t^{1/2}$ were drawn. But, for regulation coefficient is too low, they could not be given. The values characteristic constants of adsorption were calculated from the slope and intercept of $t/Q_t$ vs. $t$ (Fig. 8) and the kinetic parameters obtained for adsorption of MB on SAS were given in Table 7. Pseudo-second order kinetic model is more convenient for MB adsorption onto SAS.

### 3.5. Reusability of SAS

In order to investigate the reusability of the SAS, the adsorption-desorption cycle was repeated five times with the same adsorbent [17] and the results shown in Fig 9. It was observed that the adsorption capacity of SAS did not considerably change after five adsorption desorption cycles. This results shows that SAS are good reusable adsorbent for the removal of MB from aqueous environment.
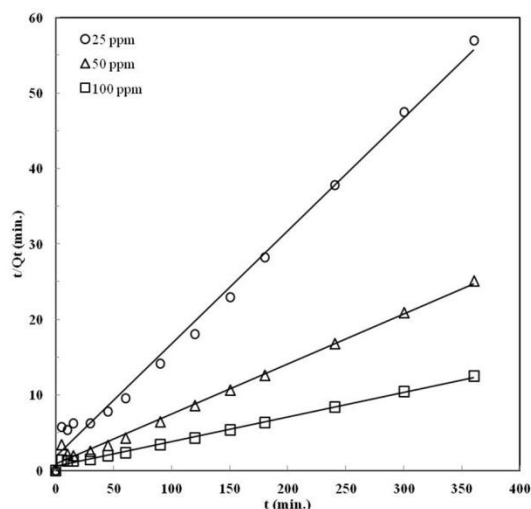


**Fig 8.** Pseudo-second-order plots for MB on almond shells. [pH = 10; T = 25 ºC]

**Table 7.** Values of pseudo second order kinetic model

| $C_o$ (mg L$^{-1}$) | $Q_{e, exp.}$ (mg g$^{-1}$) | $Q_{e, cal.}$ (mg g$^{-1}$) | $k_2$ (g mg$^{-1}$min$^{-1}$) | $R^2$ |
|---|---|---|---|---|
| 25 | 6.50 | 6.69 | 0.0110 | 0.992 |
| 50 | 14.36 | 15.06 | 0.0053 | 0.992 |
| 100 | 28.86 | 30.48 | 0.0020 | 0.995 |
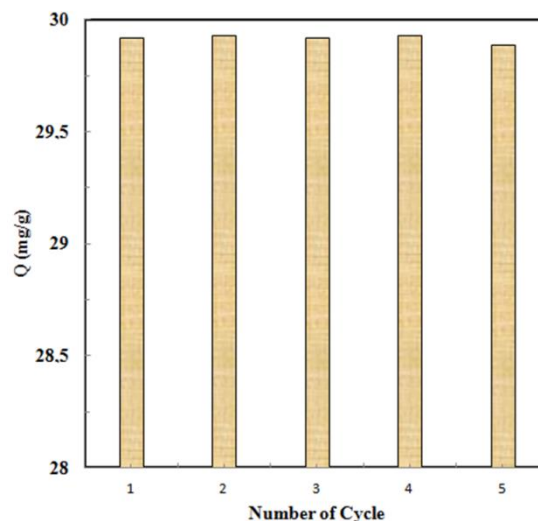


**Fig 9.** Reusability of SAS [pH = 10; $C_i$ = 100 ppm; t = 3 h; T = 25 ºC]

## 4. CONCLUSIONS

It was observed that the almond shell could be activated by a simple and easy method for increasing adsorption capacity and its the surface properties such as pore structure pore volume and surface area of the almond shells could be changed by activation. It has been determined that SAS can be used as an effective adsorbent to remove MB at a wide pH and concentration range. MB adsorption on SAS was determined to be suitable to Langmuir isotherm and second order kinetic model. Also, it was observed that SAS could be regenerated with 5 M HNO$_3$ and can be reusable at least five times without losing their adsorption capacity. As a result, almond shells may be an alternative adsorbent to more costly adsorbents for removing dye in wastewater treatment processes.

### REFERENCES

[1]. T. Madrakian, A. Afkhami, H. Mahmood-Kashani and M. Ahmadi, "Adsorption of some cationic and anionic dyes on magnetite nanoparticles-modified activated carbon from aqueous solutions: equilibrium and kinetics study",

*Journal of Iranian Chemical Sciety*, Vol. 10 (3), pp. 481-489, 2013.

[2]. X.-G. Li, X.-L. Ma, J. Sun and M.-R. Huang, "Powerful reactive sorption of silver(i) and mercury(II) onto poly(o-phenylenediamine) microparticles", *Langmuir*, Vol. 25 (3), pp. 1675–1684, 2009.

[3]. X. Gu, J. Zhou, A. Zhang, P.Wang,M. Xiao and G. Liu, "Feasibility study of the treatment of aniline hypersaline wastewater with a combined adsorption/bio-regeneration system", *Desalination*, Vol. 227 (1-3), pp. 139–149, 2008.

[4]. J.G. Cai, A. Li, H.Y. Shi, Z.H. Fei, C. Long and Q.X. Zhang, "Adsorption characteristics of aniline and 4-methylaniline onto bifunctional polymeric adsorbentmodifiedby sulfonic groups", *Journal of Hazardous Materials*, Vol. 124 (1-3), pp. 173-180, 2005.

[5]. E. Forgacs, T. Cserhati and G.Oros, "Removal of synthetic dyes from wastewaters: a review", *Environment International*, Vol. 30 (7), 953-971, 2004.

[6]. T. Robinson, G. McMullan, R. Marchant and P. Nigam, "Remediation of dyes in textile effluent: a critical review on current treatment technologies with a proposed alternative", *Bioresource Technology*, Vol. 77 (3), pp. 247-255, 2001.

[7]. S. Papic, N. Koprivanac, A.L. Bozic and A. Metes, "Removal of some reactive dyes from synthetic wastewater by combined Al(III) coagulation/carbon adsorption process", *Dyes and Pigments*, Vol. 62 (3), pp. 293-300, 2004.

[8]. T.H. Kim, C.H. Park, E.B. Shin and S.Y. Kim, "Decolorization of disperse and reactive dye solutions using ferric chloride", *Desalination*, Vol. 161 (1), pp. 49-58, 2004.

[9]. K. Nakagawa, A. Namba, S.R. Mukai, H. Tamon, P. Ariyadejwanich and W. Tanthapanichakoon, "Adsorption of phenol and reactive dye from aqueous solution on activated carbons derived from solid wastes", *Water Research*, Vol. 38 (7), pp. 1791-1798, 2004.

[10]. K.G. Bhattacharyya and A. Sharma, "Kinetics and thermodynamics of methylene blue adsorption on neem (Azadirachta indica) leaf powder", *Dyes and Pigments*, Vol. 65 (1), pp. 51-59, 2005.

[11]. A. Bhatnagar, M. Sillanpää and A. Witek-Krowiak, "Agricultural waste peels as versatile biomass for water purification — a review", Chemical Engineering Journal, Vol. 270, pp. 244-271, 2015.

[12]. R.K. Gautam, A. Mudhoo, G. Lofrano and M.C. Chattopadhyaya, "Biomass-derived biosorbents for metal ions sequestration: Adsorbent modification and activation methods and adsorbent regeneration". *Journal of Environmental Chemical Engineering,* Vol. 2 (1), pp. 239-259, 2014.

[13]. I. Ali, M. Asim and T.A. Khan, "Low cost adsorbents for the removal of organic pollutants from wastewater", *Journal of Environmental Management*, Vol. 113, pp. 170-183, 2012.

[14]. M.V. Dinu and E.S. Dragan, "Heavy metals adsorption on some iminodiacetate chelating resins as a function of the adsorption parameters", *Reactive and Functional Polymers*, Vol. 68 (9), pp. 1346-1354, 2008.

[15]. X. Zhao, G. Zhang, Q. Jia, C. Zhao, W. Zhou and W. Li, "Adsorption of Cu(II), Pb(II), Co(II), Ni(II), and Cd(II) from aqueous solution by poly(aryl ether ketone) containing pendant carboxyl groups (PEK-L): equilibrium, kinetics, and thermodynamics", *Chemical Engineering Journal*, 171 (1), pp. 152-158, 2011.

[16]. S. Cavus, G. Gurdag, K. Sozgen and M.A. Gurkaynak, "The preparation and characterization of poly(acrylic acid-co-methacrylamide) gel and its use in the non-competitive heavy metal removal", *Polymers for Advanced Technologies*, Vol. 20, 165-172, 2009.

[17]. C. Ramazan and D. Ali, "Removal of methylene blue from aqueous solutions by poly (2-acrylamido-2-methylpropane sulfonic acid-co-itaconic acid) hydrogels", *Polymer Bulletin*, Vol. 68 (7), pp. 1889–1903 2012.

[18]. Y. Bulut and H. Aydin, "A kinetics and thermodynamics study of methylene blue adsorption on wheat shells", *Desalination*, Vol. 194 (1-3), pp. 259-267, 2006.

[19]. R. Mohd, S. Othman, H. Rokiah and A. Anees, "Adsorption of methylene blue on low-cost adsorbents: a review", *Journal of Hazardous Materials*, Vol. 177 (1-3), pp. 70-80, 2010.

[20]. S. Deng, R. Bai and J.P. Chen, "Aminated polyacrylonitrile fibers for lead and copper removal", *Langmuir*, Vol. 19 (12), pp. 5058-5064, 2003.

[21]. C. Ramazan, S. Cengiz and S. Mehmet, "Adsorption of copper(II), nickel(II) and cobalt(II) ions from aqueous solution by methacrylic acid/acrylamide monomer mixture grafted poly(ethylene terephthalate) fiber", *Separation and Purification Technology*, Vol. 49 (2), pp. 107–114, 2006.

[22]. C. Ramazan, S. Cengiz and S. Mehmet, "Removal of some heavy metal ions from aqueous solution by adsorption using poly(ethylene terephthalate)-g-itaconic acid/ acryl- amide fiber", *Reactive and Functional Polymers*, Vol. 66 (6), pp. 599–608, 2006.

[23]. M. Ismail, M.A.K.M Hanafiah, M.S.Z. Abidin, Z.M. Hussin and K. Khalid, "Kinetics of Methylene Blue Adsorption on Sulphuric Acid Treated Coconut (Cocos nucifera) Frond Powder", *American Journal of Environmental Engineering*, Vol. 5(3A), pp. 33-37, 2015.

[24]. C. Ramazan, Y. Abdurrahim and D. Ali, "Removal of Methylene Blue Using Fast Sucking Adsorbent", *Journal of materials and Environmental Sciences*, Vol. 8(2), pp. 398-409, 2017.

[25]. K. Beyhan and K. Erdem, "Batch and column removal of the dye blue 3R over pumice", *Desalination and Water Treatment*, Vol. 57, pp. 1-14, 2016.

[26]. D. Hui, L. Guoxue, Y. Hongbing, T. Jiping and T. Jiangyun, "Preparation of activated carbons from cotton stalk by microwave assisted KOH and $K_2CO_3$ activation", *Chemical Engineering Journal*, Vol. 163 (3), pp. 373-381, 2010.

[27]. Y. Tang, X. Wang and L. Zhu, "Removal of methyl orange from aqueous solutions with poly(acrylic acid-co-acrylamide) superabsorbent resin", *Polymer Bulletin*, Vol. 70 (3), pp. 905-918, 2013.

[28]. D. Hui, L. Jianjiang, L. Guoxue, Z. Genlin and W. Xugen, "Adsorption of methylene blue on adsorbent materials produced from cotton stalk", *Chemical Engineering Journal,* Vol. 172 (1), pp. 326-334, 2011.

[29]. L. Hem, V.K. Garg and R.K. Gupta, "Removal of a basic dye from aqueous solution by adsorption using Parthenium hysterophorus: An agricultural waste", *Dyes and Pigments*, Vol. 74 (3), pp. 653-658, 2007.

[30]. P. Waranusantigul, P.Pokethitiyook, M. Kruatrachue and E.S. Upatham, "Kinetics of basic dye (methylene blue) biosorption by giant duckweed (Spirodela polyrrhiza)", *Environmental Pollution*, Vol. 125 (3), pp. 385-392, 2003.

[31]. V.K. Garg, A. Moirangthem, R. Kumar and R. Gupta, "Basic dye (methylene blue) removal from simulated waste water by adsorption using Indian Rosewood Sawdust: timber industry waste". *Dyes and Pigments,* Vol. 63 (3), pp. 243-250, 2004.

[32]. Y. Bulut and H. Aydin, "A kinetics and thermodynamics study of methylene blue adsorption on wheat shells", *Desalination*, Vol. 194 (1-3), pp. 259-267, 2006.

[33]. C.H. Weng and Y.F. Pan, "Adsorption of a cationic dye (methylene blue) onto spent activated clay", *Journal of Hazardous Materials*, Vol. 144 (1), pp. 355-362, 2007.

[34]. M.T. Yagub, T.K. Sen and H. Ang, "Equilibrium, kinetics, and thermodynamics ofmethylene blue adsorption by pine tree leaves", *Water Air Soil Pollution*, Vol. 223 (8), pp. 5267–5282, 2012.

[35]. T.K. Sen, S. Afroze and H. Ang, "Equilibrium, kinetics and mechanism of removal of methylene blue from aqueous solution by adsorption onto pine cone biomass of Pinus radiata", *Water Air Soil Pollution*, Vol. 218 (1-4), pp. 499-515, 2011.

[36]. R.K. Ghosh and D.D. Reddy, "Tobacco Stem Ash as an adsorbent for removal of methylene blue from aqueous solution: equilibrium, kinetics, and mechanism of adsorption". *Water Air Soil Pollution*, Vol. 224 (6), pp. 1-12, 2013.

[37]. K.V. Kumar, V. Ramamurthi and S. Sivanesan, "Modeling the mechanism involved during the sorption of methylene blue onto fly ash", *Journal of Colloid and Interface Science*, Vol. 284 (1), pp. 14-21, 2005.

[38]. N. Kannan and M.M. Sundaram, "Kinetics and mechanism of removal of methylene blue by adsorption on various carbons—a comparative study", *Dyes and Pigments*, Vol. 51 (1), pp. 25-40, 2001.

[39]. W. Zou, H. Bai S. Gao and K. Li, "Characterization of modified sawdust, kinetic and equilibrium study about methylene blue adsorption in batch mode", *Korean Journal of Chemical Engineering*, Vol. 30 (1), pp. 111-122, 2013.

[40]. S. A. Omotayo, O. O. Akeem, O. A. Abass, G. F. Abolaji and A. A. Segun, "Adsorption of methylene blue from aqueous solution using steam-activated carbon produced from *Lantana camara* Stem", *Journal of Environmental Protection*, Vol. 5 (13), pp. 1352-1363, 2014.

[41]. D. Sara, K. S. Tushar and P. Chi, "Adsorption removal of Methylene Blue (MB) dye from aqueous solution by bio-char prepared from Eucalyptus sheathiana bark: kinetic, equilibrium, mechanism, thermodynamic and process design", *Desalination and Water Treatment*, Vol. 57 (59), pp. 28964–28980, 2016.

[42]. A. R. Tehrani-Bagha, H. Nikkar, N. M. Mahmoodi, M. Markazi and F. M. Menger, "The sorption of cationic dyes onto kaolin: kinetic, isotherm and thermodynamic studies", *Desalination*, Vol. 266 (1), pp. 274-280, 2011.

[43]. P. S. Kumar, M. Palaniyappan, M. Priyadharshini, A.M. Vignesh, A. Thanjiappan, P. S. A. Fernando, R. T. "Ahmed and R. Srinath, Adsorption of basic dye onto raw and surface-modified agricultural waste", *Environmental Progress & Sustainable Energy*, Vol. 33 (1), pp. 87-98, 2013.

[44]. J. Yener, T. Kopac, G. Dogu and T. Dogu, "Dynamic analysis of sorption of Methylene Blue dye on granular and powdered activated carbon", *Chemical Engineering Journal*, Vol. 144, pp. 400-406, 2008.

[45]. S. Ragupathy, K. Raghu and P. Prabu, "Synthesis and characterization of $TiO_2$ loaded cashew nut shell activated carbon and photocatalytic a activity on BG and MB dyes under sunlight radiation, Spectrochim", *Spectrochimica Acta Part A: Molecular and Biomolecular Spectroscopy*, Vol. 138, pp. 314-320, 2015.

[46]. Z.A. AlOthman, M.A. Habila, R. Ali, A. Abdel Ghafar and M.S. El-din Hassouna, "Valorization of two waste streams into activated carbon and studying its adsorption kinetics, equilibrium isotherms and thermodynamics for methylene blue removal", *Arabian Journal of Chemistry*, Vol. 7 (6), pp. 1148-1158, 2014.

[47]. A. Aygun, S. Yenisoy-Karaka and I. Duman, "Production of granular activated carbon from fruit stones and nutshells and evaluation of their physical, chemical and adsorption properties", *Microporous Mesoporous Materials*, Vol. 66 (2-3), pp. 189-195, 2003.

[48]. D. Kavitha and C. Namasivayam, "Experimental and kinetic studies on methylene blue adsorption by coir pith carbon", *Bioresource Technology*, Vol. 98 (1), pp. 14-21, 2007.

Turkish **JournalPark** ACADEMIC

## Environmental Research & Technology

**RESEARCH ARTICLE**

# The treatment of baker's yeast wastewater by an up flow anaerobic sludge blanket (UASB) reactor

Abdullah Saghir[1,*], Salwa Hajjar[2],

[1,*] Dept of Civil Engineering, Faculty of Engineering of Aljazeera University, SYRIA
[2] Dept of Environmental, Faculty of Civil Engineering University of Aleppo, SYRIA

## ABSTRACT

The objective of the research is to study the ability of baker's yeast wastewater (BYW) treatment by a Up Flow - Anaerobic Sludge Blanket (UASB) reactor. The effect of the temperature of BYW on the efficiency of treatment in a UASB was investigated and the experiments showed that it is possible to achieve good removal efficiency of chemical oxygen demand (COD) (10200-16320) mg $L^{-1}$ when the temperature of BYW is about $(35\pm2)°C$ and hydraulic retention time (HRT) = 24 h. The removal efficiency fit with temperature value of wastewater in UASB reactor for the following values of temperature of $(11\pm2; 16\pm2; 26\pm2; 26\pm2; 31\pm2; 35\pm2)$ °C. The removal efficiencies of COD were: (36.6%; 37.9%; 43%; 44.2%; and 48.8%) respectively. The effect of changing the values of HRT on the efficiency removal at a temperature $(35\pm2)$ °C value was investigated. The experiments illustrated that it is possible to achieve good removal efficiency for high concentrations of COD when the temperature of the BYW is fixed at $(35\pm2)$ °C and HRT>=24 h. The removal efficiency fits with HRTs values. For the following values of HRTs: (18; 24; 30; 36) h, the removal efficiencies of COD were: (32.9%; 48.8%; 48.95%; 51.3%) respectively.

*Keywords:* Anaerobic biological treatment, UASB reactor, baker's yeast wastewater

## 1. INTRODUCTION

The high organic load wastewater discharged from industries is one of the most critical causes of pollution in the nature if left untreated. It contaminates the groundwater and, if it is discharged into the sewer network without sufficient treatment, it causes an increase in the organic and hydraulic loads in sewage treatment plants [1]. This may cause operational problems that can reduce the efficiency of treatment. In spite of the existence of BYW in many governorates of Syria, there are no treatment plants to treat the wastewater from baker's yeast. This wastewater is heavily polluted so it is very important to find the best way to treat it. In anaerobic reactors, maintenance of sufficient methanogenic population is critical for stable performance of the systems. Also, the methanogenic activity is very important for operation UASB reactors [2].

The production of baker's yeast by fermentation which generally uses molasses as the raw materials includes operations and processes such as molasses preparation, fermentation, and separation and drying

of yeast, it produces a large quantity of wastewater [3, 4]. Various treatment methods like biological process, physico-chemical treatment, adsorption, membrane process, reverse osmosis, coagulation/flocculation and oxidation processes, have been attempted for the treatment of BYEs [3].

The objective of the research is to study the ability of BYW treatment by a UASB reactor and recognize the effect of changing the temperature degree of baker's yeast wastewater on the efficiency removal of the pollutants and define the best HRT for achieving the best efficiency removal of pollutants.

In this research, the effect of the temperature of baker's yeast wastewater on the efficiency of treatment in UASB was investigated. UASB reactor was selected because UASB reactors have been strongly used for industrial and domestic wastewater treatment [5] UASB reactors have not mechanical equipment and there is no need for primary sedimentation and sludge thickeners, and low sludge production with good settling properties in general. Also UASB reactors are economical to build, their

operational conditions are suitable for the climate in Syria and they are easy to operate and produce $CH_4$ which can be used to generate electricity and heat.

The flow of Aleppo BYW is about 853 $m^3$ $day^{-1}$. The efficiency of treatment of BYW of Aleppo baker's yeast factory was studied by the UASB reactor with continuous flow. The characteristics of BYW which was studied in the research are :COD(12385-27600) mg $L^{-1}$, Total dissolved solids (TDS):(13482-23106) mg $L^{-1}$, Total suspended solids (TSS): (428-1460) mg $L^{-1}$, pH: (6.42-7.65) mg $L^{-1}$, $SO_4^{2-}$:(1850-3980) mg $L^{-1}$, $PO_4^{3-}$: (290-500) mg $L^{-1}$, $NH_4^+$: (243-740) mg $L^{-1}$, oil and grease (160-359) mg $L^{-1}$, $Na^+$: (738-1038) mg $L^{-1}$, and $K^+$ (621-1090.5) mg $L^{-1}$.

The BYW is considered highly polluted the concentration of COD in it is about (12385-27600) mg $L^{-1}$, and the average value of concentration of COD is 13650 mg $L^{-1}$. The average value of COD is very high and it is higher than value of COD of domestic wastewater in Aleppo city which is about 650 mg $L^{-1}$, about 21 times. So, it causes an increase in organic loads on Aleppo wastewater treatment plant. pH value of BYW for most samples is below than 7 which mean that BYW is the value of acidic wastewater same result reported by the references [6, 7] which can lead to a serious danger to the public sewer system because acid water causes erosion in the public sewer system. BYW contains high concentrations of $SO_4^{2-}$ and sometimes its value is up to 3500 mg $L^{-1}$, which causes the release of $H_2S$, which is considered as a hazardous gas that can lead to risks to the workers working in the maintenance of sewerage networks. As well as causing damage to public sewerage systems a high concentration of sulphate reduces the efficiency of anaerobic biological treatment [8], it also contains high concentration of oil and grease. sometimes its value is up to 350 mg $L^{-1}$, which damages the public sewerage system, the pumping station and the treatment plant, and contains high concentrations of TDS, TSS, and TS, increasing the amount of sludge formed at the main treatment plant and increasing the value of organic loads. The average flow of BYW in Aleppo is about 850 $m^3$ $day^{-1}$, which equals to the discharged flow of 5667 persons of Aleppo as the organic load of this factory is equal to the organic load from 119000 persons so it is necessary for treat this wastewater. The concentration of TDS for the industrial wastewater of baker's yeast is (13482-23016) mg $L^{-1}$. So, it is expected to be inhibited the activity of methanogenic/anaerobic bacteria because of the high the salinity which will minimize the efficiency of BYW treatment according to the references, [7, 9]. Because the biological wastewater treatment was inhibited by high concentration of $SO_4^{2-}$, total nitrogen, eventually becoming reduced to toxic $H_2S$ and high total nitrogen content [10].

Authors hope that the outcomes of this research contribute to solving the problem of pollution of the environment by BYW. Anaerobic treatment is the preferred biological treatment because of its effectiveness in treating high-strength wastewater [11]. Anaerobic treatment is one of the most

important processes used for the treatment of high organic load wastewater.

## 2. MATERIALS AND METHODS

All experiments were performed according to the international Standard Methods for the Examination [12] adopted in the field of wastewater and industrial analysis and a real (not make up the laboratory) BYW was used in all stages of the research.

### 2.1. Design of Experimental UASB Reactor

Laboratory experiments were carried out in a plastic reactor with a total height of 92. 5 cm. The high-water level was 85 cm leaving 7.5 cm free height above the surface of the wastewater. The diameter of the reactor around the sludge bed was 10 cm, Fig 1. The temperature of wastewater in UASB reactor was controlled by a thermostat. The reactor was surrounded by insulant material to keep the temperature in the reactor steady, also a thermostat was used to control the temperature inside the reactor.
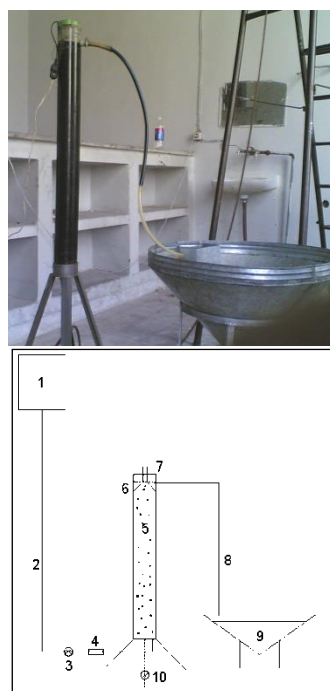


1- Feeding tank of raw wastewater

2- Pipes for carrying treated wastewater form UASB

3- Valves for control HRT value in the reactor

4-Flow meter

6- Dome for gas separating

7- Opening for exhaust the gases.

8- Pipes for carrying treated wastewater form UASB

9- Small tank for treated wastewater

10-Pipes and valve for drawing surplus sludge for UASB reactor.

**Fig 1.** Longitudinal section and pic of the experimental UASB Reactor

## 3. RESULTS AND DISCUSSION

### 3.1. UASB start up

The characteristics of the untreated BYW which was studied in startup phase of the treatment are showed in the following the Table 1.

**Table 1.** The characteristics of BYW which used in startup stage

| Parameter | Value |
|-----------|-------|
| pH | 7.65 |
| T°.C | 16.5 |
| TS (mg L$^{-1}$) | 23946 |
| TDS (mg L$^{-1}$) | 23106 |
| TSS (mg L$^{-1}$) | 840 |
| COD (mg L$^{-1}$) | 27600 |

All the volume of wastewater during startup phase was recycled and the HRT values was :24 hours according to the reference [13]. The temperature of wastewater was (16±2) °C within the laboratory reactor this temperature without any controlling it is the temperature of the laboratory room, that mean there was not any heating or cooling to control the temperature control, this operational conditions are suitable for the climate in Syria .

The entire flow was also recycled and no sedimentation was made to circulate the waster water to increase the concentration of the biomass within the laboratory UASB.

The results of start up phase are showed in the Table 2. After 34-38 days of the reactor. The value of the COD was fixed and there was no change in its value .

The startup of UASB rector was achieved after 38 days of starting feed the wastewater and the recycle ratio was 100% in closing loop. The removal efficiency of COD was about 49% because the biological wastewater treatment was inhibited by high concentration of $SO_4^{2-}$, total nitrogen [10] and high total dissolved solids.

### 3.2. The effect of the temperature of BYW on the efficiency of treatment in UASB

The effect of temperature on the efficiency of treatment of BYW by a UASB reactor was investigated by opeating the UASB reactor for 132 days after achieving startup, the duration of any stage under various operating temperatures continued about 6 days during it many samples were taken and analyzed and the average value showed in the Table 3, the temperature of BYW inside UASB was controlled by automatic thermostat which was used only for heating the BYW inside UASB reactor.

According to the reference [14] when COD value is more than 10000 mg L$^{-1}$, it is recommended that HRT in UASB equal or more than 24 hours, so HRT was fixed at 24 hours.

**Table 3.** The efficiency removal of pollutants of the experimental UASB according to the different values of the temperature of BYW

| Parameters | Temperature (°C) | | | | |
|------------|--------|--------|--------|--------|--------|
| | 11±2 | 16±2 | 26±2 | 31±2 | 35±2 |
| pH$_i$ | 7.15 | 6.6 | 6.5 | 6.42 | 6.67 |
| pH$_e$ | 7.64 | 7.44 | 7.56 | 7.79 | 7.82 |
| COD$_i$ (mg L$^{-1}$) | 15840 | 15133 | 15040 | 15065 | 12385 |
| COD$_e$ (mg L$^{-1}$) | 10042.6 | 9397.6 | 8572.8 | 8406.3 | 6341.1 |
| COD removal % | 36.6 | 37.9 | 43 | 44.2 | 48.8 |
| ORL (kg COD | 15.84 | 15.133 | 15.040 | 15.065 | 12.4 |
| TS$_i$ (mg L$^{-1}$) | 17603 | 14603 | 24290 | 19418 | 14700 |
| TS$_e$ (mg L$^{-1}$) | 17022 | 14123 | 22046 | 18081.4 | 13220.4 |
| TS removal % | 3.3 | 3.3 | 9.2 | 6.9 | 10.1 |
| TSS$_i$ (mg L$^{-1}$) | 1460 | 428 | 1063 | 881 | 1218 |
| TSS$_e$ (mg L$^{-1}$) | 1367 | 398 | 426.7 | 548.8 | 727.4 |
| TSS removal % | 6.4 | 7.0 | 59.9 | 37.7 | 40.3 |
| TDS$_i$ (mg L$^{-1}$) | 16768 | 14175 | 23227 | 18537 | 13482 |
| TDS$_e$ (mg L$^{-1}$) | 16236 | 13725 | 21619.3 | 17292.6 | 12493 |
| TDS removal % | 3.17 | 3.2 | 6.92 | 6.7 | 7.3 |

**Table 2.** Startup phase results

| Parameter | The time from startup (time) day | | | | | | | | |
|-----------|---|---|---|---|---|---|---|---|---|
| | 1 | 3 | 5 | 18 | 20 | 25 | 27 | 34 |
| COD (mg L$^{-1}$) | 20 | 22320 | 21600 | 17971 | 16320 | 16800 | 15400 | 14000 | 14100 |
| COD removal efficiency (%) | 0 | 19.1 | 21.7 | 34.9 | 40.9 | 39.1 | 44.2 | 49.3 | 49 |
| TSSe (mg L$^{-1}$) | 840 | --- | 126 | 450 | 105 | 175 | 145 | -- | --- |
| TSS removal efficiency (%) | -- | -- | 85 | 43 | 88 | 79 | 83 | -- | --- |
| TSe (mg L$^{-1}$) | 23946 | --- | 22216 | -- | 22760 | 22840 | -- | --- | -- |
| TS removal efficiency (%) | -- | --- | 7.2 | -- | 5.2 | 4.6 | -- | -- | -- |

The relation between temperature and the efficiency for COD removal is represented in the following equation and Fig 2.

$$COD_r = 0.4433 \times (T) + 31.13 \qquad (1)$$

Where T is temperature of wastewater in UASB reactor (°C) and $COD_r$ is COD removal efficiency (%).
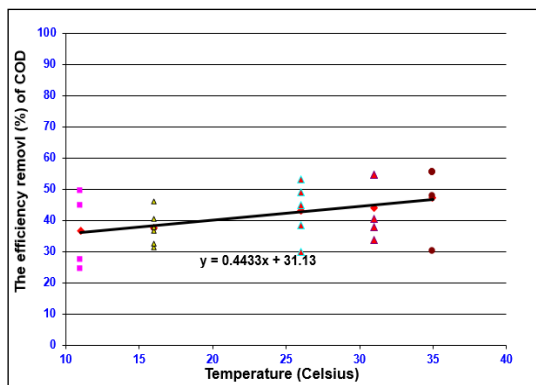


**Fig 2.** The relation between Temperature and the efficiency removal of COD

The volume organic rate load (ORL) applied to the laboratory UASB with in temperature (9-37) °C for BYW was (12.4-15.84) kg COD removal m$^{-3}$ day$^{-1}$ for COD value 12000-16000 mg L$^{-1}$ and HRT=24hours and the same result reported by the references [6, 15]. Whereas: OLR=COD$_i$ /HRT, COD$_i$: COD value before the treatment.

The efficiency removal of COD did not exceed 48.8% it is probably due to the high value of salinity, which studies the effect of methanogenic inhibitors: IC50 (inhibitory concentration 50%) for TDS: Salts (eg. Na$^+$, K$^+$, Ca$^{2+}$) of the anaerobic toxicity is IC50 = 4.700-7.600 mg L$^{-1}$. The concentration of TDS for the industrial wastewater of baker's yeast is (10790-23860) mg L$^{-1}$. So it is expected to be inhibited the activity of methanogenic/anaerobic bacteria because of the high the salinity, which will minimize the efficiency of BYW treatment. The same result was reported by the references [9, 10].

The efficiency removal of COD, TDS and TS increase with increasing the temperature of wastewater.

The efficiency removal of TDS and TS in UASB rector which treating BYW is too low (about 3.17 to 7.34% for TDS and 3.3-10% for TS). Increasing of wastewater temperature had not a very clear effect of removal TDS and TS.

pH we observed that slight increase in pH values of treated water from wastewater because of the development of reactions in anaerobic reactors that may be dependent, the release of CO$^2$ gas increases the value of treated wastewater pH because it is known that CO$_2$ has acidic properties when dissolved in water [16].

### 3.3. The effect of HRT on efficiency removal of UASB reactor with in temperature (35±2) °C

The effects of HRT on the efficiency of treatment in a UASB reactor was studied so that HRT was changed and the temperature in the reactor constant between (35±2) °C this value was choosed because it is the normal temperature of wastewater in Syria during Summer season and it is found that the best removal of COD occurs at it. The temperature of BYW was controlled by automatic thermostat which was used only for heating the BYW inside UASB reactor.

The duration of any stage under various operating HRT continued about 5 days during it many samples were taken and analyzed and the average value showed in the Table 4.

**Table 4.** The efficiency removal of pollutants of the experimental UASB according to the different values of HRT

| Parameters | HRT (hours) | | | |
|---|---|---|---|---|
| | 18 | 24 | 30 | 36 |
| pHi | 6.61 | 6.67 | 7.22 | 6.55 |
| pHe | 7.46 | 7.76 | 7.37 | 7.82 |
| COD$_i$ (mg L$^{-1}$) | 10540 | 12384 | 10200 | 13320 |
| COD$_e$ (mg L$^{-1}$) | 7072.3 | 6341 | 5207 | 6487 |
| COD removal % | 32.9 | 48.8 | 48.95 | 51.3 |
| ORL (kg COD m$^{-3}$.day$^{-1}$) | 14.05 | 12.38 | 8.18 | 8.89 |
| TS$_i$ (mg L$^{-1}$) | 13883 | 14700 | 13473 | 16313 |
| TS$_e$ (mg L$^{-1}$) | 11776.2 | 13220.4 | 11683.3 | 13130 |
| TS removal % | 15.2 | 10.1 | 13.3 | 19.5 |
| TSS$_i$ (mg L$^{-1}$) | 1073 | 1218 | 1163 | 890 |
| TSS$_e$ (mg L$^{-1}$) | 353.4 | 727.4 | 446.5 | 364.6 |
| TSS removal % | 67.1 | 40.3 | 61.6 | 59.0 |
| TDS$_i$ (mg L$^{-1}$) | 12810 | 13482 | 12310 | 15423 |
| TDS$_e$ (mg L$^{-1}$) | 11422.6 | 12493 | 11237 | 12799.4 |
| TDS removal % | 10.8 | 7.3 | 8.7 | 17.0 |

ORL applied to the laboratory UASB with in HRT value (18-36) h for BYW was (8.18-14.05) kg COD m$^{-1}$ day$^{-1}$ in a temperature value (35±2) °C. The same result reported by the reference [6, 15].

The efficiency removal of COD for BYW in UASB reactor is about (32.9-51.3) % and depends on HRT and temperature of wastewater in HRT value (18-36) hours and a temperature value (35±2) °C. The efficiency removal of COD did not exceed 51.3%. It is probably due to the high value of salinity.

It is higly recommended that using UASB reactor for treatment of high organic loading wastewater such as wastewater from yeast factories but the efficiency for COD removal would not exceed 48 % at HRT =24 hour and the temperature is between (35±2) °C, which can be obtained by heating UASB reactor by CH$_4$. The maximum efficiency removal of COD was:51.3% at

HRT value=36 hours, temperature is between (35±2) °C the same result reported by the references [9, 10].

It was found that the relation between HRT and the efficiency for COD removal was (Fig 3):

$COD_r = -0.0941 \times HRT^2 + 6.0037 \times HRT - 43.782$    (2)

Where: HRT: is the hydraulic retention time (h),$COD_r$: is the efficiency removal (%)of COD.
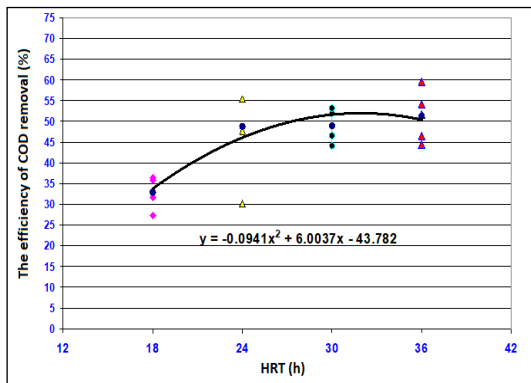


**Fig 3.** The relation between Temperature and the efficiency removal of COD

pH: We observed that slight increases in pH values of treated water from waste water.

The efficiency removal of TDS and TS in UASB rector which treating the industrial wastewater of baker's yeast is too low about 3.17 to 7.34% for TDS and 3.3-10% for TS. Increasing of wastewater temperature had not a very clear effect of removal TDS and TS.

If wastewater from yeast factories would be treated by a UASB reactor,another sequential reactor must be put. To achieve good quality of treated wastewater. It is highly recommended to investigated other method for treat baker's yeast wastewater such as evaporation because it contains high concentration of TS and TDS, so it is recommended to the advanced treatment of biologically treated BYW with membrane processes was studied to produce recovered water that was suitable for agricultural irrigation. In addition to water recover, the reference reported that electrocoagulation (EC) was employed for removals of color, COD and total organic carbon (TOC) from baker's yeast effluents in a batch EC reactor using aluminum electrodes[3]. The removal efficiencies showed a high significance of the model. The maximum color, COD and TOC were 88%,48% and 49% [3].

## 4. CONCLUSIONS

The startup of UASB rector was achieved after 38 days of starting feed the wastewater and the recycle ratio was 100% in a closing loop. The removal efficiency of COD was about 49% at the end day of startup face.
The relation between temperature and the efficiency for COD removal is represented in the following equation:

$COD_r = 0.4433 \times (T) + 31.13$    (3)

Whereas: T: temperature of wastewater in UASB reactor (°C), $COD_r$: COD efficiency removal (%).

It is highly recommended to investigated other method for treat baker's yeast wastewater, such as evaporation, because BYW contains high concentration of TS and TDS, so it is recommended to the advanced treatment of biologically treated BYW with membrane processes or any other advanced method to reuse the treated wastewater for irrigation.

## REFERENCES

[1]. A. Saghir, "Industrial wastewater treatment in Arabic world," *Arabic scientific publishers*, Lebanon, 2017.

[2]. R. Rajakumar, T. Meenambal, P.M. Saravanan, P. Ananthanarayanan, "Treatment of poultry slaughterhouse wastewater in hybrid upflow anaerobic sludge blanket reactor packed with pleated poly vinyl chloride rings," *Bioresource Technology,* Vol. 103 (1), pp. 116–122, 2012.

[3]. E. Gengec, M. Kobya, E. Demirbas, A. Akyol and K. Oktor, "Optimization of baker's yeast wastewater using response surface methodology by electrocoagulation," *Desalination,* Vol. 286, pp. 200–209, 2012.

[4]. Y. Zhou, Z. Liang and Y. Wang, "Decolorization and COD removal of secondary yeast wastewater effluents by coagulation using aluminum sulphate," *Desalination,* Vol. 225, pp. 301-311, 2008.

[5]. A. Saghir. and S. Hajjar, "Anaerobic treatment for high organic load industrial wastewater by UASB reactor," *Research Journal of Aleppo university Engineering series*. Vol. 58, 2007.

[6]. T. Ciftci. and I. Ozturk, "Nine years of full-scale anaerobic-aerobic treatment experiences with fermentation industry effluent," *Water Science and Technology,* Vol. 32 (12), pp. 131-139, 1996.

[7]. N. Deveci and G. Ciftci, "A mathematical model for the anaerobic treatment of Baker's yeast effluents," *Waste Management*, Vol. 21 (1), pp. 99-103, 2001.

[8]. S.K. Khanal, J.C. Huang, "Effect of high influent sulfate on anaerobic wastewater treatment," *Water Environment Research,* Vol. 77 (7), pp. 3037-3046, 2005.

[9]. K.V. Lo, A. Chen and P.H Liao, "Anaerobic Treatment of Baker's Yeast Wastewater:II.Sulfate Removal," *Biomass: of British*, Vol. 23 (1), pp. 25-37 ,1989.

[10]. M. Koplimaa, A. Menert, V. Blonskaja, T. Kurissoo, S. Zub, M. Saareleht, E. Vaarmets and T. Menert, "Liquid and gas chromatographic studies of the anaerobic degradation of baker's yeast wastewater," *Procedia Chemistry,* Vol. 2 (1), pp. 120–129, 2010.

[11]. M.E Ersahin, H. Ozgun, R.K. Dereli and I. Ozturk, "Anaerobic Treatment of Industrial Effluents:An Overview of Applications," Available: https://www.intechopen.com/books/waste-water-treatment-and-reutilization/anaerobic-treatment-of-industrial-effluents-an-overview-of-applications, DOI: 10.5772/16032, 2011.

[12]. E.W. Rice, "*Standard Methods for the Examination of Water and Wastewater,*" 22nd

Edition, American Public Health Association, American Water Works Association and Water Environment Federation, Washington DC, USA, 2014.

[13]. M.M. Ghangrekar, "Design of an UASB Reactor," Available. https://docslide.net/documents/design-of-an-uasb-reactor.html, 2005.

[14]. S. Sung, "Anaerobic Water Treatment Technologies," Accessed:

http://www.wpeiic.ncku.edu.tw/resources/Aeaerobic%20Water%20Treatment.pdf, (2008).

[15]. M.M. Ghangrekar, "Design of an UASB Reactor," https://www.scribd.com/document/86683056/Design-of-an-UASB-Reactor, 2002.

[16]. L.F Burton and G. Tchobanoglous,"*Wastewater Engineering-Treatment- Disposal- Reuse*," 3rd Ed, Metcalf and Eddy. Inc ,McGraw- Hill, New York, 1991

Environmental Research & Technology

**RESEARCH ARTICLE**

# Application of mathematical model for design of an integrated biodiesel-petroleum diesel blends system for optimal localization of biodiesel production on a Bulgarian scale

Boyan Ivanov[1,*], Stoyan Stoyanov[2], Evgeniy Ganev[1]

[1] Institute of Chemical Engineering, Bulgarian Academy of Ssciences, Sofia, BULGARIA
[2] Centre of Ecology, University of Chemical Technology and Metallurgy, Sofia, BULGARIA

## ABSTRACT

This paper proposes a mixed integer linear programming (MILP) model for optimal design and planning of biodiesel supply chain for Bulgarian case study. Sunflower and rapeseed are used as raw materials for biodiesel production. The country has been divided into twenty-seven regions corresponding to its districts. The existing in each region crops, oil and biodiesel plants and potential ones are represented as discrete variables in the model. The mathematical model is developed using GAMS software and represents a complete decision-making tool. The proposed strategy can be applied for other countries or regions by adjusting the required for the modeling data

*Keywords:* Integrated biofuel supply chain, optimal design, MILP model, minimum total GHG emission, minimum annualized total cost, Bulgarian scale

## 1. INTRODUCTION

To replace the increasing amount of fossil-based diesel by biodiesel is one of the targets of the sustainable development, because the biodiesel production can ensure significant economical and environmental benefits. Each country has to analyze the needs of the economical and environmental feasibility in order to produce its own biodiesel. The analysis has to include a complete production chain starting from the availability of raw materials, their intermediate transformations up to the end products and also the storing and the distribution of the products to internal and external markets. The development of a large network with several stages and possible different alternatives in each stage is required, according to the availability of the biomass crops, the location of products storage, conversion facilities, way of transportation of biomass and products between the regions, etc.

With the aim of mitigating emissions, diversifying the energy supply and reducing the dependence on imported fossil fuels, the European Union (EU) has set ambitious targets for a transition to renewable energy [1]. An integrated energy and climate change policy adopted in 2008 requires the following general targets: 20% greenhouse gas reduction, 20% reduced energy use through increased energy efficiency and a 20% share of renewable energy by 2020 [2]. As a key to reach these targets the increased production and use of bioenergy is promoted [3]. It is expected the biomass to replace the fossil fuels in stationary applications, such as heat or electricity production, as well as in the transport sector. In order to explicitly stimulate a shift to renewables in transportation, the European Commission has, in addition to the overall 20% renewable energy target, set a mandatory target of 10% renewable energy in transport by 2020 [4], with a transitional target of 5.75% for 2010 an achievement of 10% up to 2020 [5].

It can be achieved using biofuels (biodiesel and bioethanol) as a tool for decreasing the emissions of [6]. Study [7] emphasis on the main biofuels sources used for first generation biofuels production as well as global biofuel projections for coming decades.

Other research works are devoted of development of mixed integer linear programming (MILP) modeling approaches for optimal design and planning of the supply chains activities in the biodiesel [8] production.

In Ref. [9], an approach for optimal design of integrated biodiesel-petroleum diesel blend system is proposed. It is based on mixed integer linear programming (MILP) model.

Recently, (2013-2015) a variety of research works have been published which deal with the problems associated with biofuel supply chains.

In some of them new methods of synthesis and optimization have been proposed [10]. Other works [11], [12] are focused on sustainability at operation of biofuel supply chain as well as the problems solution considering different aspects of sustainable development [13].

In Ref. [14] an effective method for the synthesis of biofuel supply chain is proposed. Its efficiency has been proved on a specific numerical example. As a case study a biofuel supply chain in North Dakota, USA is considered. The problem is solved using MATLAB and GAMS software on a Sony Vaio Laptop of 5 GB RAM, and processor's speed of 3.5 GHz.

In [15] a modeling approach for design of biofuel supply chain is presented. In order to demonstrate its performance in the presence of data uncertainty it has been proved on a hypothetical case study. The proposed model could be used for design of biofuel supply chain, which results in optimization of the total life cycle cost uncertainty. The designed model is complicated with multiple variables representing uncertainty of the yield of crops for biofuel production, the price of raw materials (grains for biofuel production), unit cost of each mode of transport, the production capacity of each plant and office price, etc.

In [16] a supply chain integration strategy for simultaneously consideration of selection and production planning based on mixed integer linear programming model accounting for uncertainty of supply and demand has been proposed. The model is solved using tailored algorithm optimization. County level cases in Illinois are analyzed and compared to show the advantage of the proposed framework for optimization.

Ref. [17] addresses the optimal design and planning of sustainable industrial supply chains considering three key performance indicators: total cost, total GHG emission, and total lead time. A multi-objective optimization framework, incorporating these sustainability indicators has been developed and applied to an industrial case study drawn from a Dow business.

The proposed mathematical programming model in Ref. [18] optimizes the numbers, locations and capacities of Jatropha CurcasL (JCL) cultivation centers and Waste Cooking Oil (WCO) collection centers, bio-refineries, and distribution centers. The proposed approach is implemented in Iran for 10 years planning horizon. The obtained results show the usefulness and efficiency of the proposed method in assisting the policymakers to make suitable strategic and tactical decisions related to biodiesel supply chain planning.

Supply chain (SC) analysis and optimization have been extensively reported in the literature applied to different process industries. However, biofuel production is mainly focused on such individual aspects of supply chain, as plantation or transportation and there are only a few papers that address analysis and optimisation of the entire biofuel supply chain. A mathematical model to solve the problem of designing and managing the biofuel supply chain (BSC) for biodiesel, based on the theoretical method of MILP of crop rotation has been proposed in the first part of Ref. [9]. The aim of this study is application of the mathematical model developed in Ref. [9] for the case of integrated biodiesel-petroleum diesel blends system at the real conditions in Bulgaria.

## 2. CASE STUDY: POTENTIAL BIODIESEL PRODUCTION IN BULGARIA FOR 2010-2020

The model described in Ref. [9] has been applied to a case study of biodiesel production in Bulgaria. Two major types of biomass resources in this case, sunflower and rapeseed for production of first generation biodiesel (B100) are used.

The demand scenario that is investigated in this paper is based on both the Bulgaria domestic target for 2010 (5.75% by energy content) [19] and the EU target for 2020 10% by energy content) [4] to promote the use of biofuels.

### 2.1. Input data

#### 2.1.1. Territorial division of Bulgaria and data on energy consumption of petroleum diesel for transport

According to the Geodesy, Cartography and Cadastre Agency at the Ministry of Regional Development and Public Works, the total area of the Republic of Bulgaria as of 31.12.2000, is 111001.9 square kilometers of which 63764.8 square kilometers is used for agriculture. From this land arable land and utilized agricultural area for 2011 is 3,162,526 hectares [20], [21]. The main energy crops for biodiesel (B100), which are suitable for growing in Bulgaria are sunflower and rapeseed. These crops are now grown mainly for ensuring food security. Areas that are employed for this purpose for 2011 are: 734,314 [ha] for sunflower and 209,347 [ha], for industrial oleaginous crops including rapeseed. Bulgaria has almost 0.7 [ha] per inhabitant agricultural land, compared to an average of 0.4 [ha] in the EU-25 [22]. Therefore, to produce required feedstock internally in Bulgaria is not difficult. The correlation between feedstock availability and land availability is positive and significant and this factor is crucial and important for feedstock amount.

#### A. Territorial Division of Bulgaria, current cultivated area and the region's population

Bulgaria comprises 27 regions (see Fig. 1) [23]. In this case study, each region in Bulgaria is considered to be

a feedstock production region, a potential location of a biorefinery facility and a demand zone. In other words, the biofuel supply chain network consists of 27 areas for feedstock production, 27 potential biorefinery locations, 27 costumer zones and 3 refineries for petroleum diesel. We assume a 10-year service life of biorefineries in the present study, and the fixed cost parameter for building refineries is amortized into annual cost to be consistent with other cost components.

For the purposes of this study, data on population, cultivated area, as well as the free cultivated area, which in principle can be used for the production of energy crops for biodiesel (B100) production are taken from Ref. [20].

Table 1 presents data on the distribution of cultivated area for each region and population size.
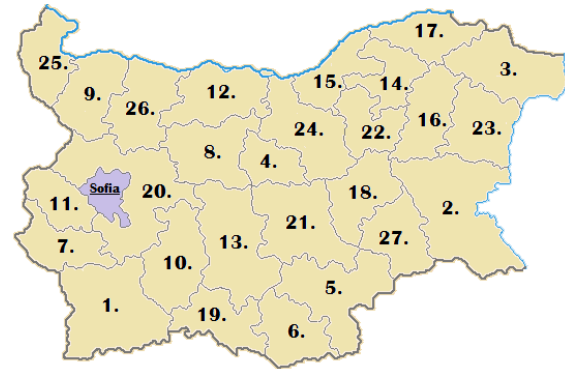


**Fig 1.** Map of the administrative territorial division of Bulgaria used for the purposes of the study [24]

**Table 1**. Cultivated area by region and population **[20], [25]**

| No | Name of regions | | Population | Cultivated area |
|----|----|----|----|----|
| | **Units** | | | **[ha]** |
| 1 | Region-1 | Blagoevgrad | 322 025 | 20 512 |
| 2 | Region-2 | Bourgas | 414 947 | 177 572 |
| 3 | Region-3 | Dobrich | 188 088 | 329 809 |
| 4 | Region-4 | Gabrovo | 121 389 | 21 507 |
| 5 | Region-5 | Haskovo | 243 955 | 116 657 |
| 6 | Region-6 | Kardjali | 152 009 | 12 751 |
| 7 | Region-7 | Kyustendil | 134 990 | 18 537 |
| 8 | Region-8 | Lovech | 139 609 | 66 834 |
| 9 | Region-9 | Montana | 145 984 | 130 243 |
| 10 | Region-10 | Pazardjik | 273 803 | 57 675 |
| 11 | Region-11 | Pernik | 131 987 | 33 980 |
| 12 | Region-12 | Pleven | 266 865 | 289 355 |
| 13 | Region-13 | Plovdiv | 680 884 | 179 416 |
| 14 | Region-14 | Razgrad | 123 600 | 140 215 |
| 15 | Region-15 | Ruse | 233 767 | 170 072 |
| 16 | Region-16 | Shtumen | 179 668 | 140 824 |
| 17 | Region-17 | Silistra | 118 433 | 146 411 |
| 18 | Region-18 | Sliven | 196 712 | 85 021 |
| 19 | Region-19 | Smolyan | 120 456 | 5 095 |
| 20 | Region-20 | Sofia | 1 542 231 | 68 201 |
| 21 | Region-21 | St.Zagora | 331 135 | 173 465 |
| 22 | Region-22 | Targovishte | 119 865 | 98 038 |
| 23 | Region-23 | Varna | 474 344 | 160 786 |
| 24 | Region-24 | V.Tarnovo | 256 279 | 168 194 |
| 25 | Region-25 | Vidin | 99 481 | 90 853 |
| 26 | Region-26 | Vratsa | 184 662 | 175 528 |
| 27 | Region-27 | Yambol | 130 056 | 149 686 |
| | | **Total** | **7 327 224** | **3 162 526** |

### B. Data on the energy consumption of petroleum diesel for transport for the period 2010 to 2020

In setting national indicative targets for the consumption of biofuels in Bulgaria the indicative targets set out in Directive 2003/30/EC and adopted by the European Council (8-9 March 2007) are considered. These targets for biofuels are 5% for 2010 and 10% for the total consumption of petrol and petroleum diesel for transport in the EU by 2020. These targets have to be achieved in a cost effective way.

Produce biodiesel (B100) is used as a component in mixtures of petroleum diesel oil produced in a specific proportion [26]. In Bulgaria in 2011 this proportion is a biodiesel–petroleum diesel blend of 6% biofuel (B100) and 94% petroleum diesel.

Table 2 shows the diesel consumption for transport over the period 2010-2012 we know it from Ref [20] while the estimated diesel consumption for the period 2013 to 2020 is taken from Ref. [27].

For the purposes of this study we assume that the consumption of petroleum diesel fuel for each region is taken approximately proportional to its size.

**Table 2.** Petroleum diesel consumption for transport and energy crops for food security in 2010-2020 [27]

| No | Year | 2010 | 2012 | 2014 | 2016 | 2018 | 2020 |
|---|---|---|---|---|---|---|---|
| **Status** | **Units** | **Diesel consumption** | | **Estimated diesel consumption** | | | |
| Proportion biodiesel/diesel | [%] | 5% | 6% | 7% | 8% | 9% | 10% |
| Petroleum Diesel | | 1891300 | 2050000 | 2219000 | 2401000 | 2583000 | 2775500 |
| Sunflower for food security | [ton year$^{-1}$] | 1321765 | 1321765 | 1321765 | 1321765 | 1321765 | 1321765 |
| Rapeseed for food security | | 376824 | 376824 | 376824 | 376824 | 376824 | 376824 |

### 2.1.2. Potential feedstock's for biodiesel (B100) for production in Bulgaria

Vegetable oils are the main raw material for producing biodiesel (B100) and the oils are derived from the seeds or the pulp of a range of oil-bearing crops. The most suitable oil crops for Bulgarian climate are sunflower and rapeseed. Rapeseed oil was the first type used for biodiesel (B100) production and is still the main feedstock for biodiesel (B100) production in Bulgaria. This is because the climate is more suitable for its growth throughout the country, while sunflower seed crops are grown mainly in the warmer south areas. Rapeseed and sunflower have been traditionally cultivated in Bulgaria and both of these crops have great potential for the future. This is the reason rapeseed and sunflower to be discussed as main energy crops, in this study for biodiesel (B100) production.

### 2.1.3. Data for emission factor for cultivation of biomass and yields

GHG emissions in the agronomy phase for cultivation of sunflower and rapeseed lifecycle phases include soil preparation, seeding, tillage, fertilization, and finally harvest.

For different regions in Bulgaria GHG emissions aggregation for the entire life cycle of growing energy crops vary greatly depending on terrain, weather conditions, the technology of growing crops and imported fertilizer to increase yields. Table 3 gives GHG emissions in the agronomy phase to rapeseed and sunflower and the yield cultivation for different regions of the Bulgaria.

### 2.1.4. Data for the production cost of energy crops produced in Bulgaria

Unit biomass cultivation cost includes all costs associated with the cultivation of biomass, and a final selling price in the region (not including shipping costs for delivery to biorefineries). Cultivation cost is variable and is a function of the regional climate, the technology of cultivation of the species on earth and bio cultures.

At Table 3 is shown the specific annual yield of sunflower and rapeseed as raw material for biodiesel (B100) production. The specific annual yield of each raw material per hectare of cultivated area differs significantly between regions because of the climate, soil, rainfall, etc. The maximum biomass production from each region in Bulgaria is shown in Table 4. The minimum biomass production from each region in Bulgaria is 250 ton year$^{-1}$.

### 2.1.5. Potential locations of biodiesel and petroleum diesel refineries

The most appropriate possible locations for biorefinery throughout the regions are chosen on the basis of the accessibility to the transportation infrastructures, urban planning and zoning conditions. All 27 regions have been selected as candidate biorefinery locations, which are therefore dispersed across the Bulgarian territory. Refineries for the production of petroleum diesel are located in the regions of Bourgas, Ruse and Sofia.

**Table 3.** GHG emissions in the agronomy phase and potential yields from rapeseed and sunflower in the regions in Bulgaria **[20]**

| No | Regions | GHG emissions in the agronomy phase | | The yield cultivation in regions | |
|---|---|---|---|---|---|
| | Units | [kg $CO_2$ – eq ton$^{-1}$ biomass] | | [ton ha$^{-1}$] | |
| | Energy crops | Sunflower | Rapeseed | Sunflower | Rapeseed |
| 1 | Region-1 | 1700 | 1350 | 1.5 | 1.8 |
| 2 | Region-2 | 1425 | 1120 | 2.8 | 2.8 |
| 3 | Region-3 | 600 | 430 | 3.4 | 3.5 |
| 4 | Region-4 | 1425 | 1120 | 1.8 | 2.2 |
| 5 | Region-5 | 1425 | 1120 | 1.8 | 2.2 |
| 6 | Region-6 | 1700 | 1350 | 1.5 | 1.8 |
| 7 | Region-7 | 1700 | 1350 | 1.5 | 1.8 |
| 8 | Region-8 | 1425 | 1120 | 1.8 | 3.2 |
| 9 | Region-9 | 1150 | 890 | 2.2 | 2.6 |
| 10 | Region-10 | 1700 | 1350 | 2.2 | 3.2 |
| 11 | Region-11 | 1425 | 1120 | 1.8 | 2.2 |
| 12 | Region-12 | 600 | 430 | 2.8 | 3.5 |
| 13 | Region-13 | 1425 | 1120 | 1.8 | 2.2 |
| 14 | Region-14 | 875 | 660 | 2.8 | 3.0 |
| 15 | Region-15 | 600 | 430 | 3.3 | 3.5 |
| 16 | Region-16 | 875 | 660 | 2.8 | 3.0 |
| 17 | Region-17 | 875 | 660 | 2.8 | 3.0 |
| 18 | Region-18 | 1150 | 890 | 2.4 | 2.6 |
| 19 | Region-19 | 1700 | 1350 | 1.5 | 1.8 |
| 20 | Region-20 | 1700 | 1350 | 1.5 | 1.8 |
| 21 | Region-21 | 875 | 660 | 2.8 | 3.0 |
| 22 | Region-22 | 1150 | 890 | 2.2 | 2.6 |
| 23 | Region-23 | 875 | 660 | 2.8 | 3.0 |
| 24 | Region-24 | 875 | 660 | 2.4 | 3.0 |
| 25 | Region-25 | 1425 | 1120 | 2.8 | 2.2 |
| 26 | Region-26 | 875 | 660 | 1.8 | 2.0 |
| 27 | Region-27 | 1150 | 890 | 2.6 | 2.6 |

### 2.1.6. The technology of biodiesel (B100) production used in this study

In our case, we assume that classical esterification technology [29] will be used for the production of biodiesel (B100) from raw sunflower and rapeseed.

The average price of glycerin by Ref. [30] is 1.088 $ kg$^{-1}$. Another co-product is the residue seed cake from him crushing of the oilseeds, which is rich in protein and is used for animal feed. According to Ref. [29] approximately 1.575 ton of seed cake is produced per ton of biodiesel (B100). The average price of seed cake for sunflower by [31] is 115 $ ton$^{-1}$.

The technology for extraction oil from oilseeds has not changed significantly during the last 10-15 years. The process of biodiesel production from the oil is a relatively simple and the expectations for efficiency improvement are small, but utilization of co-products has improved significantly in this time.

### 2.1.7. Biomass to biodiesel (B100) conversion factor

The feedstock conversion ratio of the process is defined here as the amount of the feedstock input divided by the amount of the main product. It is a measure of how much biomass is needed for a unit mass of biofuel.

Conversion efficiency of rapeseed and sunflower biodiesel (B100) ranges from 454 L ton$^{-1}$ to 422 L ton$^{-1}$. We use a conversion efficiency of 422 L ton$^{-1}$ in the Aglink model [32], which is the average of the lowest and highest conversion efficiency found in literature.

In Table 5, are given the differentiated value of the conversion factor for sunflower and rape, applicable to conditions in Bulgaria under traditional method to extract biodiesel (B100). In this study the used value of the conversion factor is 371 kg ton$^{-1}$ biomass for sunflower and 303 kg ton$^{-1}$ biomass rapeseed applicable to the conditions in Bulgaria by the traditional method for extracting biodiesel (B100).

**Table 4.** Unit biomass cultivation cost and maximum amount of biomass that can be produced in the regions of Bulgaria [28]

| No | Regions | Cultivation costs per unit of | | Maximum biomass production | |
|----|---------|--------------|----------|-----------|----------|
| | Units | [\$ ton$^{-1}$ biomass] | | [ton year$^{-1}$] | |
| | Energy crops | Sunflower | Rapeseed | Sunflower | Rapeseed |
| 1 | Region-1 | 227 | 239 | 10768 | 9230 |
| 2 | Region-2 | 213 | 236 | 93225 | 79907 |
| 3 | Region-3 | 192 | 227 | 173150 | 148414 |
| 4 | Region-4 | 213 | 233 | 11291 | 9678 |
| 5 | Region-5 | 213 | 236 | 61245 | 52496 |
| 6 | Region-6 | 227 | 239 | 6694 | 5738 |
| 7 | Region-7 | 227 | 239 | 9732 | 8342 |
| 8 | Region-8 | 213 | 236 | 35087 | 30075 |
| 9 | Region-9 | 198 | 233 | 68378 | 58609 |
| 10 | Region-10 | 227 | 239 | 30279 | 25954 |
| 11 | Region-11 | 213 | 236 | 17839 | 15291 |
| 12 | Region-12 | 192 | 227 | 151911 | 130210 |
| 13 | Region-13 | 213 | 236 | 94193 | 80737 |
| 14 | Region-14 | 195 | 230 | 73613 | 63097 |
| 15 | Region-15 | 192 | 227 | 89287 | 76532 |
| 16 | Region-16 | 195 | 230 | 73932 | 63370 |
| 17 | Region-17 | 195 | 230 | 76866 | 65885 |
| 18 | Region-18 | 198 | 233 | 44636 | 38259 |
| 19 | Region-19 | 227 | 239 | 2675 | 2293 |
| 20 | Region-20 | 227 | 239 | 35806 | 30690 |
| 21 | Region-21 | 195 | 230 | 91069 | 78059 |
| 22 | Region-22 | 198 | 233 | 51469 | 44117 |
| 23 | Region-23 | 195 | 230 | 84412 | 72353 |
| 24 | Region-24 | 195 | 230 | 88301 | 75687 |
| 25 | Region-25 | 213 | 236 | 47698 | 40884 |
| 26 | Region-26 | 195 | 230 | 92152 | 78987 |
| 27 | Region-27 | 198 | 233 | 78585 | 67358 |

**Table 5.** Biomass to biodiesel (B100) conversion factor

| | Type of Energy Crops | Conversion factor $\gamma_{ij}$ | Energy equivalent of biomass |
|---|---------------------|------------------------|------------------------------|
| | Units | (ton biofuel) (ton biomass)$^{-1}$ | GJ ton$^{-1}$ |
| 1 | Sunflower | 0.371 | 14.023 |
| 2 | Rapeseed | 0.303 | 11.453 |

### 2.1.8. Biorefinery costs and capacity

The refinery capital cost consists of fixed and variable capital cost. If the plant technology is considered mature, the variable capital cost of biomass-to-biodiesel (B100) plants are depending only on the size of the plant. The variable capital costs are scaled using the general relationship [33].

$$\frac{Cost_p}{Cost_{base}} = \left(\frac{Size_p}{Size_{base}}\right)^R \qquad (1)$$

where $Cost_p$ and $Size_p$ represent the investment cost and plant capacity respectively for the new plant, $Cost_{base}$ the known investment cost for a certain plant capacity $Size_{base}$, and $R$ is the scaling factor. The scaling factor $R$ for biomass systems is generally between 0.6 and 0.8 [34]. The fixed capital cost varies by the refinery locations.

Capital cost of biorefinery for each region is determined by the equation:

$$Cost^F_{pf} = M^{cost}_f \, Cost_p, \forall p \in P, \forall f \in F \qquad (2)$$

where $M_f^{cost}$ is a correction factor in the price of bio-refineries in the region $f \in F$ according to its installed $M_f^{cost} \geq 1$. The value of this coefficient is a different for geography region. It reported indicators such as, land prices, labor costs, etc.

According to Ref. [32] capital costs biorefinery size about 1000 ton year$^{-1}$ are within 334 – 412 \$ ton$^{-1}$. In biorefinery with basic performance $Size_{base} = 8500$ ton year$^{-1}$ and then adopted base price $412 \$ ton^{-1}$, $Cost_{base} = 3.5M \$$ and a $R = 0.8$ capacity shown in Table 6 are the values of certain capital expenditures for each of them.

In our case it is assumed that for all 27 regions $M_f^{cost} = 1, \forall f \in F$.

The capacity of the refinery at all appointed locations can be up to 10000 ton year$^{-1}$ and they are ordered down into discrete order shown in Table 6.

### 2.1.9. Biodiesel(B100) production costs

Production costs per unit of biodiesel (B100) biorefinery installed in the region in case the Keys to Manufacturing Operating expenses such as: Chemicals and catalysts, gas, electricity, make-up water, wastewater treatment and disposal, administrative and operating costs and direct labor and Benefits. As discussed in Ref [28] average cost are respectively 125 \$ ton$^{-1}$ for each region of biodiesel (B100) (not including the costs of raw materials).

In the present case study, we accept a 10 year service life of biorefineries, and the fixed cost parameter for building refineries is amortized into annual cost to be consistent with other cost components.

### 2.1.10. Data for petroleum diesel plants

In the present study we examine three bases in Bulgaria for diesel fuel supply over the regions. Two central fuel depots are in Region-20 (Sofia) and Region-15 (Ruse) and one fuel depot is in Region-2 (Bourgas). The three basic fuel depots are supplied with diesel fuel by the refinery Lukoil – Bourgas and also with imported fuel by other sources. The minimum annual capacity of the fuel depots is 100000 ton year$^{-1}$ and the maximum capacity is 1200000 ton year$^{-1}$ for Region-20 and 900000 ton year$^{-1}$ for Region-15 and Region-2.

**Table 6.** Total specific investment cost of biodiesel (B100) production plants as a function of the size of the plant [35], [36]

| Size of biodiesel (B100) plant | Capital cost of biodiesel (B100) plant $Cost_p$ | MIN capacity of biodiesel (B100) plant $PB_p^{MIN}$ | MAX capacity of biodiesel (B100) plant $PB_p^{MAX}$ | Average capital costs per unit of biodiesel (B100) |
|---|---|---|---|---|
| Units | [M\$] | [ton year$^{-1}$] | | [\$ ton$^{-1}$] |
| Size-1 | 3.5000 | 1000 | 8500 | 411.76 |
| Size-2 | 4.3018 | 6000 | 11000 | 391.07 |
| Size-3 | 6.3790 | 8000 | 18000 | 354.39 |
| Size-4 | 8.0297 | 10000 | 24000 | 334.57 |
| Size-5 | 10.8589 | 14000 | 35000 | 310.25 |
| Size-6 | 14.4447 | 25000 | 50000 | 288.89 |
| Size-7 | 18.4731 | 30000 | 68000 | 271.66 |
| Size-8 | 19.7660 | 38000 | 74000 | 267.11 |
| Size-9 | 22.0835 | 44000 | 85000 | 259.81 |
| Size-10 | 25.1497 | 55000 | 100000 | 251.50 |

### 2.1.11. Data for biodiesel (B100) and petroleum diesel

**Table 7.** Emission coefficient of fuel and energy equivalent

| Type of fuel | Emission coefficient | Energy equivalent | Energy equivalent | Density (average) | Price of biofuel |
|---|---|---|---|---|---|
| Source | Ref. [37] | | Ref. [38] | | Ref. [39] |
| Unit | [kg $CO_2$ – eq ton$^{-1}$] | [GJ ton$^{-1}$] | [MWh ton$^{-1}$] | [ton m$^{-3}$] | [\$ ton$^{-1}$] |
| Petroleum Diesel | 3623 | 42.80 | 11.880 | 0.840 | 1192.70 |
| Biodiesel(B100) | 1204 | 37.80 | 7.720 | 0.880 | |

### 2.1.12. Data for cost transportation, and emission factors for biomass and biodiesel (B100)

A GIS-based transportation network has been used for cost estimation of transporting feedstock and fuels in the entire supply chain system, introduced. This network contains local, rural, urban roads and major highways. The shortest distances between feedstock fields, refineries, and demand cities have been calculated based on this network. Since only in-state production and delivery are considered, we assume that all transportations are performed by tractor, truck and rail for transporting biomass (Sunflower and Rapeseed) and for transportation biodiesel (B100) with truck and rail. Transportation costs include three components: loading/unloading cost, time dependent travel cost, and distance dependent travel cost. Time dependent cost includes labor and capital cost of trucks, while distance dependent cost includes fuel, insurance, maintenance, and permitting cost.

The biomass transportation cost is described by Ref. [9], and summarized in Table 8 and Table 9, for transportation by tractor, truck and train for biomass (Sunflower and Rapeseed) and biodiesel (B1000). They include the fixed cost and the variable cost. The loading and unloading costs, which are not dependent on distance of transport, are included in fixed costs. The costs for fuel, driving, maintenance, etc. are included in variable costs.

The biomass transportation cost $UTC_{igfl}$ is described by [9], for transportation by tractor, truck and train $UTC_{ftb}$. They are composed of a fixed cost ($IA_{il}$, $OA_b$) and a variable cost ($IB_{il}$, $OB_b$). Fixed costs include loading and unloading costs. They do not depend on the distance of transport ($ADG_{gfl}$, $ADF_{fcb}$, $ADD_{dcb}$). Variable costs include fuel cost, driver cost, maintenance cost etc. They are dependent on the distance of transport [40].

$$UTC_{igfl} = IA_{il} + \left(IB_{il}ADG_{gfl}\right)$$

$$UTB_{fcb} = OA_b + \left(OB_b ADF_{fcb}\right)$$

$$UTD_{dcb} = OAD_b + \left(OBD_b ADD_{dcb}\right)$$

$IA_{il}$ and $IB_{il}$ is fixed and variable cost for transportation biomass type $i \in I$, ($OA_b$, $OB_b$) is fixed and variable cost for transportation biodiesel (B100) and ($OAD_b$, $OBD_b$) is fixed and variable cost for transportation petroleum diesel.

The simplest approach to estimating emissions from road and rail transport is based on the amounts of each fuel consumed. The approach for $CO_2 - eq$ is indicated in Table 10. This is based directly on the carbon content of the fuel. The default average emission factors used in this guideline are based on the average emission factors recommended by Refs. [41], [42].

**Table 8.** Unit transportation cost for each mode of transport and type of the biomass [9]

| | Energy crops | Fixed cost $IA_{il}$ [44] | | | Variable cost $IB_{il}$ [44] | | |
|---|---|---|---|---|---|---|---|
| | Unit | [$ ton⁻¹km⁻¹] | | | | | |
| | Type of transport | Tractor | Truck | Train | Tractor | Truck | Train |
| 1. | Sunflower | 2.486 | 9.28 | 19.63 | 0.14 | 0.209 | 0.029 |
| 2. | Rapeseed | 2.486 | 9.28 | 19.63 | 0.14 | 0.209 | 0.029 |

**Table 9.** Unit costs for each transport mode and biodiesel (B100) [9]

| | | Fixed cost $OA_b$, $OAD_b$ [44] | | Variable cost $OB_b$, $OBD_b$ [44] | |
|---|---|---|---|---|---|
| | Unit | [$ton⁻¹km⁻¹] | | | |
| | Type of transport | Truck | Train | Truck | Train |
| 1. | Biodiesel(B100) | 24.11 | 7.86 | 0.436 | 0.173 |
| 2. | Petroleum diesel | 24.11 | 7.86 | 0.436 | 0.173 |

### 2.1.13. Data for actual delivery distance between regions in Bulgaria

Distances in kilometers between different locations in Bulgaria for the purpose of this survey are taken by the National Transport Agency for each type of transport (tractor, truck and rail).

The distance between regions will be the average distance of the feedstock being transported to the factory (assuming it is installed in a certain place of the region). In order to calculate the transport

distance, the coordinates of each biomass site and the potential biorefinery location have been determined. The data used in this case study are taken at the county level, therefore the coordinates of the center point of a county are used to calculated the geographical distances between locations. The average distance can be calculated using the following equation:

$$d_{gg}{'} = \frac{\sum_{m \in M_g}\left(S_{gm}d_m^{Plant}\right)}{\sum_{m \in M_g}S_{gm}} \tag{3}$$

where $d_{gg}$ the average distance which is supposed to be transported feedstock produced in the region g ∈ G, g = g' to the factory installed in place *Plant* (Fig. 2.), which is installed in the specified location in this region, $S_{gm}$ is the area of $m \in M_g$ these sub-region, and $d_m^{Plant}$ the distance landmark center sub region $m \in M_g$ and places in which it is permissible to install biorefinery. For our case, the distances calculated according to equation 3 for the individual regions are shown in Table 11.

**Table 10.** Emission factor of transportation for mode $I \in L$

| | Type of transport | Emission factor of transportation biomass | Emission factor of transportation biofuel |
|---|---|---|---|
| | Unit | [kg CO₂ – eq km⁻¹ton⁻¹] | |
| 1. | Tractor | 0.591 | |
| 2. | Truck(average) | 0.228 | 0.228 |
| 3. | Van < 3.5 t | 1.118 | 1.118 |
| 4. | Truck, 16 t | 0.304 | 0.304 |
| 5. | Truck, 32 t | 0.153 | 0.153 |
| 6. | Train, freight | 0.038 | 0.038 |
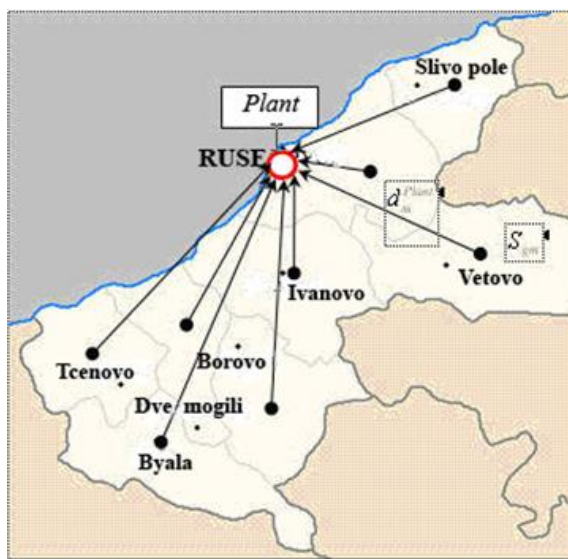


**Fig 2.** The actual delivery distance between sub regions

### 2.2. Computational results and analysis

The results from the case study described above, determining the optimal system design, the system costs, and the feedstock supply strategies are presented in this section.

Two possible scenarios for synthesis of the structure of the integrated biofuel supply chain (IBSC) are used in the present study. According to the proposed model [9] in the first scenario it is presumed that for a given time interval a factory with a given capacity is chosen to be built in particular geographic region and it will be the same factory with either the same or a bigger capacity is chosen in that region in the current and in the subsequent time interval. Applying the first

scenario is presumed that for a given time interval a factory with a given capacity is chosen to be build in particular geographic region and it will be the same factory with either the same or a bigger capacity chosen in that region in the current and in the subsequent time interval. Applying the second scenario is presumed that for a given time interval a factory with a given capacity is chosen the same factory with the same capacity in the same region will remain in the current and all subsequent time intervals.

The proposed models in Ref. [9] has been solved by GAMS 22.8 [43] using CPLEX 11.1 solver on an Intel Core 2 Duo P8600 2.4 GHz with 4 GB RAM on a 32-bit platform. The mixed integer linear model is formed by 6843 binary and 10368 positive continuous variables and includes 18453 constraints, which represent the investment possible decisions and required management.

**Table 11.** The actual delivery distance between regions in different models of transport

| No | Name of regions / Type of transport | Tractor or Truck or Rail |
|---|---|---|
| | Unit [km] | |
| 1 | Blagoevgrad to Blagoevgrad | 44 |
| 2 | Bourgas to Bourgas | 44 |
| 3 | Dobrich to Dobrich | 32 |
| 4 | Gabrovo to Gabrovo | 13 |
| 5 | Haskovo to Haskovo | 40 |
| 6 | Kardjali to Kardjali | 26 |
| 7 | Kyustendil to Kyustendil | 36 |
| 8 | Lovech to Lovech | 38 |
| 9 | Montana to Montana | 27 |
| 10 | Pazardjik to Pazardjik | 25 |
| 11 | Pernik to Pernik | 17 |
| 12 | Pleven to Pleven | 35 |
| 13 | Plovdiv to Plovdiv | 33 |
| 14 | Razgrad to Razgrad | 22 |
| 15 | Ruse to Ruse | 25 |
| 16 | Shumen to Shumen | 31 |
| 17 | Silistra to Silistra | 24 |
| 18 | Sliven to Sliven | 27 |
| 19 | Smolyan to Smolyan | 39 |
| 20 | Sofia to Sofia | 46 |
| 21 | St.Zagora to St.Zagora | 33 |
| 22 | Targovishte to Targovishte | 18 |
| 23 | Varna to Varna | 27 |
| 24 | V.Tarnovo to V.Tarnovo | 36 |
| 25 | Vidin to Vidin | 25 |
| 26 | Vratsa to Vratsa | 27 |
| 27 | Yambol to Yambol | 21 |

### *2.2.1. Biomass cultivation*

The total amount of two kinds of biomass used to produce biofuels allocated per year in regions is given on Table 12 and Table 12a.

The results of the optimal synthesis for second scenario using the two basic evaluation criteria show that the regions with concentrated production of sunflower and rapeseed for biodiesel (B100) production are in considerably narrow bounds. Using the evaluation criteria „Minimum Total GHG Emissions", the production of sunflower and rapeseed is concentrated in 3 basic regions in Bulgaria. At the same time the sown areas ensure the yield sustainability.

Using the criteria "Minimum Annualized Total Cost" for optimal synthesis of the structure of the integrated biofuel supply chain the number of the regions for sunflower and rapeseed production are increases to 7 with additional new 4 regions.

The basic bioculture for biodiesel (B100) production ensuring the „Minimum Total GHG Emissions" is the rapeseed, while using the evaluation criteria "Minimum Annualized Total Cost" for optimal synthesis of IBSC the basic feedstock is sunflower.

### *2.2.2. Distribution of land*

One of the most significant conclusions obtained from applying the mathematical model for optimal synthesis of IBSC [9] concerns the area of land in Bulgaria required to produce the national biofeedstock needs in 2020.

Using the "Minimum Total GHG Emission" criterion to model the quantity of biofeedstock required (see Fig. 3) for 10 % component of biodiesel (B100) it is predicted that 3% of available agriculture land would be required for production of biodiesel (B100) from sunflower and and 12% of available agriculture land for production of biodiesel (B100) from rapeseed.

Using the "Minimum Annualized Total Cost" criterion the predictions for areas of agricultural land required to produce the necessary biofeedstock (see Fig. 4) for biodiesel (B100) is 14% for sunflower and 2% for rapeseed cultivation.

For ensuring Minimum Total GHG Emissions the basic biofeedstock is rapeseed, while for ensuring the Minimum Annualized Total Cost the sunflower has to be used as a bioculture.

Comparing the cases we reach the conclusion that when the Minimum Annualized Total Cost criterion is used, sunflower cultivation is indicated whereas use of the Minimum Total GHG Emission criterion indicates that rapeseed cultivation is more efficient.

**Table 12.** Biomass cultivation per years in regions to produce biofuels for second scenario in case (a) – Minimum Total GHG emissions

| Years | 2010 | 2012 | 2014 | 2016 | 2018 | 2020 |
|---|---|---|---|---|---|---|
| **Sunflower [ton year⁻¹]** | | | | | | |
| Region-3 | 250 | 250 | 500 | 500 | 3750 | 3750 |
| Region-12 | 500 | 500 | 7221 | 22040 | 48869 | 173524 |
| Region-15 | 250 | 5157 | 500 | 500 | 9584 | 7407 |
| **Rapeseed [ton year⁻¹]** | | | | | | |
| Region-3 | 74483 | 65647 | 159732 | 236099 | 288583 | 288487 |
| Region-12 | 214786 | 233326 | 236954 | 236954 | 253186 | 253186 |
| Region-15 | 19804 | 97916 | 104246 | 131449 | 148813 | 148813 |

**Table 12a.** Biomass cultivation per years in regions to produce biofuels for second scenario in case (b) – Minimum Annualized Total Cost

| Years | 2010 | 2012 | 2014 | 2016 | 2018 | 2020 |
|---|---|---|---|---|---|---|
| **Sunflower [ton year⁻¹]** | | | | | | |
| Region-3 | 70460 | 87439 | 113597 | 134566 | 134950 | 157273 |
| Region-12 | 182351 | 23819 | 235744 | 239146 | 194126 | 253186 |
| Region-14 | 0 | 0 | 0 | 0 | 40613 | 40227 |
| Region-15 | 0 | 0 | 67181 | 104867 | 90500 | 148813 |
| Region-21 | 0 | 0 | 0 | 0 | 22706 | 22706 |
| Region-24 | 0 | 0 | 0 | 0 | 0 | 1491 |
| Region-26 | 0 | 0 | 0 | 22706 | 122869 | 122869 |
| **Rapeseed [ton year⁻¹]** | | | | | | |
| Region-3 | 250 | 250 | 250 | 250 | 500 | 500 |
| Region-12 | 500 | 5158 | 500 | 500 | 500 | 500 |
| Region-14 | 0 | 0 | 0 | 0 | 40613 | 0 |
| Region-15 | 0 | 0 | 250 | 17925 | 250 | 250 |
| Region-21 | 0 | 0 | 0 | 0 | 250 | 250 |
| Region-24 | 0 | 0 | 0 | 0 | 0 | 250 |
| Region-26 | 0 | 0 | 0 | 250 | 23532 | 750 |

**Table 13.** Distribution of arable land for biodiesel (B100) planted with sunflower and rapeseed for second scenario in case: (a) - Minimum Total GHG emission

| Years | | 2010 | 2012 | 2014 | 2016 | 2018 | 2020 |
|---|---|---|---|---|---|---|---|
| **Land for biodiesel (B100) busy with sunflower and rapeseed [ha]** | | | | | | | |
| **Region-3** | Sunflower | 71 | 71 | 142 | 142 | 1071 | 1071 |
| | Rapeseed | 21281 | 18756 | 45637 | 67457 | 82452 | 82424 |
| **Region-12** | Sunflower | 142 | 142 | 2063 | 6297 | 13962 | 49578 |
| | Rapeseed | 61367 | 66664 | 67701 | 67701 | 72339 | 72339 |
| **Region-15** | Sunflower | 71 | 1473 | 142 | 142 | 2738 | 2116 |
| | Rapeseed | 5658 | 27976 | 29784 | 37556 | 42518 | 42518 |

**Table 13a.** Distribution of arable land for biodiesel (B100) planted with sunflower and rapeseed for second scenario in case: (b) - Minimum Annualized Total Cost

| Years | | 2010 | 2012 | 2014 | 2016 | 2018 | 2020 |
|---|---|---|---|---|---|---|---|
| **Land for biodiesel (B100) busy with sunflower and rapeseed [ha]** | | | | | | | |
| **Region-3** | Sunflower | 20131 | 24982 | 32456 | 38447 | 38557 | 44935 |
| | Rapeseed | 71 | 71 | 71 | 71 | 142 | 142 |
| **Region-12** | Sunflower | 52100 | 68055 | 67355 | 68327 | 55464 | 72339 |
| | Rapeseed | 142 | 1473 | 142 | 142 | 142 | 142 |
| **Region-14** | Sunflower | 0 | 0 | 0 | 0 | 14504 | 14366 |
| | Rapeseed | 0 | 0 | 0 | 0 | 0 | 0 |
| **Region-15** | Sunflower | 0 | 0 | 19194 | 29962 | 25857 | 42518 |
| | Rapeseed | 0 | 0 | 71 | 5121 | 71 | 71 |
| **Region-21** | Sunflower | 0 | 0 | 0 | 0 | 8109 | 8109 |
| | Rapeseed | 0 | 0 | 0 | 0 | 83 | 83 |
| **Region-24** | Sunflower | 0 | 0 | 0 | 0 | 0 | 532 |
| | Rapeseed | 0 | 0 | 0 | 0 | 0 | 83 |
| **Region-26** | Sunflower | 0 | 0 | 0 | 8109 | 43882 | 43882 |
| | Rapeseed | 0 | 0 | 0 | 83 | 7844 | 250 |
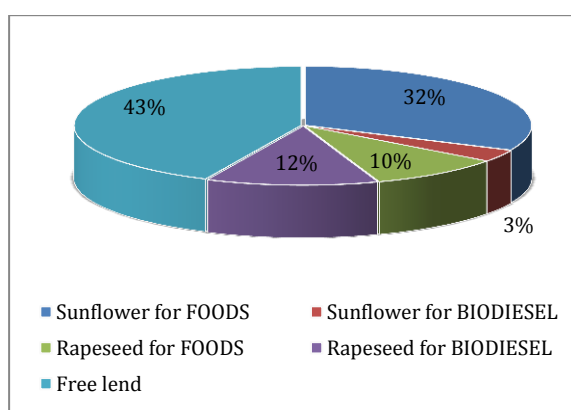


**Fig 3.** Distribution of arable land for various purposes for Sunflower and Rapeseed for 2020 year for second scenario for case: (a)-Minimum Total GHG emissions
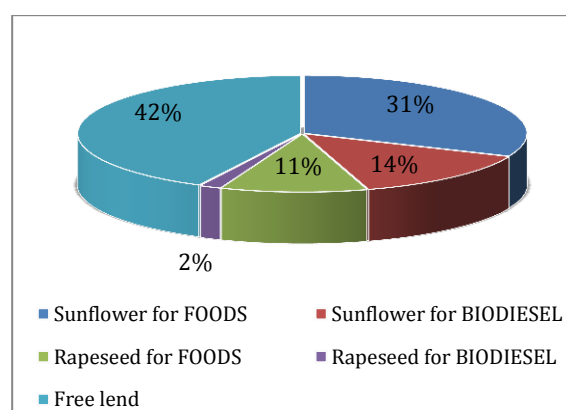


**Fig 4.** Distribution of arable land for various purposes for Sunflower and Rapeseed for 2020 year for second scenario for case: (b) - Minimum Annualized Total Cost

### 2.2.3. Biomass supply

The optimal biomass flows are given in Table 14 and Table 14a.

The analysis of the results of the optimal design of a system for IBSC in respect to the logistics show that the optimal delivery transport of the biomass from the region of production to the biorefineries is by train for both sunflower and rapeseed for all time intervals in the period (2010-2020). The railway transport can be suggested also from optimization results using the criteria "Minimum Total GHG emissions" and "Minimum Annualized Total Cost" [9]. For the transport of biodiesel (B100) and diesel from refineries to the centers of mixing and consumption is suggested also railway for both kind of fuels for the whole time period and for both criteria "Minimum Total GHG emissions" and "Minimum Annualized Total Cost" [9].

**Table 14** Flow rate biomass from grow region to biodiesel (B100) plants for second scenario in case (a) – Minimum Total GHG emissions

| Years | 2010 | 2012 | 2014 | 2016 | 2018 | 2020 |
|---|---|---|---|---|---|---|
| **Proportion biodiesel/diesel** | 5% | 6% | 7% | 8% | 9% | 10% |
| **Regions** | **Sunflower [ton day⁻¹]** | | | | | |
| Region-3 to Region-3 | 0 | 0 | 1.00 | 1.00 | 5.00 | 0 |
| Region-3 to Region-16 | 0 | 0 | 0 | 0 | 5.00 | 5.00 |
| Region-3 to Region-23 | 1.00 | 1.00 | 1.00 | 1.00 | 5.00 | 0 |
| Region-12 to Region-4 | 0 | 0 | 0 | 0 | 0 | 75.13 |
| Region-12 to Region-8 | 1.00 | 1.00 | 1.00 | 1.00 | 5.00 | 5.00 |
| Region-12 to Region-12 | 1.00 | 1.00 | 27.89 | 86.16 | 108.55 | 246.47 |
| Region-12 to Region-20 | 0 | 0 | 0 | 0 | 0 | 181.46 |
| Region-12 to Region-24 | 0 | 0 | 0 | 1.00 | 52.70 | 5.00 |
| Region-12 to Region-26 | 0 | 0 | 0 | 0 | 5.00 | 181.04 |
| Region-15 to Region-14 | 0 | 19.63 | 1.00 | 1.00 | 5.00 | 19.63 |
| Region-15 to Region-15 | 1.00 | 1.00 | 1.00 | 1.00 | 5.00 | 5.00 |
| Region-15 to Region-22 | 0 | 0 | 0 | 0 | 28.34 | 5.00 |
| **Regions** | **Rapeseed [ton day⁻¹]** | | | | | |
| Region-3 to Region-3 | 0 | 0 | 394.82 | 576.33 | 569.96 | 568.31 |
| Region-3 to Region-14 | 0 | 0 | 37.65 | 52.46 | 134.58 | 0 |
| Region-3 to Region-16 | 0 | 0 | 0 | 0 | 139.09 | 110.32 |
| Region-3 to Region-22 | 0 | 0 | 0 | 0 | 0 | 164.61 |
| Region-3 to Region-23 | 297 | 262.59 | 206.46 | 315.61 | 310.71 | 310.71 |
| Region-12 to Region-4 | 0 | 0 | 0 | 0 | 0 | 92.83 |
| Region-12 to Region-8 | 427 | 422.98 | 427.82 | 427.82 | 422.92 | 389.92 |
| Region-12 to Region-12 | 431 | 510.33 | 520.00 | 520.00 | 520.00 | 520.00 |
| Region-12 to Region-20 | 0 | 0 | 0 | 0 | 0 | 5.00 |
| Region-12 to Region-26 | 0 | 0 | 0 | 0 | 69.83 | 5.00 |
| Region-15 to Region-14 | 0 | 306.00 | 306.00 | 306.00 | 189.34 | 306.00 |
| Region-15 to Region-15 | 79 | 85.67 | 110.99 | 108.81 | 105.58 | 106.09 |
| Region-15 to Region-22 | 0 | 0 | 0 | 0 | 295.34 | 159.30 |
| Region-15 to Region-24 | 0 | 0 | 0 | 110.99 | 5.00 | 23.86 |

**Table 14a** Flow rate biomass from grow region to biodiesel (B100) plants for second scenario in case (b) - Minimum Annualized Total Cost

| Years | 2010 | 2012 | 2014 | 2016 | 2018 | 2020 |
|---|---|---|---|---|---|---|
| **Proportion biodiesel/diesel** | **5%** | **6%** | **7%** | **8%** | **9%** | **10%** |
| **Regions** | Sunflower [ton day$^{-1}$] | | | | | |
| Region-3 to Region-3 | 0 | 0 | 0 | 0 | 50 | 90 |
| Region-3 to Region-23 | 281 | 349 | 454 | 538 | 489 | 538 |
| Region-12 to Region-8 | 320 | 345 | 349 | 349 | 349 | 349 |
| Region-12 to Region-12 | 408 | 607 | 593 | 607 | 426 | 607 |
| Region-12 to Region-26 | 0 | 0 | 0 | 0 | 0 | 56 |
| Region-14 to Region-15 | 0 | 0 | 0 | 0 | 162 | 160 |
| Region-15 to Region-12 | 0 | 0 | 0 | 0 | 0 | 56 |
| Region-15 to Region-15 | 0 | 0 | 268 | 357 | 357 | 357 |
| Region-15 to Region-20 | 0 | 0 | 0 | 0 | 0 | 58 |
| Region-15 to Region-24 | 0 | 0 | 0 | 0 | 0 | 84 |
| Region-15 to Region-26 | 0 | 0 | 0 | 0 | 0 | 38 |
| Region-21 to Region-21 | 0 | 0 | 0 | 0 | 90 | 90 |
| Region-26 to Region-9 | 0 | 0 | 0 | 0 | 46 | 90 |
| Region-26 to Region-20 | 0 | 0 | 0 | 90 | 76 | 32 |
| Region-26 to Region-26 | 0 | 0 | 0 | 0 | 368 | 368 |
| **Regions** | Rapeseed [ton day$^{-1}$] | | | | | |
| Region-3 to Region-3 | 0 | 0 | 0 | 0 | 1 | 1 |
| Region-3 to Region-23 | 1 | 1 | 1 | | 1 | 1 |
| Region-12 to Region-8 | 1 | 1 | 1 | 1 | 1 | 1 |
| Region-12 to Region-12 | 1 | 19 | 1 | 1 | 1 | 1 |
| Region-15 to Region-15 | 0 | 0 | 1 | 71 | 0 | 0 |
| Region-26 to Region-9 | 0 | 0 | 0 | 0 | 42 | 0 |
| Region-26 to Region-20 | 0 | 0 | 0 | 1 | 1 | 0 |
| Region-26 to Region-26 | 0 | 0 | 0 | 0 | 51 | 0 |

### 2.2.4. The optimal system design

Table 15 and Table 15a show the results from the optimal synthesis of an IBSC using the "Minimum Total GHG emissions" criterion. The case where it is possible to increase the size of the biorefinery optimal size and use capacity and the petroleum diesel plant capacity in the subsequent time intervals (scenario 1) are given in Table 15 and the case when it is not possible (scenario 2) in Table 15a. It is possible to satisfy the EC requirements for the period (2010-2020) by increasing factory size (scenario 1) in 9 Bulgarian regions (regions 3, 4, 8, 12, 14, 15, 20, 22, 23, 26). Using the policy of not changing the installed power of the factories (scenario 2) whilst satisfying the EC criteria and the predicted diesel fuel consumption for the same period it will be necessary to build new factories with different capacity in 12 Bulgarian regions (3, 4, 8, 12, 14, 15, 16, 20, 22, 23, 24, 26) in 2020. At the same time the total investments which have to be done for building and enlargements of biorefineries (2010-2020) are 1 % more using the scenario 2 (127.257M$) comparing with scenario 1

(125.685M$). Regarding the criteria "Minimum Total GHG emissions" using both scenarios the results are equivalent towards the total investment expenditures for the whole period (2010-2020). The advantage of using the scenario 1 is that the investment loading after the first year is less while using the scenario 2 is bigger in the first time interval. The investment expenses for the first year are equal for both scenarios but for the following years are different.

**Table 15** Optimal size / optimal used capacity and location of biodiesel (B100) and optimal used petroleum diesel plants for first scenario in case (a) – Minimum Total GHG emissions

| Years | 2010 | 2012 | 2014 | 2016 | 2018 | 2020 |
|---|---|---|---|---|---|---|
| **Proportion biodiesel/diesel** | **5%** | **6%** | **7%** | **8%** | **9%** | **10%** |
| **REGIONS/** <br> Total Investment [M$] | **Biorefinery optimal size**/optimal used capacity **[ton year⁻¹]x10³** | | | | | |
| **Region-3/** <br> 19.788 | - | - | - | Size 5/ <br> 25.729 | Size 5/ <br> 35.000 | Size 8/ <br> 42.984 |
| **Region-4/** <br> 3.500/0 | - | - | - | - | - | Size 1/ <br> 3.686 |
| **Region-8/** <br> 18.473 | Size 7/ <br> 32.500 | Size 7/ <br> 32.377 | Size 7/ <br> 32.483 | Size 7/ <br> 32.500 | Size 7/ <br> 30.758 | Size 7/ <br> 32.500 |
| **Region-12/** <br> 25.149 | Size 7/ <br> 32.765 | Size 8/ <br> 39.755 | Size 8/ <br> 43.515 | Size 8/ <br> 39.482 | Size 10/ <br> 55.000 | Size 10/ <br> 62.250 |
| **Region-14** <br> 14.444 | - | - | Size 1/ <br> 8.500 | Size 6/ <br> 25.000 | Size 6/ <br> 25.000 | Size 6/ <br> 28.750 |
| **Region-15** <br> 14.444 | Size 1/ <br> 6.093 | Size 4/ <br> 23.847 | Size 4/ <br> 24.000 | Size 6/ <br> 25.000 | Size 6/ <br> 25.000 | Size 6/ <br> 26.973 |
| **Region-20** <br> 3.500 | - | - | - | - | - | Size 1/ <br> 5.002 |
| **Region-23** <br> 22.083 | Size 4/ <br> 22.661 | Size 6/ <br> 26.467 | Size 6/ <br> 46.334 | Size 9/ <br> 44.000 | Size 9/ <br> 53.566 | Size 9/ <br> 64.586 |
| **Region-26** <br> 4.301 | - | - | - | - | Size 1/ <br> 8.000 | Size 2/ <br> 11.000 |
| **TOTAL USED CAPACITY** | **94.020** | **1224.49** | **154.833** | **191.712** | **232.324** | **277.734** |
| **Investment in years [M$]** | **48.475** | **12.237** | **3.500** | **35.857** | **8.883** | **16.708** |

MIN and MAX capacity of each of size of biodiesel (B100) plant is given in table 6

| Regions diesel plant / <br> MAX capacity | **Petroleum diesel plant used capacity** | | | | | |
|---|---|---|---|---|---|---|
| | **[ton year⁻¹]x10³** | | | | | |
| **Region-2/** <br> 1200000 | 474.850 | 550.060 | 654.902 | 766.488 | 848.746 | 938.999 |
| **Region-15/** <br> 900.000 | 433.397 | 491.782 | 527.339 | 565.184 | 629.057 | 691.197 |
| **Region-20/** <br> 900.000 | 900.000 | 900.000 | 900.000 | 900.000 | 900.000 | 900.000 |
| **TOTAL USED CAPACITY** | **1808.248** | **1941.843** | **2082.241** | **2231.672** | **2377.804** | **2530.196** |

**Table 15a** Optimal size / optimal used capacity and location of biodiesel (B100) and optimal used petroleum diesel plants for second scenario in case (a) – Minimum Total GHG emissions

| Years | 2010 | 2012 | 2014 | 2016 | 2018 | 2020 |
|---|---|---|---|---|---|---|
| **Proportion biodiesel/diesel** | 5% | 6% | 7% | 8% | 9% | 10% |
| **REGIONS/** Total Investment [M$] | **Biorefinery optimal size**/optimal used capacity **[ton year⁻¹]x10³** | | | | | |
| **Region-3/** 18.473 | - | - | Size 7/ 30.000 | Size 7/ 43.750 | Size 7/ 43.638 | Size 7/ 43.513 |
| **Region-4/** 10.858 | - | - | - | - | - | Size 5/ 14.000 |
| **Region-8/** 18.473 | Size 7/ 32.500 | Size 7/ 32.133 | Size 7/ 32.500 | Size 7/ 32.500 | Size 7/ 32.500 | Size 7/ 30.000 |
| **Region-12/** 18.473 | Size 7/ 32.765 | Size 7/ 38.749 | Size 7/ 41.976 | Size 7/ 47.381 | Size 7/ 49.458 | Size 7/ 62.250 |
| **Region-14/** 14.444 | - | Size 6/ 25.000 | Size 6/ (26.124 | Size 6/ 27.245 | Size 6/ 25.000 | Size 6/ 25.000 |
| **Region-15/** 3.500 | Size 1/ 6.093 | Size 1/ 6.581 | Size 1/ 8.500 | Size 1/ 8.335 | Size 1/ 8.461 | Size 1/ **8.500** |
| **Region-16/** 4.301 | - | - | - | - | Size 2/ 11.000 | Size 2/ 8.820 |
| **Region-20/** 6.379 | - | - | - | - | - | Size 3/ 17.209 |
| **Region-22/** 14.444 | - | - | - | - | Size 6/ 25.000 | Size 6/ 25.000 |
| **Region-23** 8.029 | Size 4/ 22.661 | Size 4/ 19.983 | Size 4/ 15.732 | Size 4/ 24.000 | Size 4/ 24.000 | Size 4/ 24.000 |
| **Region-24/** 3.500 | - | - | - | Size 1/ 8.500 | Size 1/ 5.266 | Size 1/ 2.271 |
| **Region-26/** 6.379 | - | - | - | - | Size 3/ 8.000 | Size 3/ 17.170 |
| **TOTAL USED CAPACITY** | **94.020** | **122.449** | **154.833** | **191.712** | **232.324** | **277.734** |
| **Investment in years [M$]** | **48.475** | **14.444** | **18.473** | **3.500** | **25.125** | **17.237** |

MIN and MAX capacity of each of size of biodiesel (B100) plant is given in table 6

| **Regions diesel plant / MAX capacity** | **Petroleum diesel plant used capacity** | | | | | |
|---|---|---|---|---|---|---|
| | **[ton year⁻¹]x10³** | | | | | |
| **Region-2/** 1200000 | 474.850. | 550.060 | 654.902 | 766.488 | 848.746 | 938.999 |
| **Region-15/** 900.000 | 433.397 | 491.782 | 527.339 | 565.184 | 629.057 | 691.197 |
| **Region-20/** 900.000 | 900.000 | 900.000 | 900.000 | 900.000 | 900.000 | 900.000 |
| **TOTAL USED CAPACITY** | **1808.248** | **1941.843** | **2082.241** | **2231.672** | **2377.804** | **2530.196** |

**Table 16** Optimal size / optimal used capacity and location of biodiesel (B100) and optimal used petroleum diesel plants for first scenario in case (b) - Minimum Annualized Total Cost

| Years | 2010 | 2012 | 2014 | 2016 | 2018 | 2020 |
|---|---|---|---|---|---|---|
| **Proportion biodiesel/diesel** | 5% | 6% | 7% | 8% | 9% | 10% |
| **REGIONS/** Total Investments [M$] | **Biorefinery optimal size/**optimal used capacity [ton year$^{-1}$]x10$^3$ | | | | | |
| **Region-3/** 3.5000 | - | - | - | Size 1/ 6.116 | Size 1/ 8.468 | Size 1/ 3.979 |
| **Region-8/** 10.8589 | Size 5/ 29.803 | Size 5/ 32.146 | Size 5/ 32.500 | Size 5/ 32.500 | Size 5/ 32.500 | Size 5/ 32.500 |
| **Region-9/** 3.5000 | - | - | - | | Size 1/ 8.500 | Size 1/ 8.500 |
| **Region-12/** 19.7660 | Size 8/ 38.000 | Size 8/ 53.879 | Size 8/ 56.748 | Size 8/ 62.169 | Size 8/ 41.940 | Size 8/ 57.246 |
| **Region-14/** 14.4447 | - | - | - | | Size 6/ 28.579 | Size 6/ 28.750 |
| **Region-15/** 3.5000 | - | Size 1/ 7.975 | Size 1/ 8.500 | Size 1/ 8.500 | Size 1/ 8.500 | Size 1/ 8.500 |
| **Region-17/** 10.8589 | - | - | - | | | Size 5/ 14.000 |
| **Region-20/** 3.5000 | | | | Size 1/ 8.500 | Size 1/ 8.500 | Size 1/ 8.500 |
| **Region-21/** 3.5000 | - | - | - | | | Size 1/ 8.500 |
| **Region-23/** 19.7683 | Size 6/ 26.216 | Size 6/ 28.447 | Size 8/ 57.084 | Size 8/ 73.926 | Size 8/ 57.335 | Size 8/ 64.258 |
| **Region-26/** 19.7660 | - | - | - | | Size 8/ 38.000 | Size 8/ 43.000 |
| **TOTAL USED CAPACITY** | **94.020** | **122.449** | **154.833** | **191.712** | **232.324** | **277.734** |
| **Investments over years [M$]** | **45.0696** | **3.5000** | **5.3213** | **7.000** | **37.7107** | **14.3589** |

MIN and MAX capacity of each of size of biodiesel (B100) plant is given in table 6

| Region diesel plant/ MAX capacity | Petroleum diesel plant used optimal capacity | | | | | |
|---|---|---|---|---|---|---|
| | [ton year$^{-1}$]x10$^3$ | | | | | |
| **Region-2/** 1200000 | 474.850 | 550.060 | 654.902 | 766.488 | 848.746 | 938.999 |
| **Region-15/** 900.000 | 433.397 | 491.782 | 527.339 | 565.184 | 629.057 | 691.197 |
| **Region-20/** 900.000 | 900.000 | 900.000 | 900.000 | 900.000 | 900.000 | 900.000 |
| **TOTAL USED CAPACITY** | **1808.248** | **1941.843** | **2082.241** | **2231.672** | **2377.804** | **2530.196** |

**Table 16a** Optimal size / optimal used capacity and location of biodiesel (B100) and optimal used petroleum diesel plants for second scenario in case (b) - Minimum Annualized Total Cost

| Years | 2010 | 2012 | 2014 | 2016 | 2018 | 2020 |
|---|---|---|---|---|---|---|
| **Proportion biodiesel/diesel** | 5% | 6% | 7% | 8% | 9% | 10% |
| **REGIONS/** Total Investments [M$] | Biorefinery optimal size/optimal used capacity [ton year⁻¹]x10³ | | | | | |

| **REGIONS/** Total Investments [M$] | **Biorefinery optimal size/optimal used capacity [ton year⁻¹]x10³** | | | | | |
|---|---|---|---|---|---|---|
| **Region-3/** 3.500 | - | - | - | - | Size 1/ 4.713 | Size 1/ 8.500 |
| **Region-8/** 10.858 | Size 5/ 29.803 | Size 5/ 32.146 | Size 5/ 32.500 | Size 5/ 32.500 | Size 5/ 32.500 | Size 5/ 32.500 |
| **Region-9/** 3.500 | - | - | - | - | Size 1/ 7.500 | Size 1/ 8.500 |
| **Region-12/** 19.766 | Size 8/ 38.000 | Size 8/ 57.786 | Size 8/ 55.112 | Size 8/ 62.169 | Size 8/ 40.136 | Size 8/ 61.622 |
| **Region-15/** 14.444 | - | - | Size 6/ 25.000 | Size 6/ 38.543 | Size 6/ 48.255 | Size 6/ 48.111 |
| **Region-20/** 3.500 | - | - | - | Size 1/ 8.500 | Size 1/ 7.215 | Size 1/ 8.500 |
| **Region-21/** 3.500 | - | - | - | - | Size 1/ 8.500 | Size 1/ 8.500 |
| **Region-23/** 14.444 | Size 6/ 26.216 | Size 6/ 32.515 | Size 6/ 42.220 | Size 6/ 50.000 | Size 6/ 45.504 | Size 6/ 50.000 |
| **Region-24/** 3.500 | - | - | - | - | - | Size 1/ 8.500 |
| **Region-26/** 19.766 | - | - | - | - | Size 8/ 38.000 | Size 8/ 43.000 |
| **TOTAL USED CAPACITY** | 94.020 | 122.449 | 154.833 | 191.712 | 232.324 | 277.734 |
| **Investments over years [M$]** | 45.069 | | 14.444 | 3.500 | 30.266 | 3.500 |

MIN and MAX capacity of each of size of biodiesel (B100) plant is given in table 6

| Region diesel plant/ **MAX capacity** | **Petroleum diesel plant used optimal capacity** | | | | | |
|---|---|---|---|---|---|---|
| | **[ton year⁻¹]x10³** | | | | | |
| **Region-2/** 1200000 | 474.850 | 550.060 | 654.902 | 766.488 | 848.746 | 938.999 |
| **Region-15/** 900.000 | 433.397 | 491.782 | 527.339 | 565.184 | 629.057 | 691.197 |
| **Region-20/** 900.000 | 900.000 | 900.000 | 900.000 | 900.000 | 900.000 | 900.000 |
| **TOTAL USED CAPACITY** | 1808.248 | 1941.843 | 2082.241 | 2231.672 | 2377.804 | 2530.196 |

On the Table 16 and Table 16a are shown the results from the optimal synthesis of an IBSC using the criteria „Minimum Annualized Total Cost". The cases when it is possible to increase the size of the factory in the subsequent time intervals (the first scenario) the biorefinery optimal size/optimal used capacity and the petroleum diesel plant used capacity are given on Table 16 and the case when it is not possible (the second scenario) on Table 16a. To reach the EC requirements for the period (2010-2020) using the first scenario if increasing of the factory size is possible the number of Bulgarian regions with changed power of the factories is 11 (regions 3, 8, 9, 12, 14, 15, 17, 20, 21, 23, 26) at 2020. Using the policy without changing of the installed power of the factories (second scenario) during the exploitation, keeping the requirements EC criteria and the prognoses for diesel fuel consumption it is necessary to build factories with different power in 10 Bulgarian regions (3, 8, 9, 12, 15, 20, 21, 23, 24, 26) at 2020. For scenario 1 the total investments for building and enlargement of biorefineries for the period 2010-2020 figure out at 112.960 M$ while using scenario 2 the total investments are 96.780M$ respectively. The investment expenditures are equal for both scenarios for the first year, but for the next years the investment loading will be less for scenario 1 comparing with scenario 2.

### 2.2.5.　Distribution of greenhouse gases stages of the life cycle of biodiesel(B100)

The results of optimal synthesis shown on Fig. 5 and Fig. 6 indicate that carbon dioxide emissions increase when the "Minimum Annualized Total Cost" criterion is used in comparison with the case when the Minimum Total GHG Emission is used. This is mainly because of increased emissions from the transport of raw materials and biodiesel. At the same time the increased emissions of carbon dioxide in the case in Fig. 6 is because of the technology used for growing sunflowers, which are predominantly used for the production of biodiesel (B100) in this case.

The analysis of the distribution of GHG emissions show that the "Minimum Total GHG emissions" is realized basically by optimization of transport emissions and appropriate choice of the places for necessary biomass production. When using the "Minimum Annualized Total Cost" criterion for synthesis of optimal IBSC is used, an increase of the emissions is observed as a result of the transportation of biofeedstock and fuels. In both the "Minimal Total GHG" and "Minimum Annualized Total Cost" cases the source of GHG emissions is the biodiesel (100) production technology and the relevant technology for cultivation of sunflower and rapeseed. Use of rapeseed as biofeedstock for biodiesel (100) production gives better indicators for GHG emissions at the biomass growth stage than use of sunflower biofeedstock.

The conclusion made from Fig. 7 is that the "Total GHG Emissions" with criteria "Minimum Annualized Total Cost" are with 9.55% more comparing with the emissions using the criteria "Minimum Total GHG Emissions" referred to 2020.
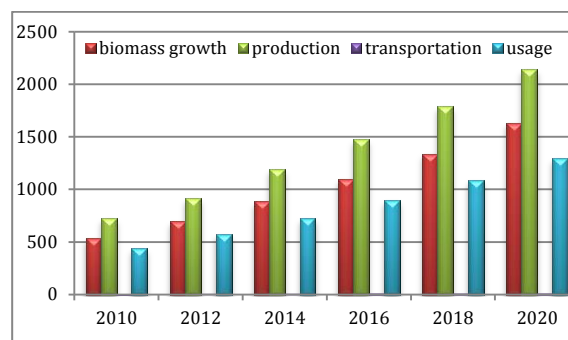


**Fig 5.** Distribution of GHG emissions for different stages of the life cycle of biodiesel (B100) for second scenario in case (a) – Minimum Total GHG emissions
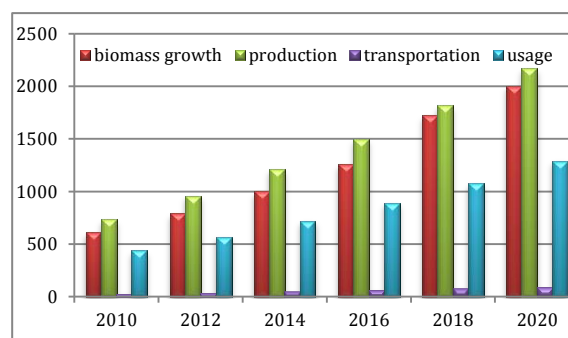


**Fig 6.** Distribution of GHG emissions for different stages of the life cycle of biodiesel (B100) for second scenario in case (b) - Minimum Annualized Total Cost
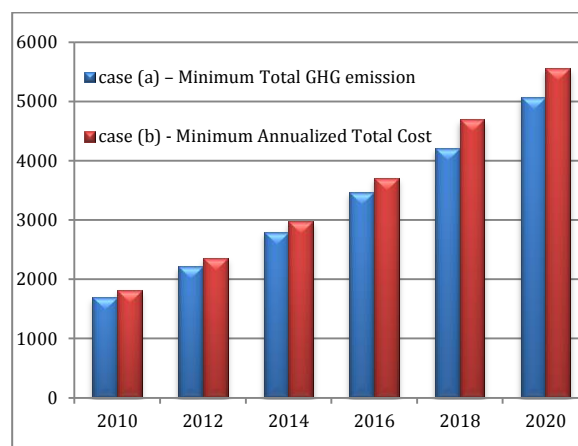


**Fig 7.** Total GHG emissions of the life cycle of biodiesel (B100) for second scenario in case (a) – Minimum Total GHG emissions and (b) - Minimum Annualized Total Cost

### 2.2.6.　Biodiesel(B100) supply chain cost structures

The analysis of the structure of the expenses using both criteria shows that there is a significant value in the byproducts such as glycerin and seed cake remaining after oil extraction. For example the inclusion of glycerin and seed cake value leads to a decrease in the net process cost by 29.77% using the "Minimum Total GHG emission" criterion and by 37.03% using the "Minimum Annualized Total Cost" criterion over the time interval 2010-2020.
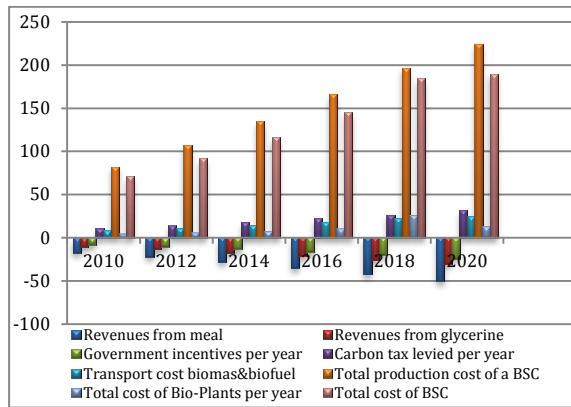
**Fig 8.** Biodiesel (B100) supply chain cost structures ($ year⁻¹)10⁶ for second scenario in case (a) – Minimum Total GHG emissions



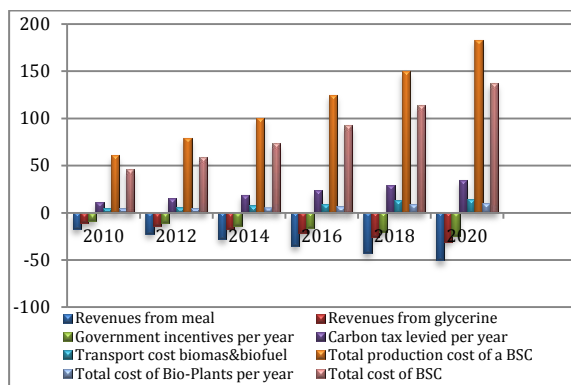**Fig 9.** Biodiesel (B100) supply chain cost structures ($ year⁻¹)10⁶ for second scenario in case (b) - Minimum Annualized Total Cost

Figure 10 shows the Annualized Total Cost for the first and second scenario for different objective functions used for optimal synthesis of IBSC for different time intervals. It is seen that factory size has a relatively small influence on the total price of the IBSC, whereas choice of the criteria for synthesis, Minimum Cost or "Minimum GHG Emission", has a significant influence on the Annualized Total Cost. For example the cost of the "Minimum Annualized Total Cost" system has a 22.56% lower price compared with the Minimum Total GHG Emission based approach. At the same time using the "Minimum Annualized Total Cost" criterion the total emissions of greenhouse gases is only 9.55% bigger than that produced using the "Minimum Total GHG emission" approach.
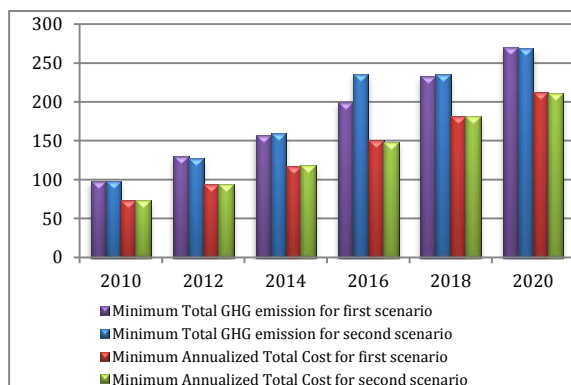


**Fig 10.** Annualized Total Cost ($ year⁻¹)10⁶ for first and second scenario using different objective functions for optimal synthesis of IBSC

### 2.2.7. Biodiesel(B100) production plant locations

The solutions obtained in the case of an optimal synthesis of BSC using the criterion "Minimum Total GHG Emissions" (case (a)) and using the criteria "Minimum Annualized Total Cost" (case (b)) showed that GHG emissions (Table 19) is only 6.6% lower in case (a) than case (b), while the price of biodiesel (B100) (Table 18) is 32% higher in case (a) than case (b). This is due to the increased capital and operational costs in case (a). Furthermore, the reduction of GHG emissions at the expenses of optimization of transport emissions in case (a) and use as rapeseed feedstock at case (b) instead of sunflower seeds in case (b). In case of design of an IBSC by using minimum greenhouse gas emissions as objective function, the best parameters are obtained if the used bio-resource for the Bulgarian conditions is rapeseed. However, it results in production of biodiesel (B100) with highest price (see Table 17 and Table 17a).
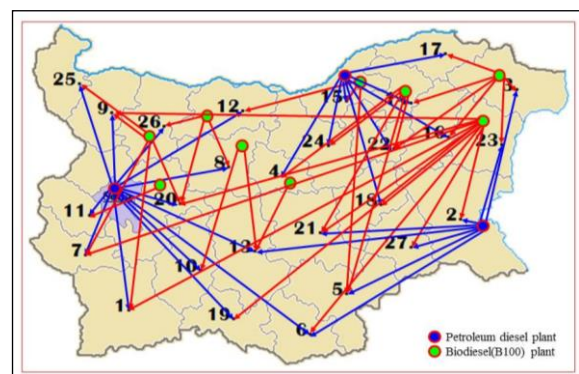


**Fig 11.** Optimal BG biodiesel (B100) supply chain configuration for 2020 year for first scenario in case: (a) – Minimum Total GHG emissions
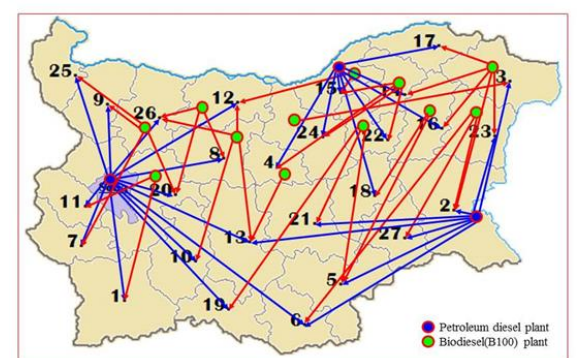


**Fig 12.** Optimal BG biodiesel (B100) supply chain configuration for 2020 year for second scenario in case:(a) – Minimum Total GHG emissions
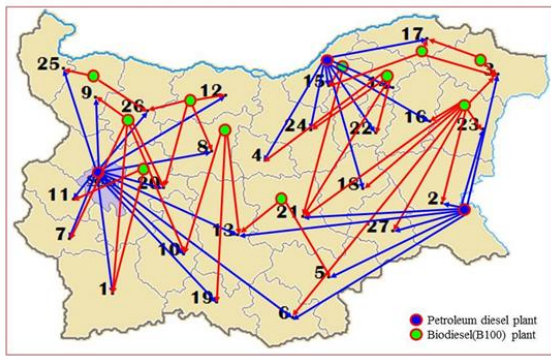
**Fig 13.** Optimal BG biodiesel (B100) supply chain configuration for 2020 year for first scenario in case: (b) – Minimum Annualized Total Cost
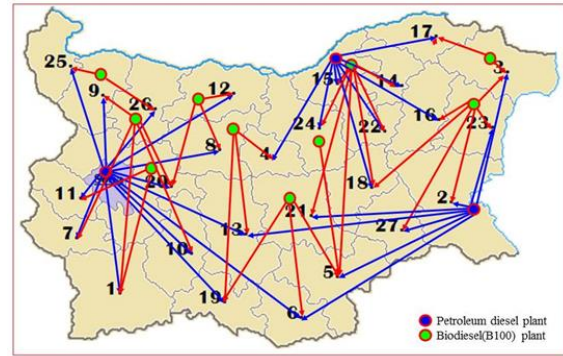


**Fig 14.** Optimal BG biodiesel (B100) supply chain configuration for 2020 year for second scenario in case: (b) – Minimum Annualized Total Cost

**Table 17.** Summary of computational results for the second scenario in case: **(a)-Minimum Total GHG emissions**

| Years | 2010 | 2012 | 2014 | 2016 | 2018 | 2020 |
|---|---|---|---|---|---|---|
| Proportion biodiesel/diesel | 5% | 6% | 7% | 8% | 9% | 10% |
| **Cost of a Biodiesel plants per year (M\$ year⁻¹)** | | | | | | |
| **Cost of a Biodiesel per year** | 98.270 | 127.101 | 159.84 | 195.67 | 235.53 | 268.93 |
| **Cost of a Diesel and Transport per year (M\$ year⁻¹)** | | | | | | |
| **Cost of a Diesel&Transport** | 1173.58 | 1261.37 | 1353.79 | 1452.15 | 1548.39 | 1648.79 |
| Transport cost Diesel | 34.38 | 38.01 | 41.98 | 46.20 | 50.37 | 54.77 |
| **Total Greenhouse gases (tonCO2-eq. year⁻¹)x10⁶** | | | | | | |
| **GHG on a Biodiesel&Diesel** | **6.98** | **7.5930** | **8.248** | **8.969** | **9.68** | **10.44** |
| GHG emissions from Biodiesel | 0.4240 | 0.5528 | 0.699 | 0.867 | 1.05 | 1.27 |
| GHG for Diesel and transportation | 6.55 | 7.0352 | 7.543 | 8.082 | 8.61 | 9.17 |
| **Greenhouse gases per day for BSC (tonCO2-eq. day⁻¹) x10⁶** | | | | | | |
| **GHG emissions on a BSC** | 0.1696 | 2.2113 | 2.79 | 3.48 | 4.22 | 5.07 |
| **Total Biodiesel and Diesel usage per year (ton year⁻¹) x10⁶** | | | | | | |
| Biodiesel usage | 0.094 | 0.122 | 0.154 | 0.192 | 0.232 | 0.278 |
| Diesel usage | 1.808 | 1.942 | 2.082 | 2.232 | 2.378 | 2.530 |
| **Distribution of arable land (ha)x10³** | | | | | | |
| Total SUM Land | | | 3227.23 | | | |
| BIOFUELS Land | 88.59 | 115.08 | 145.17 | 177.62 | 215.08 | 250.05 |
| RESERVATION Land | | | 1613.61 | | | |
| FOOD Land | | | 668.09 | | | |
| FREE Land | 856.93 | 830.91 | 800.36 | 767.92 | 731.21 | 695.48 |
| **BIOFUELS Land all regions for (ha)x10³** | | | | | | |
| Sunflower | 0.285 | 1.68 | 2.349 | 6.582 | 17.772 | 52.743 |
| Rapeseed | 88.306 | 113.34 | 143.123 | 172.715 | 197.309 | 197.281 |
| **FOODS&BIOFUELS Land all regions (ha)x10³** | | | | | | |
| Sunflower | 515.215 | 516.62 | 518.609 | 529.008 | 536.071 | 567.673 |
| Rapeseed | 241.470 | 266.56 | 294.657 | 316.701 | 346.347 | 350.472 |

**Table 17a.** Summary of computational results for second scenario in case: (b) - Minimum Annualized Total Cost

| | Years | | | | | |
|---|---|---|---|---|---|---|
| | **2010** | **2012** | **2014** | **2016** | **2018** | **2020** |
| Proportion biodiesel/diesel | 5% | 6% | 7% | 8% | 9% | 10% |
| **Cost of a Biodiesel plants per year (M$ year⁻¹)** | | | | | | |
| **Cost of a Biodiesel per year** | **72.760** | **93.723** | **11.8459** | **147.730** | **181.510** | **211.051** |
| **Cost of a Diesel and Transport per year (M$ year⁻¹)** | | | | | | |
| **Cost of a Diesel&Transport** | **1173.57** | **1261.37** | **1353.78** | **1452.15** | **1548.39** | **1648.79** |
| Transport cost Diesel | 34.38 | 38.01 | 41.98 | 46.20 | 50.37 | 54.77 |
| **Total Greenhouse gases (tonCO2-eq./year)x10⁶** | | | | | | |
| **GHG on a Biodiesel&Diesel** | **7.008** | **7.630** | **8.289** | **9.02** | **9.76** | **10.56** |
| GHG emissions from Biodiesel | 0.452 | 0.589 | 0.745 | 0.928 | 1.138 | 1.387 |
| GHG for Diesel and transportation | 6.551 | 7.035 | 7.544 | 8.085 | 8.615 | 9.167 |
| **Greenhouse gases per day for BSC (ton CO₂-eq. day⁻¹) x10³** | | | | | | |
| **GHG emissions on a BSC** | **1.809** | **2.35** | **2.98** | **3.71** | **3.90** | **5.55** |
| **Total Biodiesel and Diesel usage per year (ton year⁻¹) x10⁶** | | | | | | |
| Biodiesel usage | 0.094 | 0.122 | 0.155 | 0.192 | 0.232 | 0.278 |
| Diesel usage | 1.808 | 1.941 | 2.082 | 2.231 | 2.377 | 2.530 |
| **Distribution of arable land (ha)x10³** | | | | | | |
| Total SUM Land | | | 3227.23 | | | |
| BIOFUELS Land | 72.446 | 94.583 | 119.43 | 150.26 | 194.66 | 227.45 |
| RESERVATION Land | | | 1613.61 | | | |
| FOOD Land | | | 657.46 | | | |
| FREE Land | 883.72 | 861.58 | 826.10 | 781.65 | 731.84 | 689.87 |
| **BIOFUELS Land all regions for (ha)x10³** | | | | | | |
| Sunflower | 72.231 | 93.038 | 119.00 | 144.84 | 186.37 | 226.68 |
| Rapeseed | 0.214 | 1.545 | 0.285 | 5.419 | 8.284 | 0.773 |
| **FOODS&BIOFUELS Land all regions (ha)x10³** | | | | | | |
| Sunflower | 576.53 | 597.34 | 633.33 | 668.48 | 719.04 | 756.20 |
| Rapeseed | 153.38 | 154.71 | 154.19 | 163.50 | 165.85 | 174.44 |

**Table 18.** Summary of computational results for price of biodiesel (B100) for second scenario

**Price of biodiesel (B100) ($ ton⁻¹)**

| Criterion | Average | Years | | | | | |
|---|---|---|---|---|---|---|---|
| | | **2010** | **2012** | **2014** | **2016** | **2018** | **2020** |
| **(a) -** MIN Total GHG emissions | **1019 (132%)** | 1045 (135%) | 1041 (136%) | 1032 (135%) | 1020 (132%) | 1013 (129%) | 968 (127%) |
| **(b)** - MIN Annualized Total Cost | **769 (100%)** | 774 (100%) | 765 (100%) | 765 (100%) | 770 (100%) | 781 (100%) | 759 (100%) |

**Table 19.** Summary of computational results for total GHG emissions for the second scenario

**Total Greenhouse gases emissions (tonCO2-eq./year)x10⁶**

| Criterion | Average | Years | | | | | |
|---|---|---|---|---|---|---|---|
| | | **2010** | **2012** | **2014** | **2016** | **2018** | **2020** |
| **(a) -** MIN Total GHG emissions | **(93.42%)** | 1.696 (93.7%) | 2.211 (93.8%) | 2.798 (93.8%) | 3.465 (93.4%) | 4.216 (92.2%) | 5.083 (93.6%) |
| **(b)** -MIN Annualized Total Cost | **(100%)** | 1.809 (100%) | 2.356 (100%) | 2.981 (100%) | 3.712 (100%) | 4.696 (100%) | 5.558 (100%) |

## 3. CONCLUSIONS

The underlying conclusions of the present investigation are that in order to achieve a "smart" system design for biodiesel production and dissemination it is necessary to take into account the interactions between all components included in the production and distribution of biodiesels produced from different types of biomass. At the same time, the requirements of EC Directive 20/20/20 need to be met. Analyzing the results of the investigation, we found that the economically competitive production of biodiesel depends on the optimization of the whole integrated supply chain over the entire planning horizon for Bulgaria in the period 2010-2020. Optimization of only parts of the supply chain will not achieve an understanding of the compromises in time, in geographical location of the production and in necessary supply elements required for the optimization of biodiesel production. The approach proposed in this investigation can be applied in different geographic regions that have the capacity to produce various bio-resources for example - sunflower and rapeseed. The model can also be take into account changing policy standards and changing biodiesel production technologies in over extended system planning periods.

The results from this investigation are giving the possibility to make the following substantial conclusions:

1. The available agricultural land in Bulgaria is giving an opportunity for producing sufficient amount of biological feedstock (sunflower and rapeseed) for production of the needed quantity of biodiesel (B100) in order to satisfy the Bulgarian needs and to reach the required quota of 10 % for liquid biofuel at 2020.

2. The optimal area required for cultivation of sunflower and rapeseed is concentrated in a small number of country regions chosen independently of the objective criteria for the optimal synthesis of the IBSC.

3. The optimum mixture of biocultural feedstock using the "Minimum Annualized Total Cost" approach for synthesis of IBSC required in 2020 requires 14% of agricultural land to be used to for sunflower cultivation and 2% to be used for rapeseed cultivation. The use of the "Minimum Total GHG Emissions" criterion requires 12% of agricultural land to be used for rapeseed cultivation and 3% to be used for sunflower cultivation.

4. An important conclusion for the logistics is that the railway is an optimal type of transport which should be used as for bio-resources (sunflower and rapeseed), as well as for fuels (biodiesel (B100) and petroleum diesel).

5. The average cost of biodiesel (B100) in the period of (2010-2020) using the "Minimum Annualized Total Cost" synthesis model is 769 $ $t^{-1}$ whilst the "Minimum Total GHG Emission" model under the the same circumstances yields a cost of 1019 $ $t^{-1}$, i.e. 32.5% higher than the "Minimum Annualized Total Cost" approach. The total GHG emissions for the Minimum Annualized Cost approach are 6.6% higher when minimization of the cost of production rather than minimization of GHG emissions the primary objective.

6. The estimated cost of capital investment for the whole period (2010-2020) is 96.779 M$ for the "Minimum Annualized Total Cost" and 127.257 M$ for "Minimum Total GHG Emission" using the same input data for each calculation.

We intend also in the future to include in the model uncertainties in optimal decision-making procedures in order to improve the system reliability against uncertainties as demand variations, technological uncertainty and unexpected circumstances caused by human or natural adversity.

## ACKNOWLEDGEMENT

## REFERENCES

[1]. E. Wetterlund, S. Leduc, E. Dotzauer and G. Kindermann, "Optimal localisation of biofuel production on a European scale," *Energy.* Vol. 41, pp. 462-472, 2012.

[2]. European Commission 20 20 by 2020: Europe's climate change opportunity, COM (2008) 30 final. Brussels, Belgium: European Commission, 2008.

[3]. European Commission. Biomass action plan. COM 2005, 628.

[4]. Dir 2009/28/EC, Directive 2009/28/EC of the European Parliament and of the Council of 23 April 2009 on the promotion of the use of energy from renewable sources and amending and subsequently repealing Directives 2001/77/EC.

[5]. Dir 2003/30/EC. Directive 2003/30/EC of the European Parliament and of the Council of 8 May, 2003, on the promotion of the use of biofuels or other renewable fuels for transport.

[6]. E.M. Kondili and J.K. Kaldellis, "Biofuel implementation in East Europe: Current status and future prospects," *Renewable and Sustainable Energy Reviews*. Vol. 11, pp. 2137–2151, 2007.

[7]. A. Demirbas, "Biofuels sources, biofuel policy, biofuel economy and global biofuel projections," *Energy Conversion and Management.* Vol. 49, pp. 2106–2116, 2008.

[8]. F. Andersen, F. Iturmendi, S. Espinosa and M. S. Diaz, "Optimal design and planning of biodiesel supply chain with land competition," *Computers and Chemical Engineering.* Vol. 47, pp. 170-182, 2012.

[9]. B. Ivanov and S. Stoyanov, "A mathematical model formulation for the design of an integrated biodiesel-petroleum diesel blends

system," *Energy.* Available: http://dx.doi.org/10.1016/j.energy.2016.01.038 , 2016.

[10]. A. Azadeh, H. V. Arani and H. Dashti, "A stochastic programming approach towards optimization of biofuel supply chain," *Energy.* Vol. 76, pp. 513-525, 2014.

[11]. J.D. Nixon, P.K. Dey, P.A. Davies, S. Sagi and R.F. Berry, "Supply chain optimisation of pyrolysis plant deployment using goal programming," *Energy.* Vol. 68, pp. 262-271, 2014.

[12]. S.Y. Balaman and H. Selim, "A fuzzy multiobjective linear programming model for design and management of anaerobic digestion based bioenergy supply chains," *Energy.* Vol. 74, pp. 928-940, 2014.

[13]. B. Mota, M.I. Gomes, A. Carvalho and A.P. Barbosa-Povoa, "Towards supply chain sustainability: economic, environmental and social design and planning," *Journal of Cleaner Production.* pp. 1-14, 2014.

[14]. I. Awudu and J. Zhang, "Stochastic production planning for a biofuel supply chain under demand and price uncertainties," *Applied Energy.* Vol. 103, pp. 189–196, 2013.

[15]. J. Ren, L. Dong, L. Sun, M. E. Goodsite, S. Tan and L. Dong, "Life cycle cost optimization of biofuel supply chains under uncertainties based on interval linear programming," *Bioresource Technology.* Vol. 187, pp. 6–13, 2015.

[16]. K. Tong, F. You and G. Rong, "Robust design and operations of hydrocarbon biofuel supply chain integrating with existing petroleum refineries considering unitcost objective," *Computers and Chemical Engineering.* Vol. 68, pp. 128–139, 2014.

[17]. Q. Zhang, N. Shah, J. Wassick, R. Hellin and P. van Egerschot, "Sustainable supply chain optimisation: An industrial case study," *Computers & Industrial Engineering.* Vol. 74, pp. 68–83, 2014.

[18]. R. Babazadeh, J. Razmi, M. Rabbani and M. S. Pishvaee, "An integrated data envelopment analysise mathematical programming approach to strategic biodiesel supply chain network design problem," *Journal of Cleaner Production.* Available: http://dx.doi.org/10.1016/j.jclepro.2015.09.038 , 2015.

[19]. F. You and B. Wang, "Life Cycle Optimisation of Biomass-to-Liquids Supply Chains with Distributed-Centralized Processing Networks," *Industrial Engineering & Chemical Research,* Vol. 50 (17), pp. 10102-10127, 2011.

[20]. REPUBLIC OF BULGARIA National statistical institute. Available: http://www.nsi.bg, 2015.

[21]. Digital Library of National Statistical Institute-Online Catalogue. Available: http://statlib.nsi.bg:8181/FullT/FulltOpen/SRB _7_5_2012_2013.pdf, 2014.

[22]. E. Kondili and J. Kaldellis, "Biofuel implementation in East Europe: Current status

[23]. B. Ivanov, B. Dimitrova and D. Dobrudzhaliev, "Optimal design and planning of biodiesel supply chain considering crop rotation model. Part 2. Location of biodiesel production plants on the Bulgarian scale," *Bulgarian Chemical Communications.* Vol. 46 (2), pp. 306 – 319, 2014.

[24]. Wikimedia Commons, Available: http://commons.wikimedia.org/wiki/File:Bulga ria_administrative_divisions, 2015.

[25]. Official website of the Ministry of Agriculture and Food of Republic of Bulgaria 2010. Available: http://www.mzh.government.bg, 2014.

[26]. R. Bryan and A. Moser, "Efficacy of specific gravity as a tool for prediction of biodiesel–petroleum diesel blend ratio," *Fuel.* Vol. 99, pp. 254–261, 2012.

[27]. Ministry of Transport, Information Technology and Communications of Republic of Bulgaria. Available: http://www.mtitc.government.bg, 2014.

[28]. Available: http://www.biofuels.apec.org/pdfs/ewg_2010_ biofuel-production-cost.pdf.

[29]. International resource costs of biodiesel and bioethanol. Available: http://www.neema.ufc.br/Etanol17.pdf, 2014.

[30]. ChemWorld Glycerin. Available: http://www.chemworld.com/ChemWorld-Glycerin-p/cw-glycerin-1.htm, 2015.

[31]. BorsaAgro. Available: http://borsaagro.net, 2015.

[32]. Open Access version via Utrecht University Repository. Available: http://dspace.library.uu.nl/bitstream/handle/1 874/20687/NWS-E-2005-141.pdf?sequence=1, 2014.

[33]. A. Ozlem, N. Shah and L. Papageorgiou, "Economic optimisation of a UK advanced biofuel supply chain," *Biomass and Bioenergy.* Vol. 4 (1), pp. 57-72, 2012.

[34]. D.S. Remer and L.H. Chai, "Design cost factors for scaling-up engineering equipment," *Chemical Engineering Progress.* Vol. 86 (8), pp.77-82, 1990.

[35]. A. Ozlem, N.Shah and L. Papageorgion, "An optimisation framework for a hybrid first/second generation bioethanol supply chain," *Computers & Chemical Engineering.* Vol. 42, pp. 101-114, 2012.

[36]. G. Sara, Z. Andrea and B. Fabrizio, "Spatially explicit multi-objective optimisation for design and planning of hybrid first and second generation biorefineries," *Computers and Chemical Engineering.* Vol. 35, pp. 1782–1797, 2011.

[37]. International Energy Agency, Available: http://www.iea.org/stats/unit.asp, 2014.

[38]. World of electric vehicles. Available: http://www.evworld.com/library/energy_numb ers.pdf, 2014.

[39]. Експертен клуб за икономика и политика. Available: http://ekipbg.com/2012/05/25/gpricesbg/, 2015.

[40]. W. Elisabeth, L. Sylvain, D. Erik and K. Georg, "Optimal localisation of biofuel production on a European scale," *Energy*. Vol. 41, pp. 62-472, 2012.

[41]. European Commission, Well-to-wheels analysis of future automotive fuels and pow-ertrains in the European context. (Online). (2006), Available: <http://www. europabio.org/Biofuels%20reports/well-to-wheel.pdf, 2011.

[42]. G. Edwards-Jonesa, L.M. Canals, N. Hounsomec, M. Truningerd, G. Koerbera and B. Hounsomee, "Testing the assertion that 'local food is best': the challenges of an evidence-based approach," *Trends in Food Science & Technology*. Vol. 19, pp. 265-274, 2008.

[43]. GAMS Development Corporation -A user's guide. Washington, DC: GAMS: 2014. Available: http://www.gams.com/dd/docs/bigdocs/GAMS UsersGuide.pdf, 2014 .

[44]. P. Borjesson and L. Gustavsson," Regional production and utilization of biomass in Sweden," *Energy.* Vol. 21, pp. 747-64, 1996.

Turkish
**JournalPark**
ACADEMIC

Environmental Research & Technology

http://dergipark.gov.tr/ert

**RESEARCH ARTICLE**

# Isolation and characterization of fluoride resistant bacteria from groundwaters in Dindigul, Tamilnadu, India

K. Kirupa Sree[1], C. Edward Raja[1*], U. Ramesh[2]

[1] DST-Ramanujan Fellow, Department of Molecular Biology, School of Biological Sciences, Madurai Kamaraj University, Madurai, Tamil Nadu 625021, INDIA
[2] Assistant Professor, Department of Molecular Biology, School of Biological Sciences, Madurai Kamaraj University, Madurai, Tamil Nadu 625021, INDIA

## ABSTRACT

The use of microbes to remove fluoride from water and soil is an extent of applied research and development. This is the first attempt have been made to examine physiochemical characteristics and also isolate fluoride resistant bacteria from ground waters in selected villages at Dindigul district, Tamil nadu, India. Based on high fluoride resistance (200 mM), three bacterial isolates were selected for further studies. The isolates authentically identified as genus *Pseudomonas*. Biochemical and 16S rRNA sequencing analysis of the isolates revealed that they are closely related (97%) to *Pseudomonas* sp. (98%) to *Pseudomonas* aeruginosa and (97%) to *Pseudomonas* sp. The 16S rRNA sequences were submitted in the NCBI under accession numbers MF481852, MF481853, MG751413. The fluoride resistant bacterial strains were resistant to antibiotics such as amoxicillin, ampicillin, chloramphenicol, kanamycin and streptomycin.

*Keywords:* Ground water, Fluoride resistant bacteria, Antibiotic resistance, *Pseudomonas*

## 1. INTRODUCTION

Groundwater is a most valuable natural source that is essential for human health, socio-economic development and functioning of ecosystems [1]. The rapid urbanization, agricultural activities and other environmental fluctuations are continuously deteriorating the quality of various water resources [2, 3]. Fluoride pollution occurs in the environment through natural and anthropogenic sources [4]. The natural source of fluoride in waters are fluoride bearing minerals and soil consisting clays [5]. The wastewater released from semiconductor, aluminium and glass manufacturing industries, also contributes fluoride water pollution especially in groundwater [4]. The permissible limit of fluoride is 1.5 mg L$^{-1}$ in water [6]. It is harmful when it exceeds the acceptable limit and it can lead to various diseases for example osteoporosis, arthritis, and brittle bones cancer, infertility, brain damage, and thyroid disorder [7]. The fluoride problem has reached alarming proportion affecting at least 19 states of India [8, 9, 10]. Most of

the countries are affected by fluorosis including China, India, Srilanka, Mexico, Argentina, U.S.A, New Zealand, Japan, Egypt, Jordan, Turkey, Iran, Iraq, Kenya, Tanzania, South Africa, Australia, Thailand, Canada, Saudi Arabia, Persian Gulf, and Syria [11, 12, 13, 14]. In this study to assess the physicochemical parameters of some open wells, hand pumps and bore well samples were collected from three different villages of Dindigul district. In addition, to screen and isolate fluoride resistant bacteria from the groundwater samples.

## 2. MATERIALS AND METHOD

### 2.1. Sample Collection and analysis

Groundwater samples were collected from 22 different sites including bore wells, hand pumps, and wells covering three villages of Dindigul district (Fig 1). Dindigul is one of the district in the state of Tamil Nadu. The geological longitude of the sampling site of Tamilnadu is 11.1271$^{\circ}$ N, 78.6569$^{\circ}$ E. For

physicochemical characteristics, water samples were collected in sterile plastic bottles and then carefully sealed, labelled and transferred to laboratory for the analysis. Portable device (PCSTestr 35, Eutech), was employed to record pH, electrical conductivity(EC) and total dissolved solid (TDS). The other physiochemical parameters such as total hardness (TH), residual (free) chlorine, chloride, iron and nitrate were determined by titration method as recommended by manufacturer instructions (Himedia, Mumbai, India). The fluoride concentration was estimated by LABMAN ion meter (lumion-40) with fluoride electrode combination.
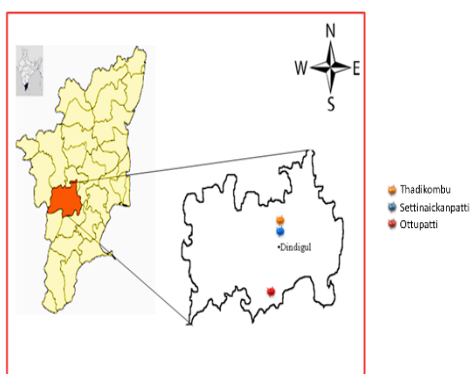


**Fig 1.** Groundwater sampling sites of three different villages in Dindigul district

### 2.2. Isolation of fluoride resistant bacteria

For isolation and enumeration of fluoride resistant bacteria, 0.1 ml of undiluted water samples were separately plated on Luria-Bertani agar (LB) (Himedia, Mumbai, India) supplemented with Sodium fluoride (NaF) (SRL, Mumbai, India). The initial concentration of 10 and 70 mM NaF was used to screen the fluoride resistant bacteria from Thadikombu, Settinaickanpatti and Ottupatti water samples. Plates were incubated at 37°C for 72 h. Fluoride resistant colonies differing in morphological, physiological and biochemical characteristics were isolated and used for further studies.
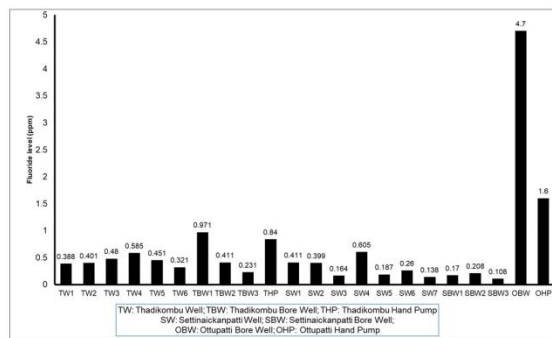


**Fig 2.** Fluoride values in groundwater analysed by ion selective electrode method. The concentration of fluoride is mentioned in parts per million (ppm) units

### 2.3. Determination of fluoride resistance

Fluoride resistance was determined on LB agar plates supplemented with different concentration of NaF starting from 10 to 250 mM. The working concentrations of NaF were prepared from 1 M stock solution of Sodium fluoride. The stock solution of fluoride was prepared in sterilized double distilled water. Minimum inhibitory concentration (MIC) was evaluated until the selected isolates were unable to grow on fluoride containing LB agar plates. Based on this analysis, MIC was determined in five days at 37 °C.

### 2.4. Biochemical Characterization of fluoride resistant bacteria

Selected fluoride resistant isolates were checked their growth on MacConkey agar, Eosin Methylene Blue agar (EMB), and *Pseudomonas* isolation agar media (Himedia, Mumbai, India). The shape and colour of the colonies were examined under the microscope after Gram staining. The isolates were identified according to Bergey's Manual of Systematic Bacteriology [15]. The optimal growth conditions with reference to pH and temperature were determined. The selected isolates were grown in LB medium, in the presence and absence of fluoride with varying pH values, i.e., 4, 5, 6, 7, 8, 9 and incubated at 25, 30, 37 and 44 oC. The optical density of the growing cultures in all the above-mentioned conditions was observed at 570 nm using a photo colorimeter (Deep vision, model 312) to determine the optimum growth.

### 2.5. Polymerase chain reaction (PCR) amplification

One colony or toothpick of every bacterial culture was suspended in 10 μl sterile double distilled water containing 1.5 ml Eppendorf tube. The tubes were kept for 15 min at 95 °C in boiling water bath and short spin at 10,000 rpm for 2 min. From the supernatant, 1μl was used as a template for PCR reaction. Amplification of 16S rRNA was carried out by using the universal bacterial 16S rRNA primers, 27 F 5'-AGA GTT TGA TCC TGG CTC AG-3' and 1429 R 5'-GGT TACC TTG TTA CGA CTT-3' [16] in thermal cycler under the following cyclic conditions as follows: 94°C for 5 min, 35 cycles of denaturation at 94°C for 30 s, annealing at 55°C for 30 s, extension at 72°C for 30 s and final extension at 72°C for 5 min. Polymerase chain reaction was performed in Agilent Technologies, SureCycler 8800. PCR product was analysed in 1.0% agarose gel electrophoresis. The amplified PCR products were eluted by GeneJET gel extraction kit (ThermoScientific, USA) and then carry out for sequencing.

### 2.6. 16S rRNA sequencing and blast analysis

The 16S rRNA gene sequencing of fluoride resistant isolates was carried out in 48-capillary ABI 3730 DNA analyser by direct sequencing of the PCR-amplified 16S rRNA gene. The sequences obtained were

compiled and compared to the sequences in the Genbank databases using BLAST analysis [17].

### 2.7. Determination of antibiotic resistance

Antibiotic sensitivity of the fluoride resistant isolates was determined by disc diffusion method. Antibiotic-impregnated discs (Himedia, Mumbai, India) were placed on Mueller Hinton (MH) agar plates swabbed with individual isolates and incubated at 37°C for 24-48 h. The diameter of the inhibition zones around the discs was measured. The antibiotic concentrations of the disc used were Amikacin (AK, 30mcg), Amoxyclav (AMC, 30mcg), ampicillin (AMP, 10mcg), chloramphenicol (C, 30mcg), ciprofloxacin (CIP, 5mcg) gentamycin (GEN, 10mcg) kanamycin (K, 30mcg) streptomycin (S, 10mcg) and tetracycline (TE, 30mcg) respectively.

### 2.8. Salt tolerance

The salt tolerance was determined in LB agar plates supplemented with different concentration of Sodium chloride (1-10%). The growth was monitored after 48 h incubation at 37°C.

## 3. RESULTS & DISCUSSION

### 3.1. Physiochemical characteristics

The physicochemical parameters and statistical measures of groundwater samples are mentioned in Table 1. In this study, pH values of all groundwater samples were ranging from 6.78 to 8.28. According to the WHO, safe limit of pH in water is 6.5-8.5 [18]. So that collected water samples pH values were within the permissible limit. The most desirable limit of EC in

drinking water is prescribed as 300 $\mu S$ cm$^{-1}$ [19]. The average value of EC is 1863 $\mu S$ cm$^{-1}$ and maximum number of samples showed above the desirable limit EC values. The WHO most desirable and maximum allowable limit of TDS is 500 and 1500 mg L$^{-1}$ respectively. The TDS values of all samples ranges from 1.09 to 935 mg L$^{-1}$ and also within the acceptable limit. The highest and average value of salinity was found to be at 942 and 491.5 mg L$^{-1}$ respectively. There were iron and residual free chlorine values not detected in all type of water samples.

In regards to total hardness, the highest values were obtained at 800 and 750 mg L$^{-1}$ for Thadikombu (SW3) and Settinaickanpatti (SW7) well waters. The permissible limit of chloride (Cl-) in water is 1000 mg L$^{-1}$ as recommended by the BIS. The Cl- content of all samples values were (100-750 mg L$^{-1}$) within the permissible limit. In general nitrate level in drinking water can also be an indicator of overall water quality. But in this study, tested nitrate values (0-25 mg L$^{-1}$) were below the desirable limit, that is 45 mg L$^{-1}$ [20]. Fluoride concertation was estimated by LABMAN ion meter and their values are shown in Fig. 2. The range (0.108-0.971 ppm) of fluoride concentrations were perceived from Thadikombu and Settinaickanpatti villages. In this analysis, maximum number of samples showed below fluoride level <0.5 ppm and it causes dental caries [21, 22]. In contrast, high fluoride values (1.6 and 4.7 ppm) were tested in Ottupatti village. Likewise, high fluoride contamination (4.34 ppm) in drinking water was reported in Ottapidaram block, Thoothukudi District [23]. Fluoride is harmful, when it exceeds the permissible limit of 1.5 ppm [24]. The concentration of fluoride above 1.5 ppm may cause dental fluorosis, intake of fluoride concentration above 3.0 ppm may cause skeletal fluorosis respectively [19].

**Table 1.** Statistical measures like, maximum, minimum, average and standard deviation of water samples in the study area

| Water quality parameters | Units | Maximum concentration | Minimum concentration | Average | Standard deviation (SD) | WHO/ISI permissible limit |
|---|---|---|---|---|---|---|
| pH | - | 8.28 | 6.78 | 7.49 | 0.39 | 6.5-8.5 |
| EC | $\mu S$ cm$^{-1}$ | 1863 | 2.24 | 983.61 | 723.56 | 300 |
| TDS | mg L$^{-1}$ | 935 | 1.09 | 215.36 | 335.20 | 500 |
| Salinity | mg L$^{-1}$ | 942 | 1.14 | 491.50 | 364.01 | - |
| Nitrate | mg L$^{-1}$ | 25 | 0 | 23.86 | 5.33 | 45(ISI) |
| TH | mg L$^{-1}$ | 800 | 50 | 393.18 | 318.64 | 500 |
| Chloride | mg L$^{-1}$ | 750 | 40 | 318.64 | 172.91 | 200 |

### 3.2. Screening and isolation of fluoride resistant bacteria

Five hundred ninety-four colonies were screened from initial level of NaF containing LB agar plates. After secondary screening, the colonies were transferred consecutively from 100-200 mM NaF supplemented LB agar plates. Finally, one colony was selected based on high growth in 200 mM NaF supplemented LB broth and agar medium. In addition, an attempt was made to screen fluoride resistant

bacteria from low desirable limit fluoride (1.0 ppm) in Thadikombu and Settinaickanpatti water samples. After screening, two high fluoride resistance (200 mM) bacterial isolates were identified only from Thadikombu water samples. The fluoride resistance (200 mM) is equivalent to the bacterium, that was isolated from high fluoride contaminated (1.6 and 4.7 ppm) Ottupatti water samples. Although, no high NaF resistance colonies were identified from Settinaickanpatti water samples. Three bacterial isolates were selected (THP6, THP41 and OHP5) and

used for further studies. The fluoride resistant isolates were made growth on MacConkey, EMB, and *Pseudomonas* isolation agar. They were gram negative, rod shaped bacteria (Fig 3). The optimum growth was observed at 37 oC and pH 7.
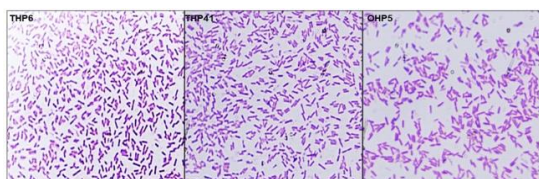


**Fig 3.** Microscopic view of fluoride resistant bacteria

Bacterial 16S rRNA gene (1.5 kb) was amplified successfully using 16S rRNA universal primers and then eluted by gel extraction kit (Fig 4). The eluted products were sequenced. Based on the morphological, biochemical and 16S rRNA sequencing analysis showed that the strains were close to the members of genus *Pseudomonas*. The highest sequences similarities were observed for THP6 (97%), THP41(97%) and OHP5 (98%) and matched highly homology to *Pseudomonas* sp. MB65 (HM597240), *Pseudomonas* sp. (GU966668) and *Pseudomonas aeruginosa* DN1 (KP119458) respectively. The 16S rRNA sequences were submitted in the NCBI database under accession numbers (MF481852, MF481853, MG751413). The evolutionary history was inferred using the UPGMA method [25]. The evolutionary distances were computed using the Maximum Composite Likelihood method [26] and phylogenetic tree was created in MEGA7 [27]. Phylogenetic analysis of fluoride resistant bacteria is shown in Fig 5. In this study, three *Pseudomonas* strains exhibited 200 mM NaF resistance was determined on LB agar plates. Previously testified fluoride resistant bacteria including *P. aeruginosa* and *Acinetobacter* sp. RH5 showed only 100 mM and 100 mg L$^{-1}$ fluoride resistance was isolated from soil and groundwater [28, 9]. Heterotrophic bacteria (Particularly *Pseudomonas* species) are ubiquitous and common bacterial species in ground water mainly because of their phenotypic plasticity [29, 30]. Bruins et al. [31] also proved that, *Pseudomonas* species exhibit resistance to a variety of heavy metals, antibiotics, toxic substances, and can use various compounds as carbon sources. Therefore, they have generated a high degree of interest in the area of environmental bioremediation.
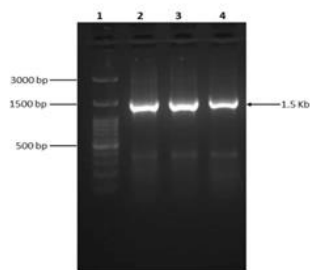


**Fig 4.** Agarose gel electrophoresis of 16r RNA gene amplification. Lane: 100bp DNA ladder H3 RTU; Lanes 2, 3 & 4: PCR products (1.5 kb) amplified from fluoride resistant bacterial strains HP6, HP41 and OHP5 isolated from groundwaters
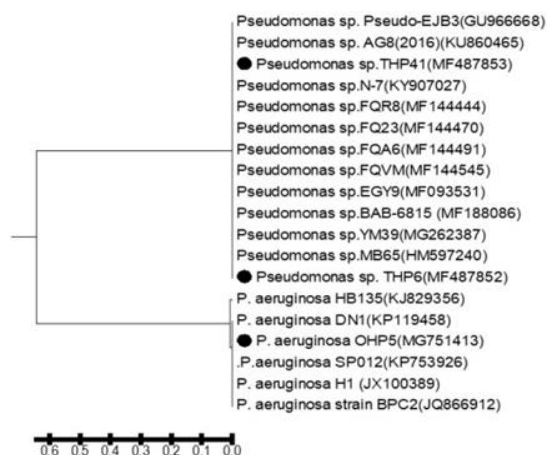


**Fig 5.** Phylogenetic analysis of fluoride resistant *Pseudomonas* and related species obtained from Genbank based on 16S rRNA sequences. The optimal tree with the sum of branch length = 1.29429242 is shown in the figure. The scale bar represents the units of the number of base substitutions per site. A total of 19 sequences involved in the analysis

### 3.3. Resistance to Salt and Antibiotics

Fluoride resistant isolates (THP6, THP41 and OHP5) exhibited 5% (w/v) salt resistance in LB agar plates. They were resistant to antibiotics such as amoxicillin, ampicillin, chloramphenicol, kanamycin and streptomycin. But they sensitive to amikacin and gentamycin antibiotics (Table 2). Isolates THP6, OHP5 was sensitive to ciproflaxin but THP41 is resistant, in other way, THP6 and OHP5 was resistant to Tetracycline in contrast THP41 is sensitive to it. Similarly, heavy metal resistant *Pseudomonas aeruginosa* BC15 showed resistance to many antibiotics such as ampicillin, tetracycline, chloramphenicol, erythromycin, kanamycin and streptomycin [32]. In contrast fluoride tolerant *Bacillus flexus* NM25 was sensitive to recommended doses of ofloxacin, kanamycin, rifampicin, levofloxacin, vancomycin, gatifloxacin, gentamicin, doxycycline, streptomycin, and nalidixic acid but only resistant to ampicillin respectively [33].

**Table 2.** Antibiotic sensitivity of Fluoride resistant isolates

| Antibiotics | Disc content (mcg) | THP6 | THP41 | OHP5 |
|---|---|---|---|---|
| Amikacin (Ak) | 30 | 21(S) | 18(S) | 18(S) |
| Amoxicillin (AMC) | 30 | NZ(R) | 8(R) | NZ(R) |
| Ampicillin (AMP) | 10 | NZ(R) | NZ(R) | NZ(R) |
| Chloramphenicol (C) | 30 | 12(R) | 8(R) | 12(R) |
| Ciprofloxacin (CIP) | 5 | 32(S) | 9(R) | 28(S) |
| Gentamycin (GEN) | 10 | 24(S) | 21(S) | 20(S) |
| Kanamycin (K) | 30 | 9(R) | 9(R) | 8(R) |
| Streptomycin (S) | 10 | 19(R) | 19(R) | 18(R) |
| Tetracycline (TE) | 30 | 9(R) | 8(S) | NZ(R) |

Note: S-sensitive, I-Intermediate, R- Resistance, NZ-No Zone, Zone of inhibition noted in (mm)

## 4. CONCLUSIONS

The study proves a variation in the Physico-chemical characteristics of groundwater. In concerning with fluoride contamination, less than desirable and higher than permissible values were detected in Thadikombu, Settinaickanpatti and Ottupatti villages. To our knowledge, this is the first report for identifying high fluoride resistant bacteria especially from Dindigul district, Tamilnadu. Fluoride resistant bacterial isolates exhibited 5% salt tolerance and also associated with resistant to multiple antibiotics. Future work will explore in terms of bacterial fluoride bioremoval, characterize fluoride resistant gene in *Pseudomonas* species and to develop biosensor for fluoride detection.

## REFERENCES

[1]. C. Steube, S. Richter, and C. Griebler, "First attempts towards an integrative concept for the ecological assessment of groundwater ecosystems," *Hydrogeology Journal,* Vol. 17, pp. 23-35, 2009.

[2]. M. Amini, K. Mueller, K.C. Abbaspour, T. Rosenberg, M. Afyuni, K.N. Møller, M. Sarr, and C.A. Johnson, "Statistical modelling of global geogenic fluoride contamination in groundwaters," *Environmental Science and Technology,* Vol. 42, pp. 3662-3668, 2008.

[3]. S. Selvam, A. Anthony Ravindran, S. Venkatramanan, and C. Singaraja, "Assessment of heavy metal and bacterial pollution in coastal aquifers from SIPCOT industrial zones, Gulf of Mannar, South Coast of Tamil Nadu, India," *Applied Water Science,* Vol. 7, pp. 897-913, 2017.

[4]. N. Drouiche, H. Lounici, M. Drouiche, N. Mameri, and N. Ghaffour, "Removal of fluoride from photovoltaic wastewater by electrocoagulation and products characteristics," *Desalination and Water Treatment,* Vol. 7, pp. 236-241, 2009.

[5]. R.K. Dey, S.K. Swain, S. Mishra, P. Sharma, T. Patnaik, V.K. Singh, B.N. Dehury, U. Jha, and R.K. Patel, "Hydro geochemical processes controlling the high fluoride concentration in groundwater: a case study at the Boden block area, Orissa, India," *Environmental Monitoring and Assessment,* Vol.184, pp. 3279-3291, 2012.

[6]. WHO, Guidelines for drinking water quality, 4th edn., *World Health Organization*, Geneva, 2011.

[7]. L. Han, D. Shubo, L. Zhijian, Y. Gang, H. Jun, "Preparation of Al-Ce hybrid adsorbent and its application for defluoridation of drinking water," *Journal of Hazardous Materials,* Vol. 179, pp. 424-430, 2010.

[8]. M. Kumar, and A. Puri, "A review of permissible limits of drinking water," *Indian Journal of Occupational and Environmental Medicine,* Vol.16, pp. 40-44, 2012.

[9]. S. Mukherjee, V. Yadav, M. Mondal, and S. Banerjee, "Characterization of a fluoride-resistant bacterium *Acenitobacter* sp. RH5 towards assessment of its water defluoridation capability," *Applied Water Science,* Vol.7, pp. 1923-1930, 2017a.

[10]. S. Mukherjee, P. Sahu, and G. Halder, "Microbial remediation of fluoride-contaminated water via a novel bacterium *Providencia vermicola* (KX926492)," *Journal of Environmental Management,* Vol. 204, pp. 413-423, 2017b.

[11]. Meenakshi, and R.C. Maheshwari, "Fluoride in drinking water and its removal," *Journal of Hazardous Materials,* Vol.137, pp. 456-463, 2006.

[12]. M. Mohapatra, S. Anand, B.K. Mishra, D.E. Giles, and P. Singh, "Review of fluoride removal from drinking water," *Journal of Environmental Management,* Vol.91, pp. 67-77, 2009.

[13]. M. Edmunds, and P. Smedley, Fluoride in natural waters-occurrence, controls and health aspects. *Essentials of Medical Geology,* O. Selinus, B. Alloway, J. A. Centerro, R. B. Finkelman, R. Fuge, U. Lindh, P. Smedley, Ed. Elsevier: Amsterdam, The Netherlands, pp. 301-329, 2010.

[14]. S. Chatterjee, and De, "Adsorptive removal of fluoride by activated alumina doped cellulose acetate phthalate (CAP) mixed matrix membrane," *Separation and Purification Technology,* Vol. 125, pp. 223-238, 2014.

[15]. D. Claus, and R.C.W. Berkeley, Genus *Pseudomonas* In: P.H.A. Sneath, N.S. Mair, M.E. Sharpe, eds. *Bergey's Manual of Systematic Bacteriology,* Vol.1 Williams & Wilkins Baltimore, pp 140-219, ISBN 0-683-04108-8, 1986.

[16]. D.J. Lane, 16S/23S rRNA sequencing. In: E. Stackebrandt, and M. Goodfellow, editors. *Nucleic acid techniques in bacterial systematics.* Chichester, United Kingdom,: John Wiley and Sons, pp. 115-175, 1991.

[17]. S.F. Altschul, T.L. Maddan, A.A. Schaffer, J. Zang, Z. Zang, W. Miller, and D.J. Lipman, "Gapped BLAST and PSI-BLAST: a new generation of protein database search programs," *Nucleic Acids Research,* Vol. 25, pp. 3389-3402, 1997.

[18]. WHO, *Guidelines for drinking water quality,* 3rd edn., World Health Organization, Geneva, 2004, vol.1.

[19]. WHO, *Guidelines for drinking water quality, Drinking water quality control in small community supplies.* World Health Organization, Geneva, Vol. 3, 1984.

[20]. BIS, (Bureau of Indian Standards) 10500, *Indian standard drinking water specification,* First revision, pp 1-8, 1991.

[21]. C.M. Jones, G.O. Taylor, J.G. Whittle, D. Evans, and D.P. Trotter, "Water fluoridation, tooth decay in 5 year olds, and social deprivation measured by the Jarman score: analysis of data from British

dental surveys," *BMJ.* Vol. 315, pp. 514-517, 1997.

[22]. G.D. Acharya, M.V. Hathi, A.D. Patel, and K.C. Parmar, "Chemical properties of groundwater in Bhiloda Taluka Region, North Gujarat, India," *European Journal of Chemistry,* Vol. 5, pp. 792-796, 2008.

[23]. V. Veeraputhiran, and G. Alagumuthu, "A report on fluoride distribution in drinking Water," *International Journal of Environmental Sciences,* Vol. 1, pp. 4, 2010.

[24]. WHO, *Guidelines for drinking water quality*, 1st addendum to 3rd edn., recommendations, World Health Organization, Geneva, Vol. 1, 2006.

[25]. P.H.A. Sneath, and R.R. Sokal, Numerical Taxonomy. Freeman, San Francisco, 1973.

[26]. K. Tamura, M. Nei, and S. Kumar, "Prospects for inferring very large phylogenies by using the neighbor-joining method," *PNAS*. Vol. 101, pp. 11030-11035, 2004.

[27]. S. Kumar, G. Stecher, and K. Tamura, "MEGA7: molecular evolutionary genetics analysis version 7.0 for bigger datasets," *Molecular Biology and Evolution,* Vol. 33, pp. 1870-1874, 2016.

[28]. S. Chouhan, U. Tuteja, and S.J.S. Flora, "Isolation, identification and characterization of fluoride resistant bacteria: possible role in bioremediation," *Applied Biochemistry and Microbiology,* Vol. 48, pp. 43-50, 2012.

[29]. H. Leclerc, *Relationships between common water bacteria and pathogens in drinking-water, in Heterotrophic Plate Counts and Drinking-Water Safety, Eds.:* J. Bartram, J. Cotruvo, M. Exner, C. Fricker, A. Glasmacher, IWA Publishing, London, UK, pp. 80-118, 2003.

[30]. M. Patel, K. Baxi, P. Dayma, D. Upadhyay, N. Parmer, S. Kundu, S. Halder, K.H. Mody, and B. Jha, "Assessment of groundwater quality with respect to bacterial contamination in Bhavnagar, Gujarat, India," *Clean-Soil, Air, Water,* Vol. 42, pp. 1351-1362, 2014.

[31]. M.R. Bruins, S. Kapil, and F.W. Oehme, "Characterization of a small plasmid (pMBCP) from bovine *Pseudomonas pickettii* that confers cadmium resistance*," Ecotoxicology and Environmental Safety,* Vol. 54, pp. 241-248, 2003.

[32]. C. Edward Raja, K. Anbazhagan, and G.S. Selvam, "Isolation and characterization of a metal resistant *Pseudomonas aeruginosa* strain*," World Journal of Microbiology and Biotechnology* Vol. 22, pp. 577-585, 2006.

[33]. K.C. Pal, N.K. Mondal, S. Chatterjee, T.S. Ghosh, and J.K. Datta, "Characterization of fluoride-tolerant halophilic *Bacillus flexus* NM25 (HQ875778) isolated from fluoride-affected soil in Birbhum district, West Bengal, India," *Environmental Monitoring & Assessment,* Vol. 186, pp. 699-709, 2014.